



FACILITY FORM 602

N64-33289	
(ACCESSION NUMBER)	(THRU)
166	1
(PAGES)	(CODE)
NASA CR 59243	18
(NASA CR OR TMX OR AD NUMBER)	(CATEGORY)

DEVELOPMENT OF WELDING TECHNIQUES AND FILLER
METALS FOR HIGH STRENGTH ALUMINUM ALLOYS

Annual Summary Report
Project No. 07-1063

to

National Aeronautics and Space Administration
George C. Marshall Space Flight Center
Purchasing Office
Huntsville, Alabama
Attn: PR-RDC

Contract No. NAS8-1529
Control No. TP2-85364

10 August 1964

OTS PRICE

	\$ 5.00
XEROX	\$
MICROFILM	\$ 1.00

SOUTHWEST RESEARCH INSTITUTE
SAN ANTONIO HOUSTON

SOUTHWEST RESEARCH INSTITUTE
8500 Culebra Road, San Antonio, Texas 78206

DEVELOPMENT OF WELDING TECHNIQUES AND FILLER
METALS FOR HIGH STRENGTH ALUMINUM ALLOYS

Annual Summary Report
Project No. 07-1063

by

N. G. Lenamond
K. K. Speirs
H. C. Burghard, Jr.
José McDonald, Jr.

Reporting Period
27 June 1963 to 27 June 1964

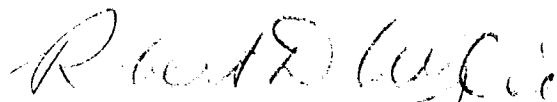
for

National Aeronautics and Space Administration
George C. Marshall Space Flight Center
Purchasing Office
Huntsville, Alabama
Attn: PR-RDC

Contract No. NAS8-1529
Control No. TP2-85364

10 August 1964

APPROVED:



Robert D. Wylie, Director
Department of Materials Engineering

FOREWORD

This report entitled, "Development of Welding Techniques and Filler Metals for High Strength Aluminum Alloys", was prepared by the Southwest Research Institute under Contract No. NAS8-1529 for the George C. Marshall Space Flight Center of the National Aeronautics and Space Administration.

The work was administered under the direction of the Propulsion and Vehicle Engineering Division, Engineering Materials Branch of the George C. Marshall Space Flight Center with Mr. Richard A. Davis acting as project manager.

ABSTRACT

33289 OVER

An investigation was undertaken to study the phases formed in the weld joint of 2219-T87 aluminum with 2319 aluminum filler metal. Of equal importance was a study of the variation in mechanical properties across the welded joint.

The predominant intermetallic phase occurring in the various zones of a 2219-T87 aluminum weldment is CuAl_2 . In most of the weld deposits, this phase occurs in the grain boundaries and is discontinuous. However, in the toes of the welds, it appears as a continuous network and takes on the appearance of Chinese script. This CuAl_2 Chinese script network is brittle and causes early failure of weldments due to its limited ductility.

In some cases a "needle" like structure was found associated with the Chinese script network. It is suspected but not confirmed that the "needles" are β (Al-Cu-Fe). This phase is also thought to be brittle but because it occurs in limited amounts is not believed to be as detrimental as the CuAl_2 network.

Under the operating procedures required for the Saturn fabrication i. e. horizontal welding with no subsequent machining, a perceptible notch is formed at the intersection of the weld toe and the parent metal. The fact that the concentration of undispersed CuAl_2 is greatest in this area results in an accentuation of the notch effect so that in general tensile

failures were initiated in this area. Were fatigue a factor, the combination might even have greater potential danger.

In addition to standard tensile tests, specimens from the weldments were subjected to special tests in which the strain in tension of various elements of the weldments was determined. From these tests it was concluded that: 1) the weld deposit yields at lower stress value than is required for the parent metal and, 2) that when a two inch test length was employed something over 50 percent of the total plastic deformation took place within a relatively short weld deposit.

In addition to standard tensile tests, a special biaxial bulge test was used in examining the welded joints.

Author

LIST OF TABLES

<u>Table</u>	<u>Page</u>
I. Chemical Composition of Alloy 2219 and Filler Material 2319	3
II. Mechanical Properties of 3/4 Inch 2219-T87 Aluminum Weldments	18
III. Mechanical Properties of Specimens from 3/4 Inch Thick 2219-T87 Aluminum Weldments Having Fusion Passes in the Top Toes	25
IV. Mechanical Properties of Specimens from 3/4 Inch Thick 2219-T87 Aluminum Weldments used in Ductility Measurements	88
V. Summary of Average Strain in Weld Metal, Zone A and Zones B and C of Welded 3/4 Inch Thick 2219-T87 Aluminum Tensile Specimens	89
VI. Mechanical Properties of 2219-T87 Weldments and Base Metal before and after Explosive Impact Loading	97
VII. Effect of Explosive Loading on the Mechanical Properties of 3/4 Inch 2219-T87 Weldments and Base Metal, Summarized from Table VI	98

LIST OF ILLUSTRATIONS

<u>Figure</u>		<u>Page</u>
1.	Microstructure of 2219-T87 Parent Metal.	5
2.	Aluminum Rich End of Al-Cu Binary Phase Diagram.	6
3.	Zones in a 2219-T87 Weldment.	7
4.	Weld Metal Structure in First and Second Weld Passes of a 2219-T87 Weldment.	9
5.	Weld Metal and Zone A of a 2219-T87 Weldment.	10
6.	Structure Close to Fusion Line in a 2219-T87 Weldment.	10
7.	Zone A of a 2219-T87 Weldment.	11
8.	Weld Crown Profile Producing the Bottom Toe in a 2219-T87 Weldment.	11
9.	Concentration of Intermetallic Constituents in the Bottom Toe of a Weld.	12
10.	Tensile Specimen.	16
11.	Appearance of a Typical Gap in the Fracture Path of a Broken Tensile Specimen after Butting the Failed Pieces Together.	19
12.	Fracture Initiation in Bottom Toe of Highly Stressed Tensile Specimen.	21
13.	Fracture Path in a Tensile Specimen with Weld Crowns Machined Off.	23
14.	The Fracture Path in Adjoining First and Second Weld Passes when Tested as Separate Tensile Specimens.	23

LIST OF ILLUSTRATIONS (Continued)

<u>Figure</u>		<u>Page</u>
15.	Bar Graph Comparing 3/4 Inch Thick 2219-T87 Weldments with and without Fusion Passes.	24
16.	Schematic of Section of Specimen Used to Study Fracture Path in 2219-T87 Weldments.	29
17.	Cracks in Weld Deposit of Uniaxial Tensile Specimen after Failure.	30
18.	Fracture Surface of 2219-T87 Welded Joint Tensile Specimen Tested with Weld Crowns Machined Off.	33
19.	Fracture Surface of 2219-T87 Welded Joint Tensile Specimen Tested with Weld Crowns Intact.	33
20.	Fracture Surface of 2219-T87 Base Metal Tensile Specimen.	35
21.	Fracture Surface of 2219-T87 Base Metal Tensile Specimen.	36
22.	Fracture Surface of 2219-T87 Base Metal Tensile Specimen.	37
23.	Fracture Surface of 2219-T87 Welded Joint Tensile Specimen.	39
24.	Fracture Surface of 2219-T87 Welded Joint Tensile Specimen.	40
25.	Fracture Surface of 2219-T87 Welded Joint Tensile Specimen.	41
26.	Fracture Surface of 2219-T87 Welded Joint Tensile Specimen.	42

LIST OF ILLUSTRATIONS (Continued)

<u>Figure</u>		<u>Page</u>
40.	Location and Measurements of Surface Cracks in Panel D.	67
41.	Formation of Cracks in the Intermetallic Constituents in the Bottom Toe of a Weld Panel after Biaxial Test.	69
42.	Cross Section of Fracture at Outer Edge of Weld Panel.	70
43.	Path of Fracture in Weld Metal Resulting from Biaxial Stressing.	71
44.	Fracture Surface of 2219-T87 Weldment Bulge Test Panel. Specimen Taken from Panel A Tested with Weld Crowns Intact.	73
45.	Fracture Surface of 2219-T87 Weldment Bulge Test Panel.	74
46.	Fracture Surface of 2219-T87 Weldment Bulge Test Panel.	75
47.	Tensile Coupon with 1/64 and 1/8 Inch Miniature Strain Gages Attached to Weld Deposit, Zone A and Zone C.	78
48.	Testing and Recording Equipment.	80
49.	Stress-Strain Curves of Weld Deposit, Zone A, Zone C, and per Two Inch Extensometer of Tensile Coupon.	81

LIST OF ILLUSTRATIONS (Continued)

<u>Figure</u>		<u>Page</u>
50.	Stress-Strain Curves of Weld Deposit, Zone A, Zone C, and Per Two Inch Extensometer of Tensile Coupon with Weld Crowns Ground Flush with Base Metal.	82
51.	Stress-Strain Curves of Weld Deposit, Zone A, Zone C, and Per Two Inch Extensometer of Large Width-to-Depth Weld Ratio Tensile Coupon.	83
52.	Percent Strain in Weld Deposit at Yield Strength as Recorded by the Two Inch Extensometer.	84
53.	Location of Three Surveys across Tensile Coupon to Measure Plastic Deformation.	86
54.	Percent Strain Distribution across Weld Joint.	90
55.	Explosive Impact Loading of Butt-Welded 3/4 Inch Thick 2219-T87 Test Panels.	92
56.	Explosive Impact Loading of Butt-Welded 3/4 Inch Thick 2219-T87 Test Panels.	92
57.	Appearance of 3/4" Thick 2219-T87 Weldment after Explosion Impact Loading with a 2-Pound Charge of Pentolite (Plate No. 30).	94
58.	Appearance of 3/4" Thick 2219-T87 Weldment after Explosion Impact Loading with a 4-Pound Charge of Pentolite (Plate No. 25).	95
59.	Sequence Used in Removing All Weld Metal, Transverse Weld and Base Metal Tensile Specimens from 3/4 Inch Thick 2219-T87 Butt Welded Panels.	96

LIST OF ILLUSTRATIONS (Continued)

<u>Figure</u>		<u>Page</u>
60.	Relative Positions of 3/4 Inch Thick 2219-T87 Test Panels Numbers 25 and 30 on the Steel Base Plate .	100
61.	Cross-Section of the Weld from Test Panel No. 25.	101
62.	Cross-Section of the Weld from Test Panel No. 30 .	102
63.	Effect of Explosive Impact Loading on Weld Zone Hardness of Panel No. 30.	104
64.	Effect of Explosive Impact Loading on Weld Zone Hardness of Panel No. 30.	105
65.	Effect of Explosive Impact Loading on Weld Zone Hardness of Panel No. 25.	106
66.	Effect of Explosive Impact Loading on Weld Zone Hardness of Panel No. 25.	107
67.	Increase in Weld Zone Hardness Due to Flattening Out of Weld Crown on Bottom Side of Panel No. 25.	108
68.	Horizontal Tig Welding.	146
69.	Standard Welding Procedure.	147
70	Weld Configurations of Hydraulic Bulge Panels A, B, C and D.	149
71.	Welding Procedure Used in the Preparation of Hydraulic Bulge Test Panel B.	150
72.	Welding Procedure of Large Width-to-Depth Weld Ratio.	152
73.	Welding Procedure and Location of Fusion Passes in Toes of Weld.	153

I. INTRODUCTION

This is the annual summary report of a study of 3/4 inch, 2219-T87 aluminum alloy weldments with 2319 filler metal. The investigation was three fold and included: 1) a study of the phases formed in weld zones and their effect on the mechanical properties, 2) a study of failure mechanisms of uniaxial and biaxial loaded weldments, and 3) a study of mechanical properties. All of the work was directed to the development of data with design significance for the Saturn program. The properties studied were yield strength, ultimate tensile strength, ductility (percent elongation), and fracture mechanisms.

This report will be divided into four major parts: 1) weld zone investigation, 2) study of failure mechanisms in aluminum alloy weldments under uniaxial and biaxial loading, 3) methods of measuring yield strength and ductility of welds, and 4) explosion impact testing of weldments.

II. WELD ZONE INVESTIGATION

Aluminum alloy 2219 is one of a group of alloys in which copper serves as the principal strengthening agent. The mechanical properties of the alloy are dependent on the manner in which the precipitated CuAl_2 is dispersed throughout the metal by a combination of mechanical and thermal treatments. When fabricated by fusion welding, structural changes due to heating and/or melting will result in a welded joint having substantially lower strength than the parent material. Since one of the objectives has been a study of the effect of weld structure on the mechanical properties of 2219-T87 weldments, particular attention has been given to the development data relative to the mechanical properties of the various zones comprising these weldments.

While referring to this alloy as one of aluminum and copper, it must be understood that elements other than copper are present in small concentrations so that under certain conditions the influence of these other elements will reflect on the properties or structures. The compositions of the wrought 2219-T87 alloy and 2319 filler metal are shown in Table I. The composition of these two alloys differs only in the titanium content. A small amount of titanium is added to the filler metal for grain refinement.

TABLE I
CHEMICAL COMPOSITION OF ALLOY 2219 AND FILLER MATERIAL 2319

<u>ALLOY 2219</u>		
	<u>Nominal Percent</u>	<u>Specification Percent (Maximum Unless Shown as a Range)</u>
Si	-	0.20
Fe	-	0.30
Cu	6.3	5.8 -6.8
Mn	0.3	0.20-0.40
Mg	-	0.02
Zn	-	0.10
Ti	-	0.02-0.10
V	.10	0.05-0.15
Zr	.15	0.10-0.25
Others, Each	-	0.05
Others, Total	-	0.15
Aluminum	Remainder	

<u>ALLOY 2319</u>		
	<u>Nominal Percent</u>	<u>Specification Percent (Maximum Unless Shown as a Range)</u>
Si	-	0.20
Fe	-	0.30
Cu	6.3	5.8 -6.8
Mn	0.3	0.20-0.40
Mg	-	0.02
Zn	-	0.10
Ti	0.15	0.10-0.20
Be	-	0.0008
V	0.10	0.05-0.15
Zr	0.15	0.10-0.25
Others, Each	-	0.05
Others, Total	-	0.15
Aluminum	Remainder	Remainder

It has been found that the response of the 2219 alloy to precipitation hardening heat treatment can be accelerated and the mechanical properties improved by the introduction of a carefully controlled amount of cold work after solution heat treatment. When this work is followed by the proper artificial aging, T87 temper is developed. Figure 1 is a photomicrograph at 1500X of the structure of 2219 wrought plate in the T87 condition. The finely dispersed phase is CuAl_2 . The massive constituent is also CuAl_2 which can be anticipated from equilibrium diagram considerations. Figure 2 is an equilibrium diagram of the Al-Cu system. This diagram shows that under equilibrium the maximum solid solubility of copper in aluminum is 5.7 percent. Since the 2219 alloy has 6.3 nominal percent of copper, approximately 9.6 percent of the total copper content is insoluble at the eutectic temperature. This amount of copper is contained in the residual liquid which surrounds the primary α grains. This liquid undergoes the eutectic reaction and forms a solid solution plus $\Theta (\text{CuAl}_2)$ in the grain boundaries.

Figure 3 shows the macrostructure of the cross section of a 2219-T87 aluminum weldment. The weld deposit (first and second passes) and the heat affected base metal have been identified. For clarity, three zones in the base metal have been identified as Zones A, B and C. Zone A, immediately adjacent to the weld deposit on either side of the fusion lines, was the area most severely affected by the heat of welding. Zones B and C are areas less affected by the heat of welding and therefore are



Etchant-Keller's

1500X

FIGURE 1. MICROSTRUCTURE OF 2219-T87
PARENT METAL

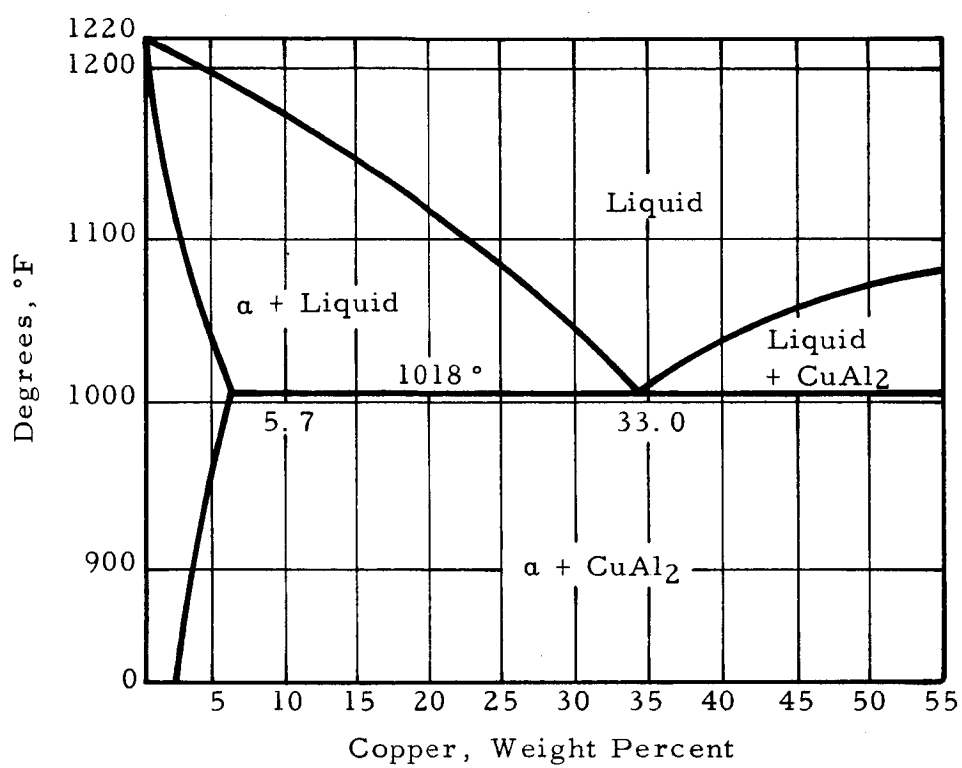
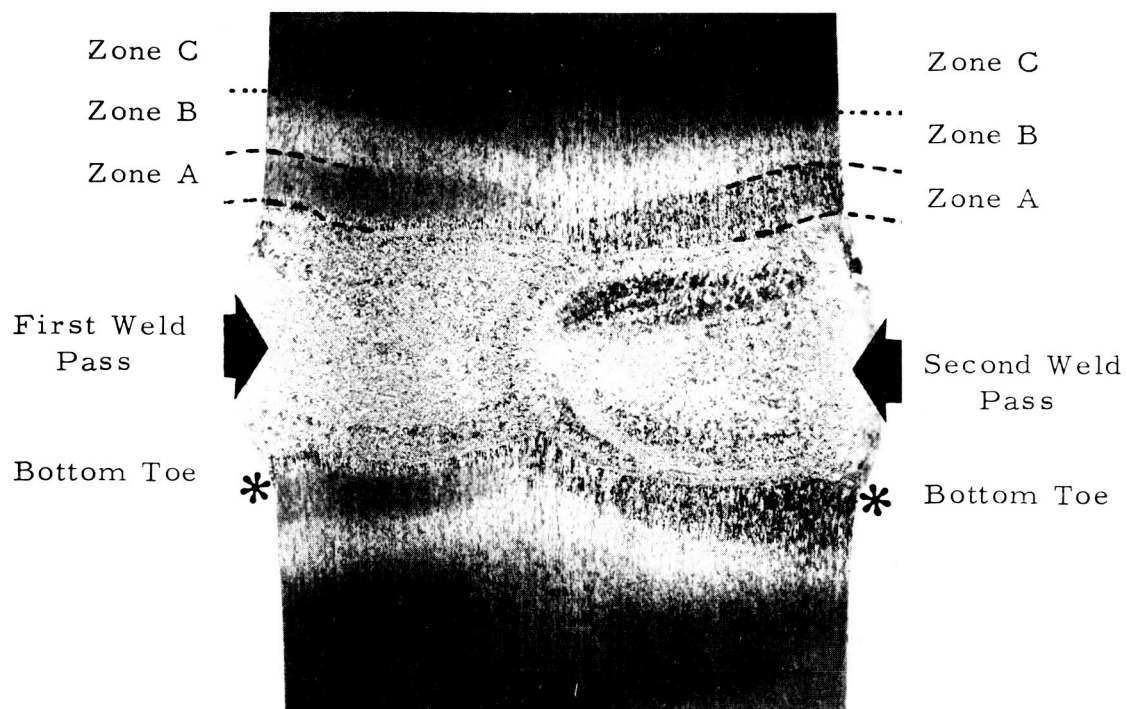


FIGURE 2 . ALUMINUM RICH END OF Al-Cu BINARY PHASE DIAGRAM.



Etchant-Keller's

4X

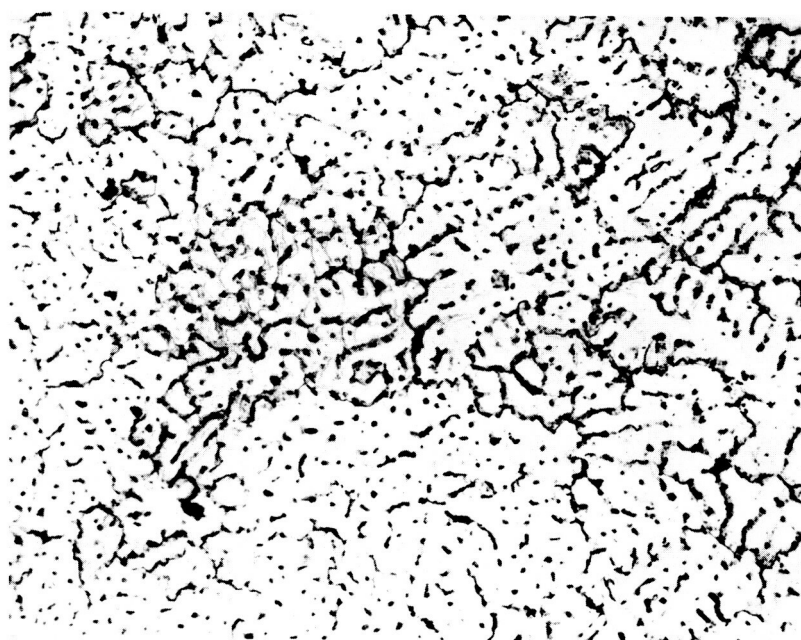
FIGURE 3. ZONES IN A 2219-T87 WELDMENT

less pronounced in the macrograph. The weld toes are also indicated in this figure.

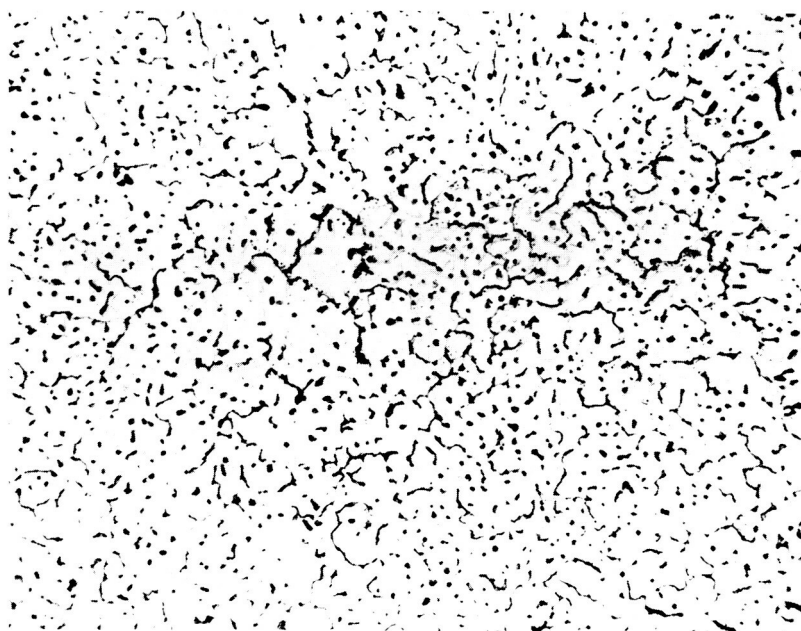
The microstructures of the first and second weld passes are shown in Figure 4. Both photomicrographs show the CuAl_2 phase in the grain boundaries of the alpha (α) solid solution matrix. During welding this material is melted and solidifies rapidly. The precipitated CuAl_2 in the matrix is taken into solution and the Cu is held in a supersaturated solution in the α phase. The CuAl_2 from the eutectic reaction coalesces as large particles of discontinuous Θ phase in the grain boundaries.

Figure 5 is a photomicrograph of the fusion found at the interface of deposit and Zone A. This structure is shown at higher magnification in Figure 6. It is evident in this photomicrograph that CuAl_2 has coalesced in the grain boundaries and another unidentified phase has precipitated in the matrix. The structural changes in Zone A are shown in Figure 7. The metal has been heated sufficiently to cause diffusion and coalescence of a portion of the Cu to the grain boundaries. This Cu forms additional CuAl_2 and adds to the CuAl_2 already present in the grain boundaries to form a continuous phase.

The microstructure of the bottom weld toes is quite different from that in the top toes, the weld deposit or any of the zones in base metal. A microstructure of a typical bottom toe at low magnification is shown in Figure 8. A portion of the weld deposit that forms the toe is seen to overlap Zone A. Figure 9 shows two micrographs of the bottom toe structure



First Weld
Pass



Second Weld
Pass

Etchant - Keller's

250X

FIGURE 4. WELD METAL STRUCTURE IN FIRST AND SECOND
WELD PASSES OF A 2219-T87 WELDMENT

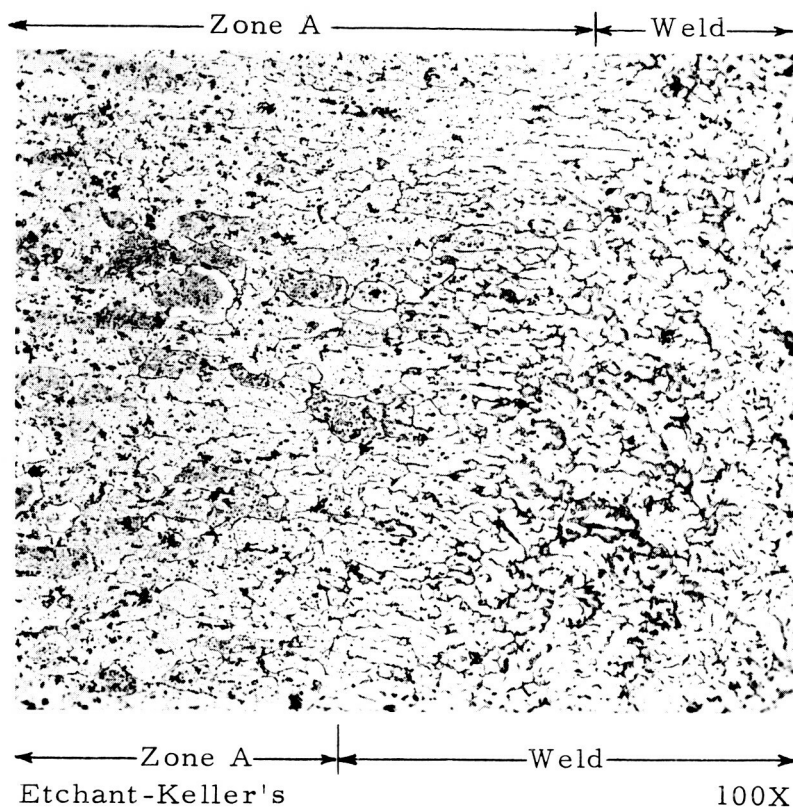


FIGURE 5. WELD METAL AND ZONE A OF A 2219-T87 WELDMENT

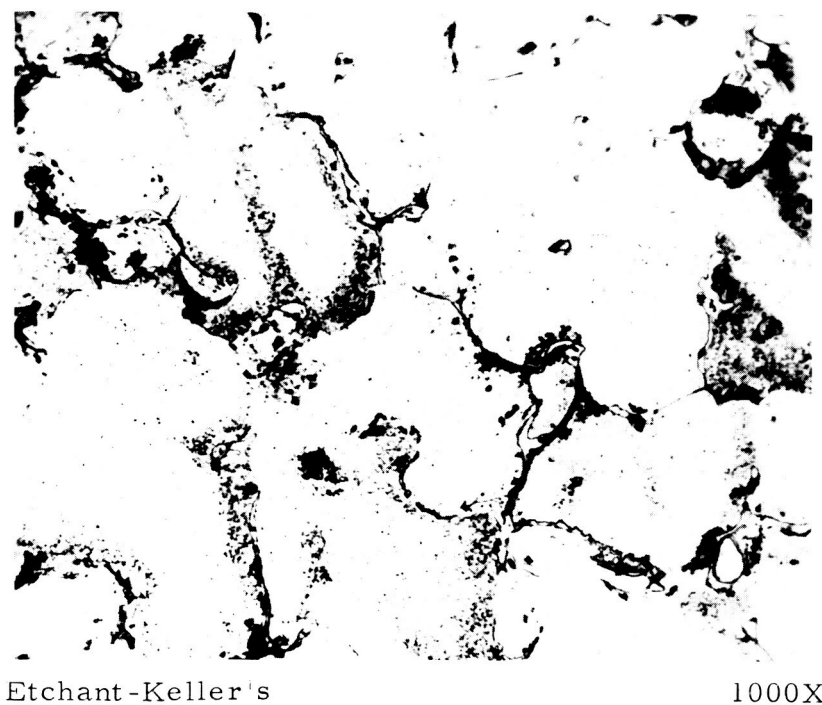
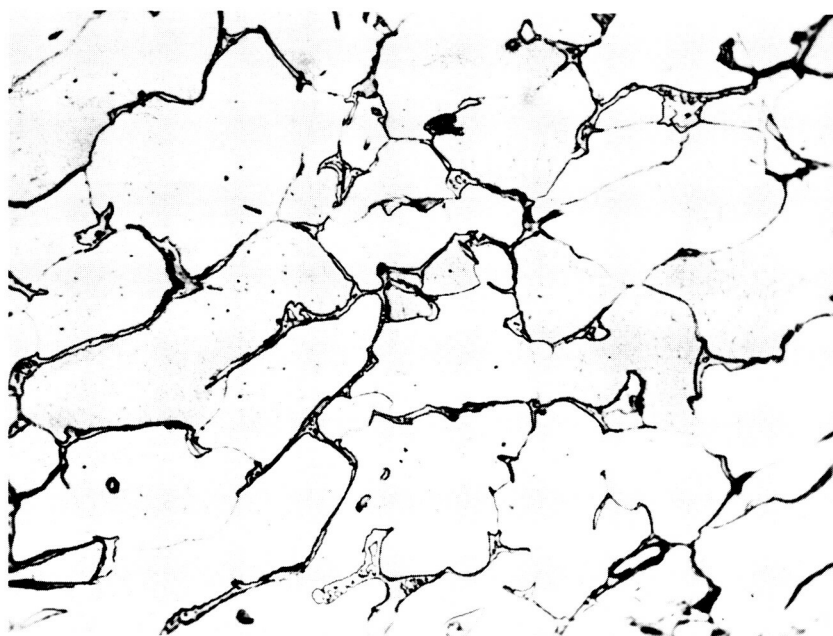


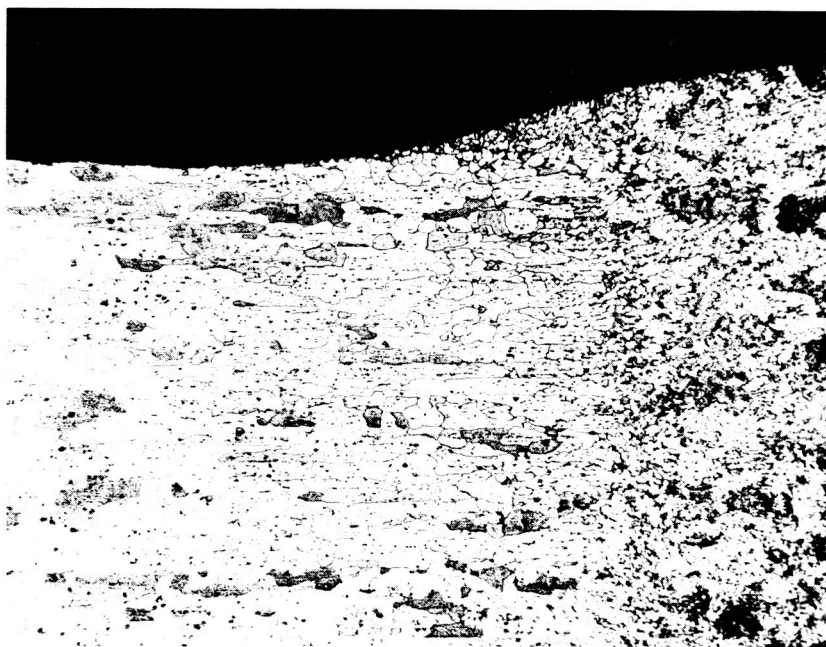
FIGURE 6. STRUCTURE CLOSE TO FUSION LINE IN A 2219-T87 WELDMENT



Etchant-Keller's

1000X

FIGURE 7. ZONE A OF A 2219-T87 WELDMENT



Zone A

Weld

Etchant-Keller's

50X

FIGURE 8. WELD CROWN PROFILE PRODUCING THE BOTTOM TOE IN A 2219-T87 WELDMENT

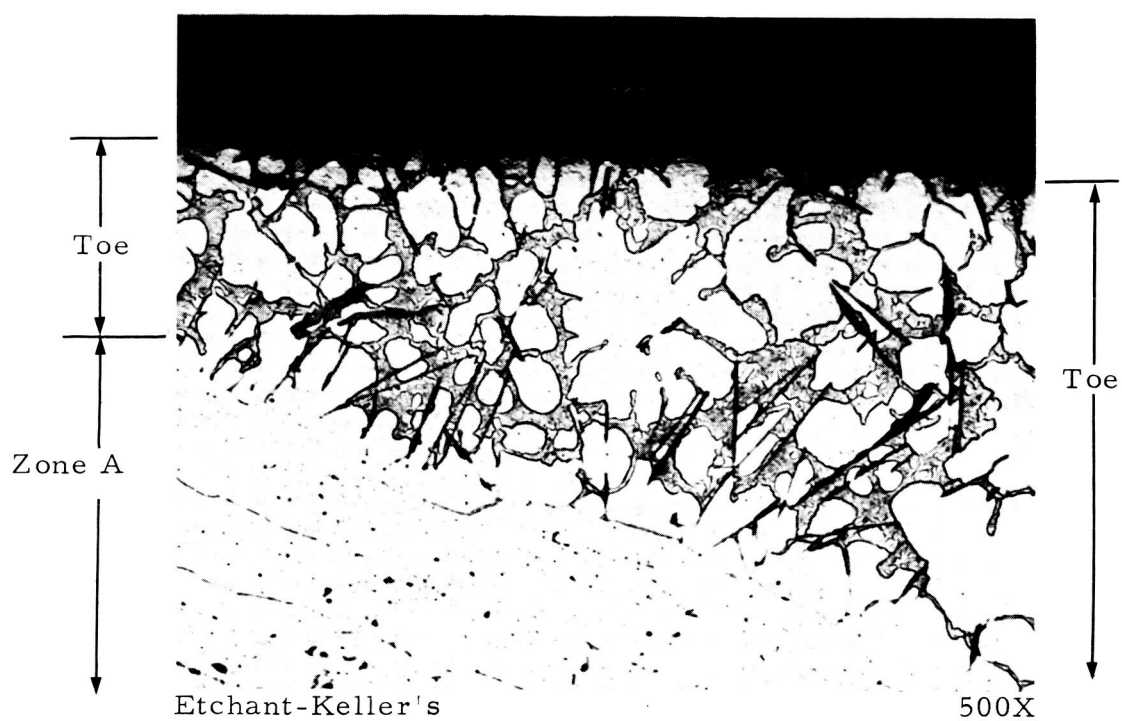


FIGURE 9. CONCENTRATION OF INTERMETALLIC CONSTITUENTS
IN THE BOTTOM TOE OF A WELD

at higher magnification. Two outstanding features may be observed in these photomicrographs. The CuAl_2 occurs as an intergranular Chinese script network. Also, there is a "needle" like phase. Both of these phases could form as a result of a unique combination of chemical composition, temperature, and cooling rate which is present at the bottom toe of the weld.

From the Al-Cu equilibrium diagram shown in Figure 2, it can be seen that upon cooling a molten alloy of less than 33 percent Cu, α solid solution is the first phase to form. At 1018°F , the eutectic of α and CuAl_2 precipitates in the grain boundaries. Under welding conditions the cooling rate is rapid and equilibrium is not established. In addition, all welding was performed in the horizontal position. Welding in this position is thought to be significant to the formation of the Chinese script and the "needle" phase. In the horizontal position, the liquid metal tends to sag at the bottom toes as shown in Figure 8. It is thought that the unique cooling rate experienced by the sagging toe of the weld may be responsible for the formation of CuAl_2 with a Chinese script appearance. Additional information concerning cooling rate as a factor in the formation of the CuAl_2 network is presented in Appendix I.

Closely allied with the Chinese script CuAl_2 is a dark "needle" like phase. Whenever this phase occurred in a weldment it was always closely associated with the CuAl_2 network. However, in some cases the massive CuAl_2 was observed without the "needle" constituent.

In an effort to identify this "needle" like phase a specimen was submitted to the Aluminum Company of America for electron microprobe analysis. This phase was tentatively identified as β (Al-Cu-Fe). It was stated by Alcoa that this phase is a common constituent in 2219 alloy weldments and forms primarily as a result of nonequilibrium conditions of welding. Another specimen containing needles was sent to Meta-Chem Laboratories, Inc., Houston, Texas. They reported a high concentration of copper, iron and manganese. Additional information on the formation of CuAl_2 and the "needle" phase is discussed in Appendix I. From the tests made it appears that the "needle" like phase is β (Al-Cu-Fe).

The toe of the weld plays an important role in the fracture mechanism and is discussed again under Section III, "Study of Failure Mechanism in Aluminum Alloy Weldments Under Uniaxial and Biaxial Loading".

III. STUDY OF FAILURE MECHANISM IN ALUMINUM ALLOY WELDMENTS UNDER UNIAXIAL AND BIAXIAL LOADING

A. Uniaxial Loading

The uniaxial tensile specimen design for determining mechanical properties of the 3/4 inch thick, 2219-T87 welded panel is shown in Figure 10. The rolling direction of the plates was perpendicular to the long axis of the weld. The welding procedures are discussed in Appendix II under "Standard Welding Procedure". Because the strength of the entire weldment was being evaluated, crowns were not normally ground flush with the base metal. The width of the specimen was 1/4-inch and a reduced section length of 4-1/2 inches was selected. Using this design a total of 32 specimens were tested. Ultimate strength, yield strength (0.2 percent offset) and percent elongation over a two-inch gauge length were determined. The results were analyzed statistically in accordance with procedures established by NASA.²² The values obtained are summarized as follows:

	<u>Yield Strength psi</u>	<u>Ultimate Strength psi</u>	<u>Percent Elongation (In 2 inches)</u>
Average	23,450	42,610	5.4
Standard Deviation	1,170	1,450	---
99 Percent Lower Tolerance with a 95 Percent Confidence Level	19,870	38,190	---

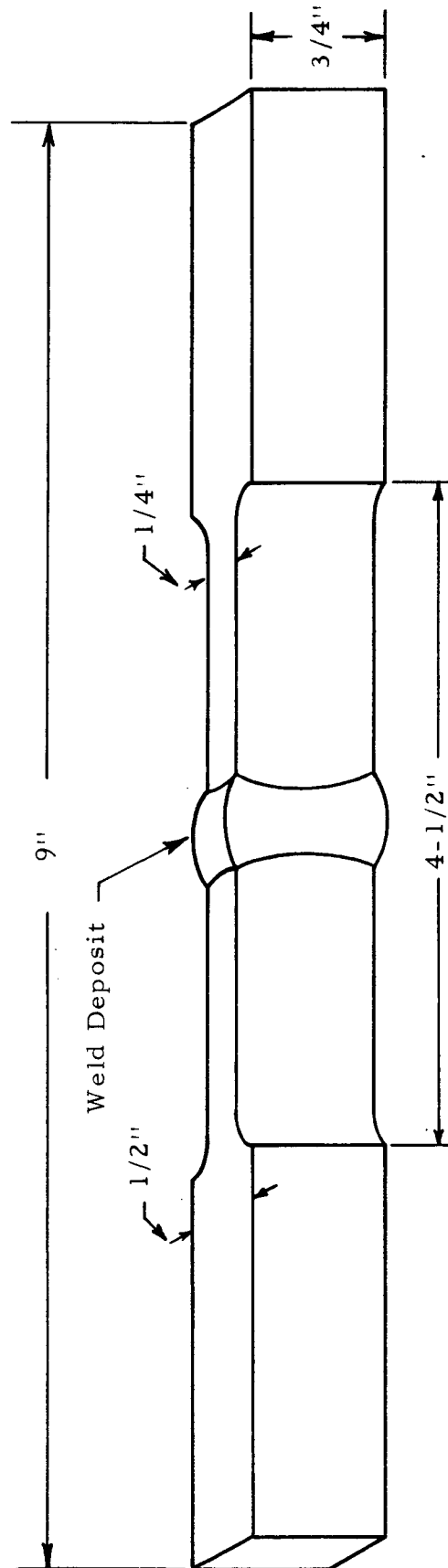


FIGURE 10. TENSILE SPECIMEN

The individual values for each test are listed in Table II. All specimens were free from porosity and other defects. This was established by X-ray examination prior to testing and visual examination of the fracture after testing. X-ray procedures are given in Appendix II, "Standard Welding Procedure."

The fracture paths in the uniaxial specimens were the same in all cases. Failure initiated in the bottom toe of the first weld pass in a region of intermetallic precipitates. These precipitates were discussed at length in Section II. After initiation in the bottom toe of the first weld pass the fracture propagated diagonally through the first pass and then into the second pass to the top toe. Figure 11 shows the fracture path of a typical specimen. That failure initiated first in the bottom toe and then progressed through the first weld pass was suggested by the appearance of the fracture path in this figure. The broken fracture faces could not be fitted together without the occurrence of a gap in the first weld pass. This gap was present in all specimens with the weld crown intact. The failure path through the toe was not unexpected as surface cracks were seen to develop in this region during tensile but prior to failure. The first cracks occurred in the stress range of 92-97 percent of the ultimate strength. This was determined by testing one specimen out of each of three welded panels. The mechanical properties had been established for the weldments prior to this test. Each specimen was loaded until yield strength (0.2 percent offset in two inches) was reached. The load was removed and the specimen

TABLE II
MECHANICAL PROPERTIES OF 3/4 INCH 2219-T87
ALUMINUM WELDMENTS¹

Specimen Number	Yield Strength (0.2 Percent Offset) psi	Ultimate Strength psi	Percent Elongation (In 2 Inches)
1	24,000	41,600	4.1
2	24,000	44,200	4.6
3	25,500	45,500	4.3
4	24,800	41,800	-
5	23,500	45,500	-
6	21,700	44,000	-
7	21,500	43,300	-
8	22,700	42,000	-
9	22,700	41,500	-
10	24,200	41,500	-
11	21,150	39,600	4.7
12	21,700	40,100	4.9
13	22,900	41,400	5.4
14	22,100	40,300	4.9
15	21,900	40,500	5.4
16	22,900	43,100	5.3
17	22,900	43,400	6.2
18	23,100	43,000	6.2
19	22,800	44,000	6.2
20	23,700	43,800	5.6
21	25,100	43,500	5.8
22	23,800	43,500	5.9
23	23,300	43,300	6.2
24	23,400	42,600	6.0
25	24,400	43,000	5.6
26	23,400	43,200	5.5
27	23,900	44,000	5.9
28	25,500	42,600	5.6
29	24,500	42,800	4.9
30	23,900	41,100	4.9
31	24,200	42,100	5.2
32	25,300	41,700	4.8
Average	23,450	42,610	5.4

¹ Horizontal welded panels, tig process square butt, one pass either side and 2319 filler

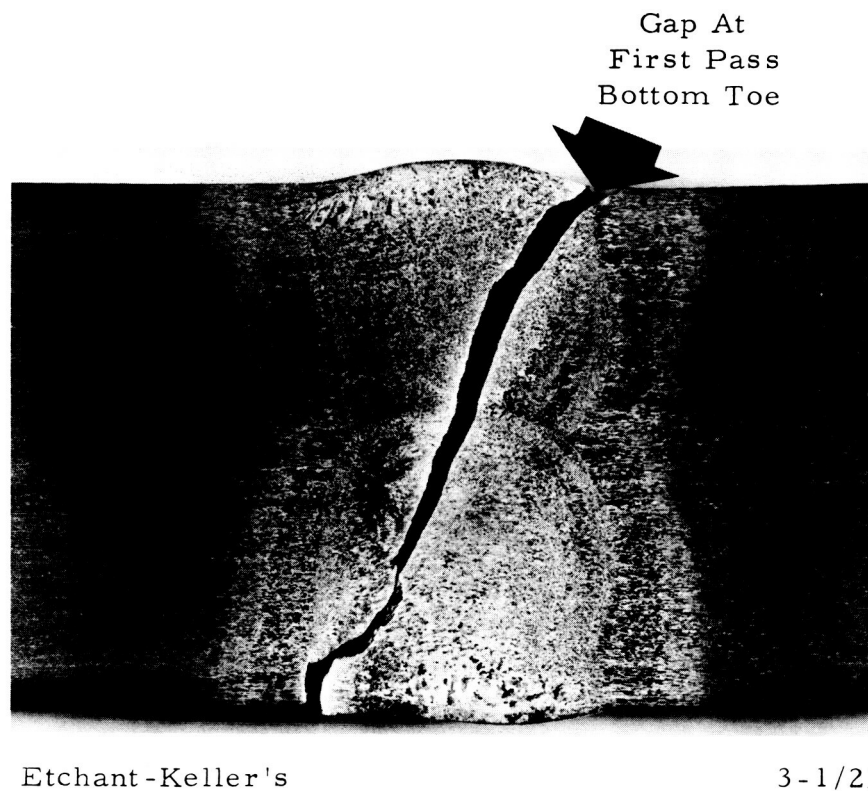
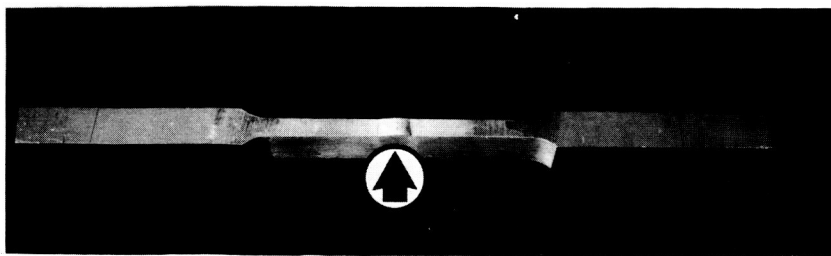


FIGURE 11. APPEARANCE OF A TYPICAL GAP IN THE FRACTURE
PATH OF A BROKEN TENSILE SPECIMEN AFTER
BUTTING THE FAILED PIECES TOGETHER

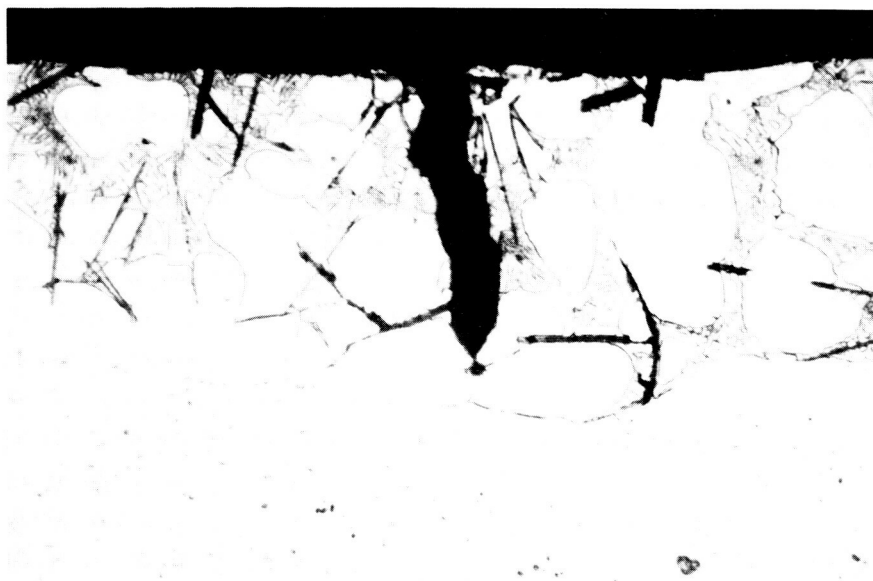
examined under a binocular microscope. In addition, a fluorescent surface penetrant was used for surface crack detection. No defects were observed at yield strength, thus the loading and examination was continued in 500-pound increments (equivalent to 2700 psi increments until failure resulted). The resulting mechanical properties of each of the three specimens treated in this manner were representative of the properties for the panels. Thus, this technique provided an indication of the stress at which fracture initiation occurred. A tensile specimen stressed until surface cracks were detected is shown in Figure 12. The top picture shows a stressed tensile specimen with the weld crown indicated by a circled arrow. The middle photograph is a macro of the top surface of the weld crown. Irregular surface cracks are visible in the bottom toe region indicated by the solid arrow. The microstructure of this area is shown in the same figure, bottom photograph. The surface crack that is evident was one of several that developed in the region of the toe. It is seen to extend through the dense CuAl_2 structure. The reason for the occurrence of this structure was explained in Section II. The depth of the crack and the depth of the intermetallic band are the same. This was observed in numerous instances. It is believed that the low fracture toughness of the intermetallic constituents in the toes of the weld accounted for this condition. Another cause for fracture initiating in the bottom toe was the geometrical stress concentration at the intersection of the weld crown and base metal.



1/4X
Stressed Tensile Specimen Showing Weld Crown



8X
Cracks In Bottom Toe Of The Weld Crown After Stressing



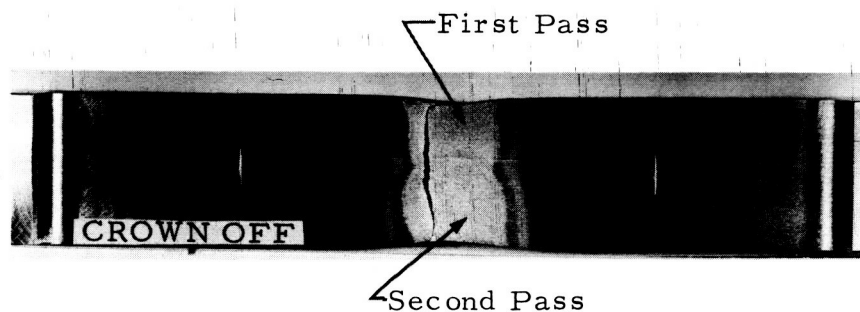
Etchant-Keller's
Microstructure Of One Of The Cracks
1000X

FIGURE 12. FRACTURE INITIATION IN BOTTOM TOE OF
HIGHLY STRESSED TENSILE SPECIMEN

Figure 13 shows the fracture path of a specimen with the weld crowns removed. The propagation was straight through the weld deposit. Observation of the fracture geometry indicated that the failure initiated in the center of the weld thickness. Tests conducted on individual tensile specimens machined out of the first weld pass and second weld pass also displayed a failure path through the weld metal. Figure 14 shows that the fracture occurred diagonally through the weld deposit in both specimens.

The influence of the geometrical stress concentration at the toe of the weld on the failure path was further evaluated by welding fusion passes in the weld toes. The welding procedure is discussed in Appendix II under "Fusion Passes". The conditions studied were: a) fusion passes in the top toes only, b) the bottom toes only, and c) in all four weld toes.

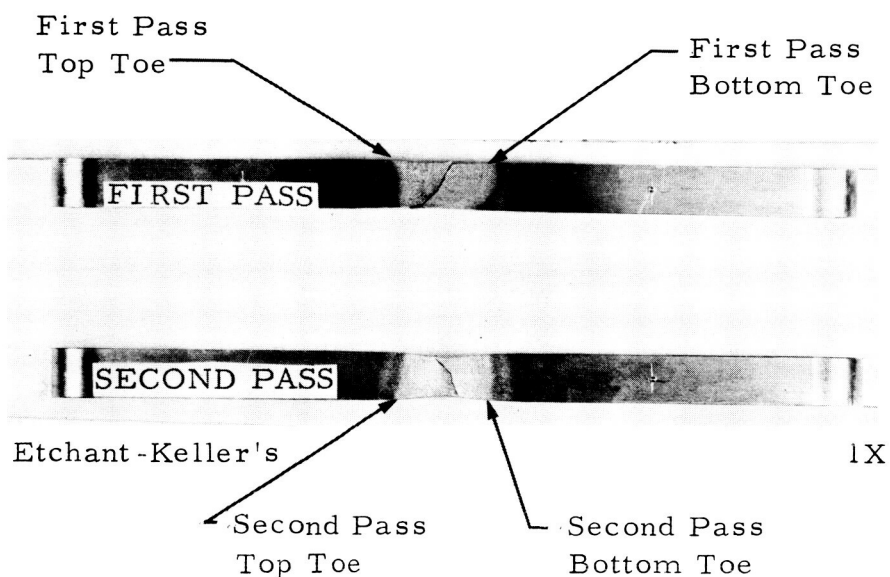
The mechanical properties of these specimens were averaged and are presented in bar-graph form in Figure 15. The average properties obtained for the specimen without fusion passes are also shown for comparative purposes. An increase in the ultimate strength and elongation was observed for the specimens with the fusion passes in the bottom toes and all four toes. The individual mechanical properties for these specimens are included in Table III. The fusion passes produced a change in the contour of the weld crown which reduced the notch effect. The concentration of intermetallic precipitates in the region of the toe was also reduced although the lower portion of the fusion pass itself represented a condition analogous to the bottom toe of the weld crown. Thus, a small amount of



Etchant-Keller's

1X

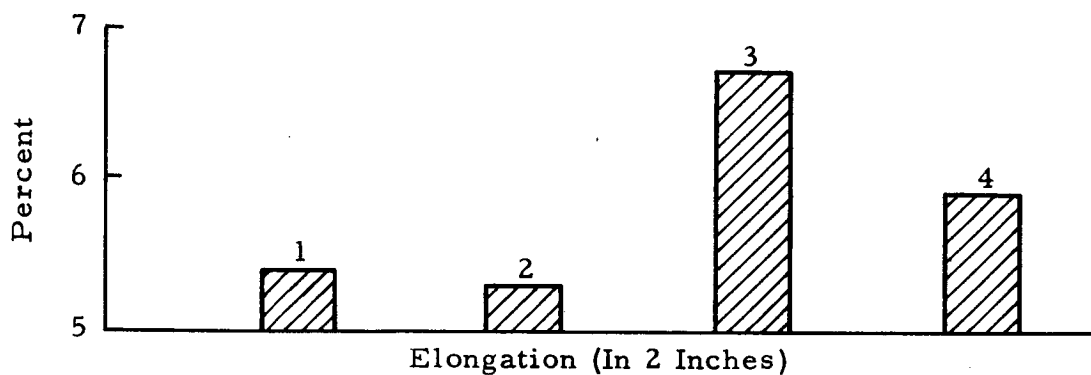
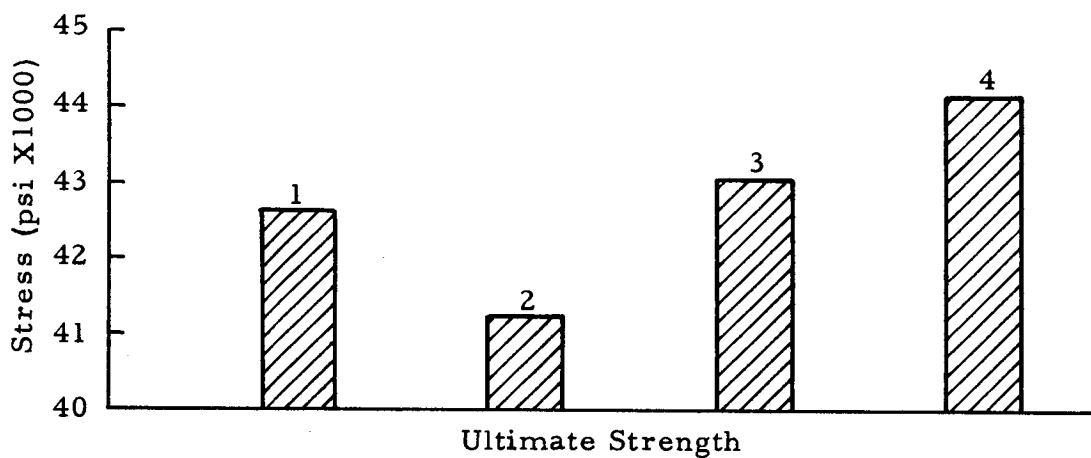
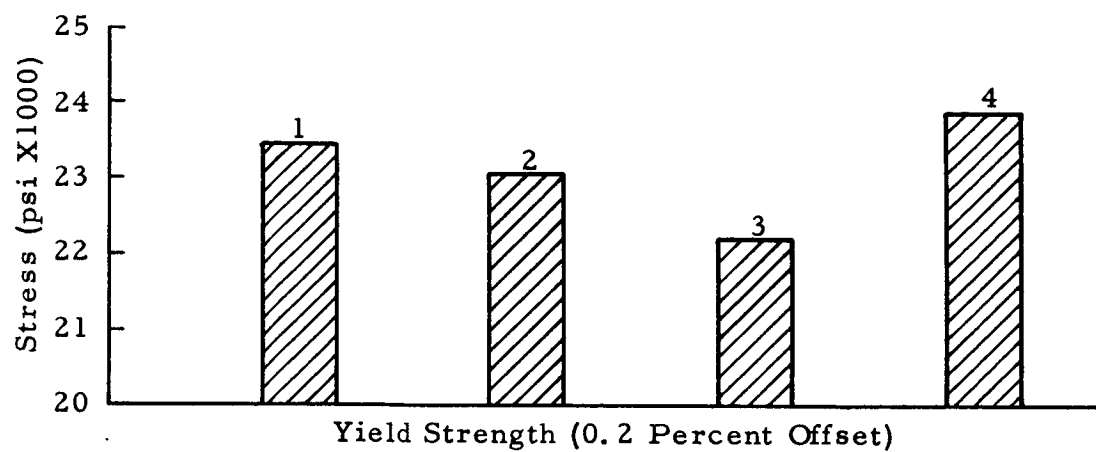
FIGURE 13. FRACTURE PATH IN A TENSILE SPECIMEN WITH WELD CROWNS MACHINED OFF



Etchant-Keller's

1X

FIGURE 14. THE FRACTURE PATH IN ADJOINING FIRST AND SECOND WELD PASSES WHEN TESTED AS SEPARATE TENSILE SPECIMENS



Legend

- | | |
|----------------------------|---------------------------------|
| 1. = No fusion passes | 3. = Bottom toe fusion passes |
| 2. = Top toe fusion passes | 4. = All four toe fusion passes |

FIGURE 15. BAR GRAPH COMPARING 3/4 INCH THICK 2219-T87 WELDMENTS WITH AND WITHOUT FUSION PASSES

TABLE III

MECHANICAL PROPERTIES OF SPECIMENS FROM 3/4 INCH
THICK 2219-T87 ALUMINUM WELDMENTS HAVING
FUSION PASSES IN THE TOP TOES ¹

<u>Location of Fusion Passes</u>	<u>Yield Strength (0.2 Percent Offset) psi</u>	<u>Ultimate Strength psi</u>	<u>Percent Elongation (in 2 Inches)</u>
Top Toe 1	22,500	41,500	5.0
Top Toe 2	22,900	41,000	4.8
Top Toe 3	23,200	41,200	5.1
Top Toe 4	22,900	40,800	5.5
Top Toe 5	23,200	40,800	5.2
Top Toe 6	23,800	42,200	6.2
Average	23,080	41,250	5.3
Bottom Toe 1	21,800	42,900	7.3
Bottom Toe 2	22,900	43,600	7.3
Bottom Toe 3	21,900	43,200	6.8
Bottom Toe 4	22,300	42,700	6.3
Bottom Toe 5	22,100	42,900	6.0
Bottom Toe 6	22,100	43,300	6.3
Average	22,180	43,100	6.7
All Toes 1	24,500	42,200	4.8
All Toes 2	24,100	44,300	6.2
All Toes 3	22,900	44,800	6.0
All Toes 4	23,600	44,700	6.2
All Toes 5	23,600	44,700	6.2
All Toes 6	24,500	44,300	6.2
Average	23,860	44,170	5.9

¹ Details of welding procedure are discussed in Appendix II.

concentrated intermetallic constituents were still present in the lower region of the fusion pass. However, where fusion passes were used in the bottom toes, fracture initiation no longer occurred in this region but rather in the weld deposit.

In some cases it is necessary to repair a vehicle because of weld defects such as porosity, cracks, lack of penetration, etc. The resulting welds generally contain a large amount of weld metal as compared to welds that have not been repaired. It was felt that this should be studied at least on a preliminary scale in this program, therefore, a panel was prepared to simulate a weld repair. The welding procedure is discussed under "Large Width-To-Depth Ratio" in Appendix II. A double "Vee" groove design was used with three beads deposited on each side of the joint. This joint design is shown in Figure 72. Tensile specimens were prepared from this panel and tested. Fracture initiated in the bottom toe of the fourth pass and propagated to the top toe of the sixth pass. This fracture was not unlike those observed in tensile specimens from panels prepared in accordance with the standard welding procedure. Probably the most interesting results from this panel were the mechanical properties. These properties were as follows:

Mechanical Properties of a Simulated Repair Weldment
in 3/4-Inch 2219-T87 Aluminum

<u>Specimen</u>	<u>Yield Strength (0.2% Offset) psi</u>	<u>Ultimate Strength psi</u>	<u>Percent Elongation (In 2 inches)</u>
38-1	22,800	44,400	6.6
38-2	21,900	43,800	6.6
38-3	22,200	44,100	7.4
38-4	21,700	43,800	7.1
Average	22,150	44,030	6.9

It is interesting to note the ultimate strength is 1,420 psi or 3.3 percent higher than the average for the weldments prepared from the standard welding procedure (Table II). The greatest difference was in elongation in which the simulated repair panel was 27.8 percent higher. This can probably be attributed to the greater volume of weld metal in the two inch gage length of the repair panel.

Elongation tests discussed in Section IV "Methods of Measuring Yield Strength and Ductility of Welds" indicate the weld metal itself to have about 20 percent elongation.

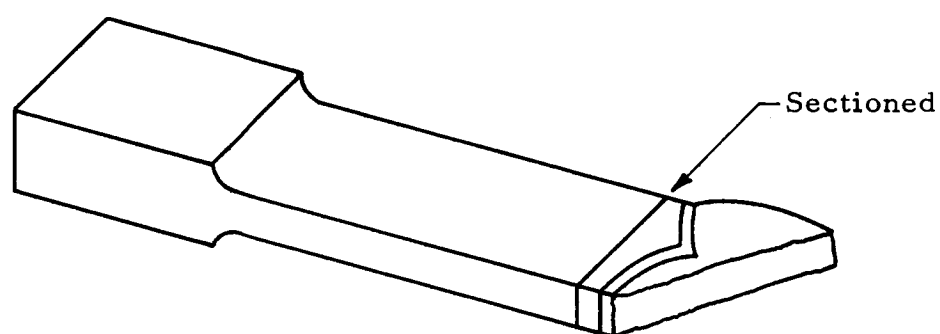
The fracture in the weld metal was studied by metallographic examination. This examination indicated that fracture was intergranular. In order to study the fracture path at high magnification it was necessary to examine secondary cracks or what might be termed branch cracks because of gross deformation associated with the fracture path. The branch cracks were small cracks which branched off from the fracture.

The procedure is illustrated schematically in Figure 16. The failed tensile specimen containing the branch cracks was sectioned and polished on planes parallel to the top surface.

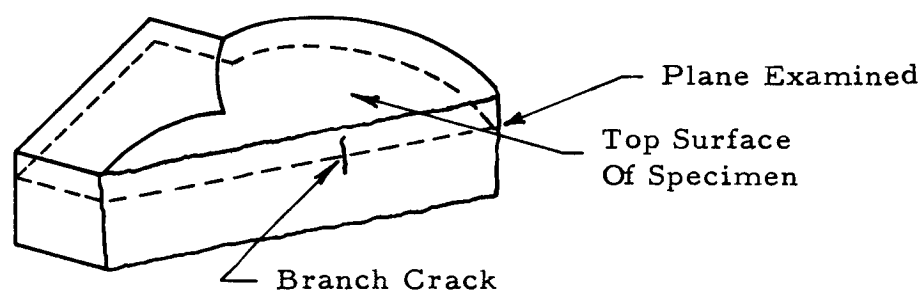
Two photomicrographs of such a crack are shown in Figure 17. These photomicrographs indicate the brittle nature of the intermetallic constituents at the grain boundaries. The fine cracks were observed in some cases to fracture the intermetallic compounds in the path of the crack. This examination also confirms that the failure in the weld deposit occurs in an intergranular manner. For further confirmation of the nature of the fracture an electron fractographic study was made.

This study of the topography of the fracture surfaces of selected test specimens was carried out to augment the microstructural studies related to fracture initiation and propagation. The particular objective of this study was that of establishing the micromechanical aspects of fracture in 2219-T87 aluminum weldments and, where possible, relate these features to the particular variables associated with such fractures.

The technique of electron fractography employs the electron microscope in the examination of replicas of fracture surfaces. The large depth of field and high resolution of this instrument provides for a definition of detail not possible with optical microscopy. In typical fractographic studies the topographical features of a given fracture are examined and evaluated at magnifications in the range of 2000 to 15,000X.

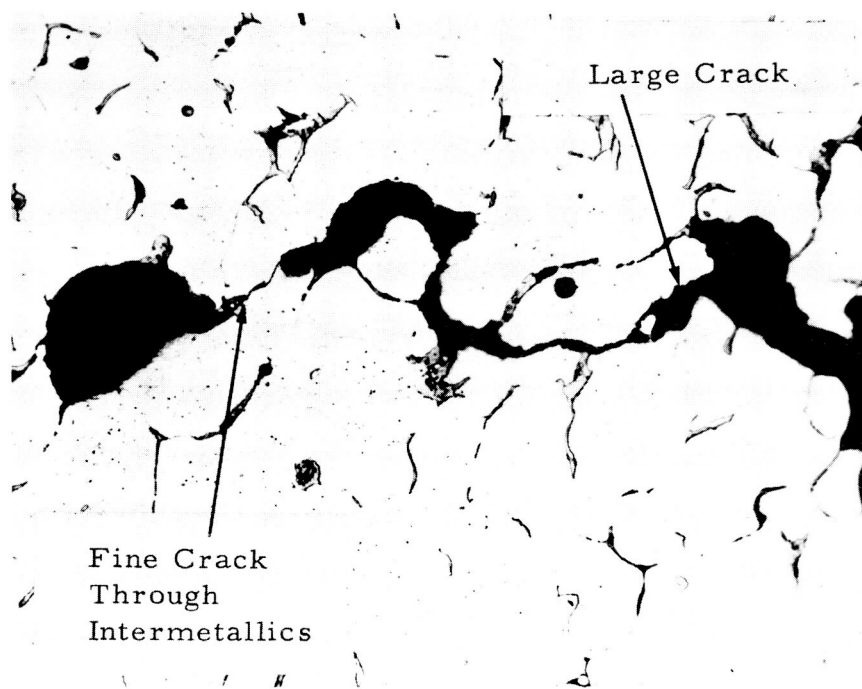
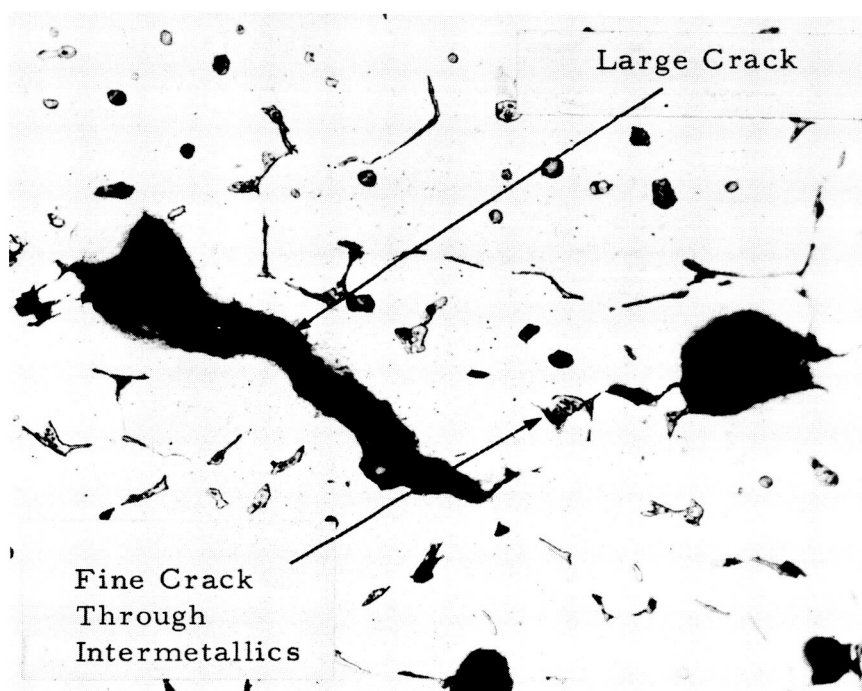


Half Of Tensile Specimen After Testing



Section Of Failure Examined

FIGURE 16. SCHEMATIC OF SECTION OF SPECIMEN USED TO STUDY FRACTURE PATH IN 2219-T87 WELDMENTS



Etchant-Keller's

1000X

FIGURE 17. CRACKS IN WELD DEPOSIT OF UNIAXIAL TENSILE SPECIMEN AFTER FAILURE. Note that the cracks follow the path of intermetallic constituents.

Recent investigations have established specific topographical characteristics associated with the various classes of fracture. Of particular interest to this program are those characteristics related to the basic mechanism of plastic fracture.

The most common type of plastic fracture occurring in constructional alloys is that of the growth and coalescence of voids in a region of plastic deformation. In such cases, voids are nucleated at preferred sites within the material, grow under the influence of triaxial stress and coalesce by localized internal necking. The coalescence of a large number of voids creates a fracture surface through the center of a sheet of voids leaving numerous concave depressions in the fracture surface. These depressions, commonly referred to as dimples, are readily observable in fractographs and are characteristic of fracture by this mechanism. These voids or dimples exhibit a characteristic shape related to the mode of fracture and have been classified as follows:

- 1) Normal Mode: Nucleation and growth under normal stresses resulting in an equiaxed simple structure.
- 2) Shear Mode: Fracture under the influence of a shear component of stress produces elongated, open dimples pointing in the direction of relative shear on each fracture surface.
- 3) Tearing Mode: Fracture under the influence of nonuniform stress results in a fracture surface exhibiting elongated open dimples pointing in a direction opposite to the macroscopic direction of crack propagation.

The nucleation sites for voids have been observed to be frequently associated with second-phase particles or inclusions within the material. The correlation of the size, distribution and properties of such particles with surface topography, however, has not yet been well established.

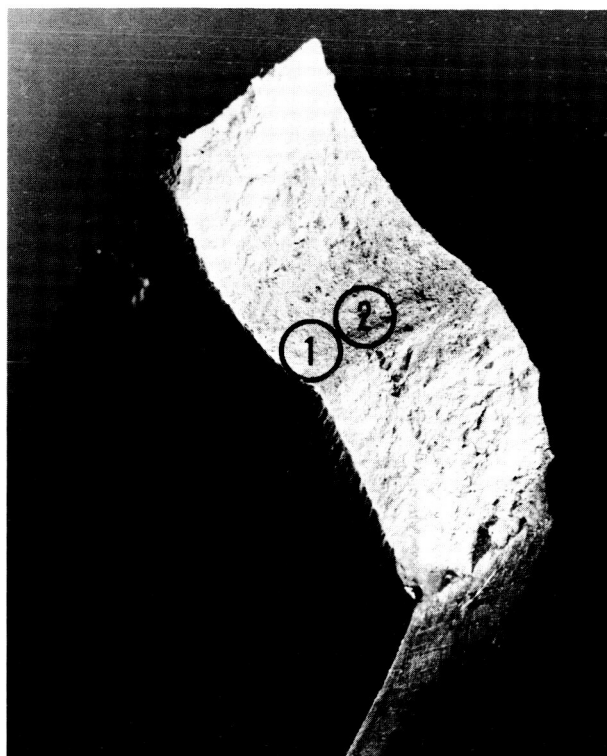
The recently published works of Beachem and Pelloux^{23, 24, 25} give a comprehensive treatment of the fractography of plastic fracture as well as that of other fracture mechanisms such as cleavage and fatigue. These references present examples of such fractographs as well as discussion of the mechanisms of basic fracture and a description of the details of the technique of electron fractography.

The principal portion of the fractographic study was carried out on four specimens representative of those tested in the program. The three uniaxial specimens examined are listed below and the fracture surfaces of the two welded joint specimens are shown in Figures 18 and 19.

1. Base metal tensile specimen. The fracture surface of this specimen was oriented essentially 45° to the wide face and 90° to the narrow face. The fracture exhibited the typical fibrous or cup zone at the center of the specimen and shear lips at the edges.

2. Weld joint tensile specimen tested with weld crowns removed. The fracture surface was oriented essentially 45° to the wide face of the specimen and 90° to the narrow face, Figure 18.

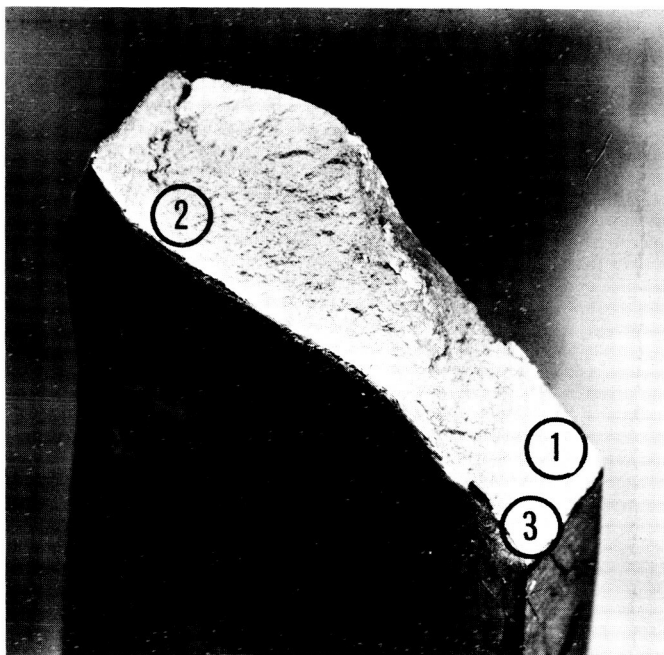
3. Welded joint tensile specimen tested with weld crown intact. Fracture surface extended diagonally across the weld between the toes of the weld, Figure 19.



4X

FIGURE 18. FRACTURE SURFACE OF 2219-T87 WELDED JOINT TENSILE SPECIMEN TESTED WITH WELD CROWNS MACHINED OFF

Numbered circles indicate location of fractographs shown in Figures 23 and 24.



4X

FIGURE 19. FRACTURE SURFACE OF 2219-T87 WELDED JOINT TENSILE SPECIMEN TESTED WITH WELD CROWNS INTACT

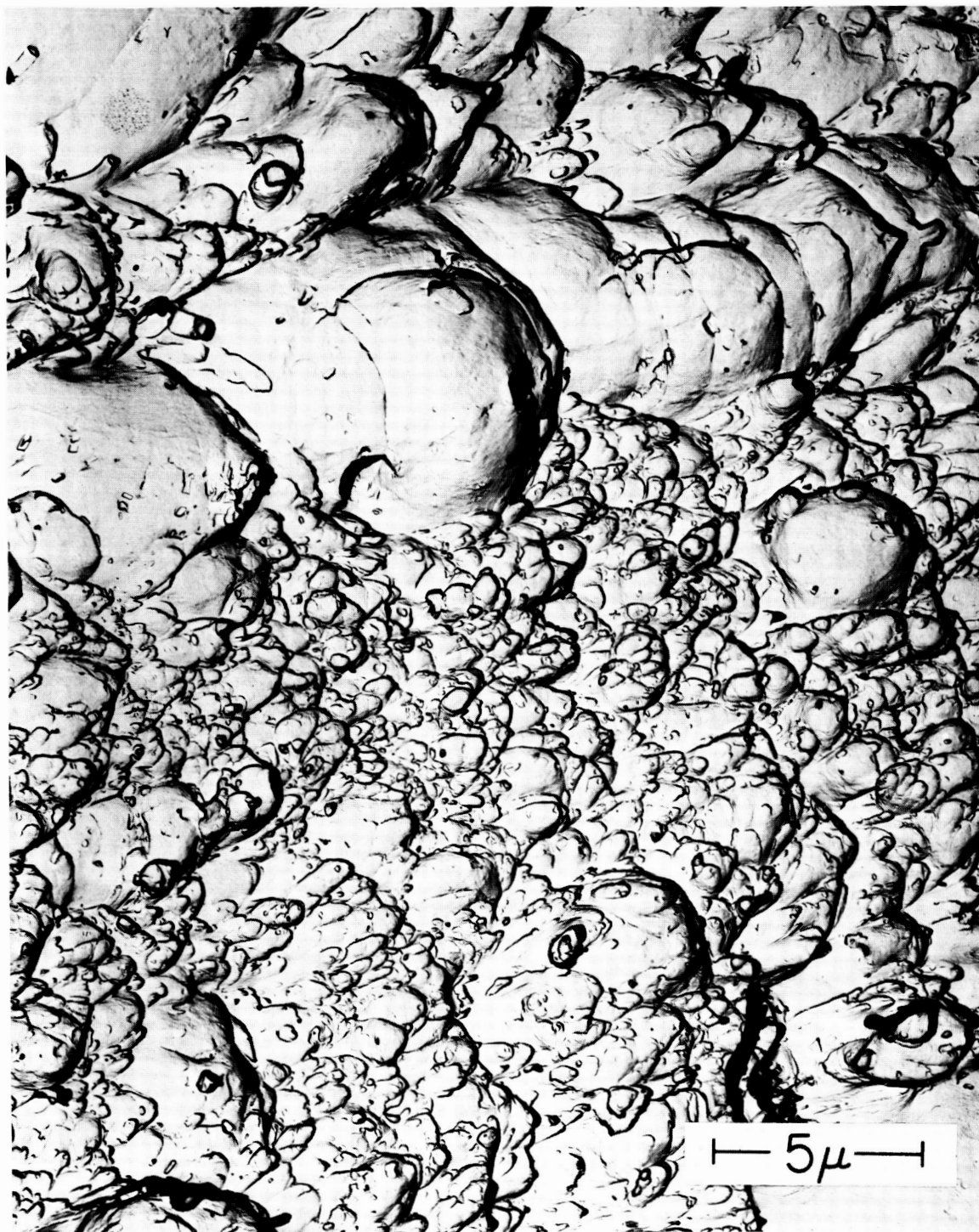
Numbered circles indicate location of fractographs shown in Figures 25, 26, 27 and 28

In general, the topographical features characteristic of various modes of plastic fracture by growth and coalescence of voids were observed in all cases investigated in this study. However, distinct differences in the size and shape of dimples were noted between specimens and between various locations on the same specimens.

Fractographs illustrating the typical surface topography observed in the base metal specimen are shown in Figures 20, 21, and 22. Regions of both transgranular and intergranular fracture were observed. All areas of this fracture which were examined exhibited a mixture of large and small dimples.

Figure 20 illustrates the range of dimple sizes noted in regions of transgranular fracture. In almost all instances, indications of the origin of the dimples at dispersed second phase particles were noted. In general, the larger dimples showed evidence of originating at larger second-phase platelets, Figure 21. This observation indicates that the mixture of dimple sizes noted can be attributed to the initiation of cracks at the interfaces of the second-phase platelets early in the deformation process, giving rise to more extensive growth of voids at such sites. The size of the platelets observed compared very closely to the size of many second-phase precipitates observed by metallographic techniques.

Figure 22 illustrates the typical structure observed in regions of intergranular fracture. In such regions facets of individual grains are



Two-Stage Plastic Carbon Replica

7000X

FIGURE 20. FRACTURE SURFACE OF 2219-T87 BASE METAL TENSILE SPECIMEN. Fractograph taken in shear lip region. Note the range of size of dimples.



Two-Stage Plastic Carbon Replica

5000X

FIGURE 21. FRACTURE SURFACE OF 2219-T87 BASE METAL TENSILE SPECIMEN. Fractograph taken in central "fibrous" region. Note the range of size of dimples. Arrows indicate origin of larger dimples at second-phase platelets.



Two-Stage Plastic Carbon Replica

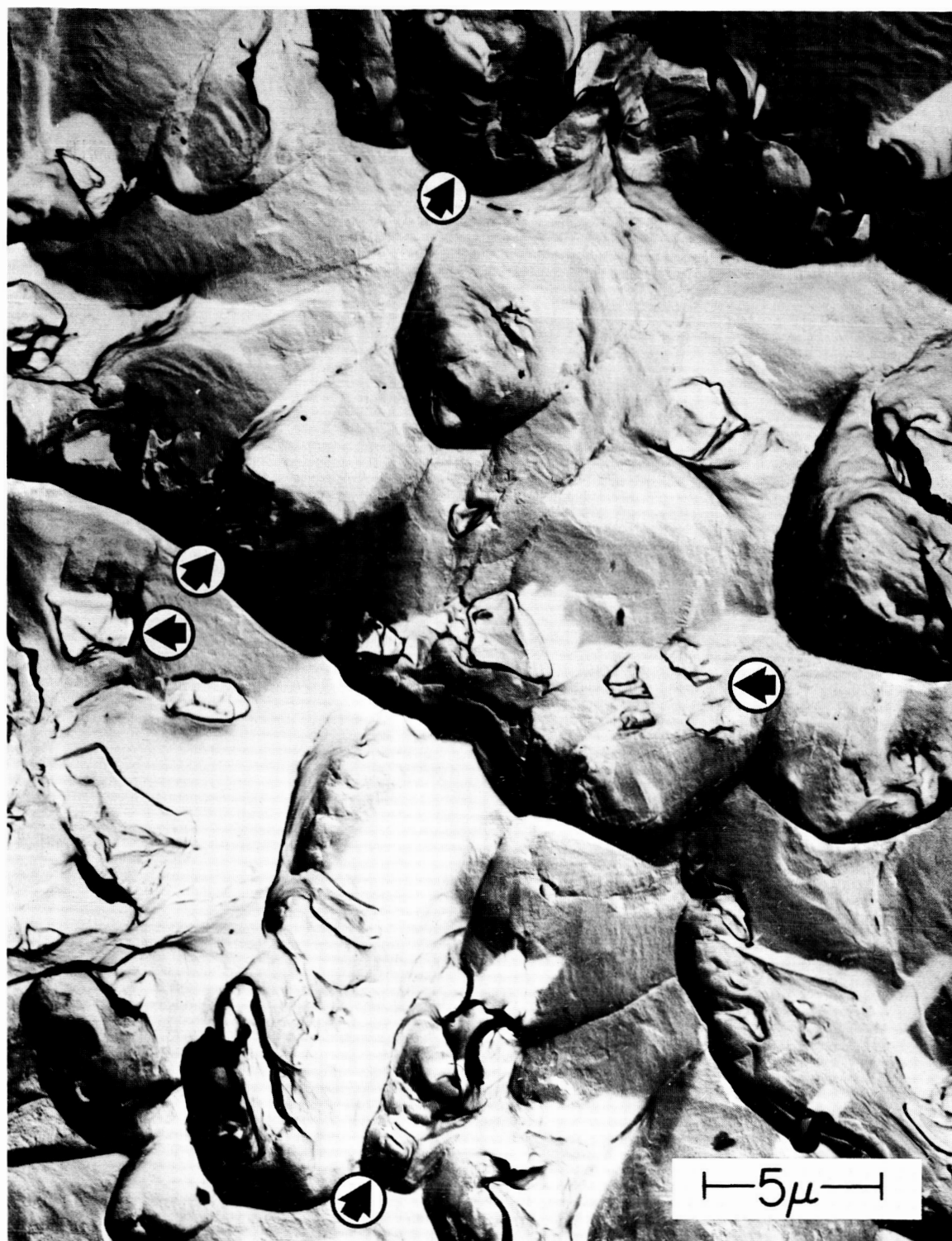
2500X

FIGURE 22. FRACTURE SURFACE OF 2219-T87 BASE METAL TENSILE SPECIMEN. Fractograph taken from central "fibrous" region. Upper portion of figure shows transgranular plastic fracture and lower portion exhibits intergranular plastic fracture. Arrows indicate two intergranular facets.

defined by areas of small flat dimples resulting from void growth within a limited volume of material containing the grain boundary.

Fractographs typical of those made of the fractures in the two welded joint tensile specimens are shown in Figures 23 through 26. In both welded joint specimens, the dimples observed were larger and more uniform in size than those observed in the base metal. In addition the dimples exhibited a noticeably irregular periphery. This feature is particularly evident in Figures 23 and 25. In addition, the presence of irregular shaped second-phase particles in the fracture surface was noted frequently in both welded joint tensile specimens, Figure 23. One region of very large and extremely uniform dimples was noted in the central portion of the welded joint specimen tested with the crowns machined off, Figure 24. In this case, as in the base metal specimen, clear indications of the initiation of the dimples at second-phase platelets were noted.

The irregularity in dimple shapes and the presence of precipitate particles in the fracture surface of the welded joint indicate a strong influence of the distribution and size of precipitates on the fracture characteristics of the weld deposits. Apparently these particles in the weld deposits not only serve as sites for the initiation of voids but also influence the direction and degree of growth of the voids. The overall large average dimple size in the welded specimens, as compared to that of the base metal specimen, indicates that a larger number of voids may be initiated early in the process of deformation in the case of the weld metal. The early



Two-Stage Plastic Carbon Replica

6000X

FIGURE 23. FRACTURE SURFACE OF 2219-T87 WELDED JOINT TENSILE SPECIMEN. Specimen tested with weld crowns machined off. Fractograph taken from location near root of weld passes (Area 1, Figure 18). Note irregular shape of shear dimples (oblique arrows) and dispersed second-phase particles in fracture surface (horizontal arrows).



Two-Stage Plastic Carbon Replica

6000X

FIGURE 24. FRACTURE SURFACE OF 2219-T87 WELDED JOINT TENSILE SPECIMEN. Specimen tested with weld crowns machined off. Fractograph taken from location near root of weld passes (Area 2, Figure 18). Note the large, uniform, equiaxed dimples. Arrows indicate origin of dimples at second-phase platelets.



Two-Stage Plastic Carbon Replica

6000X

FIGURE 25. FRACTURE SURFACE OF 2219-T87 WELDED JOINT TENSILE SPECIMEN. Specimen tested with weld crowns intact. Fractograph taken from location within second weld pass (Area 1, Figure 19). Note irregular shape of shear dimples.



Two-Stage Plastic Carbon Replica

6000X

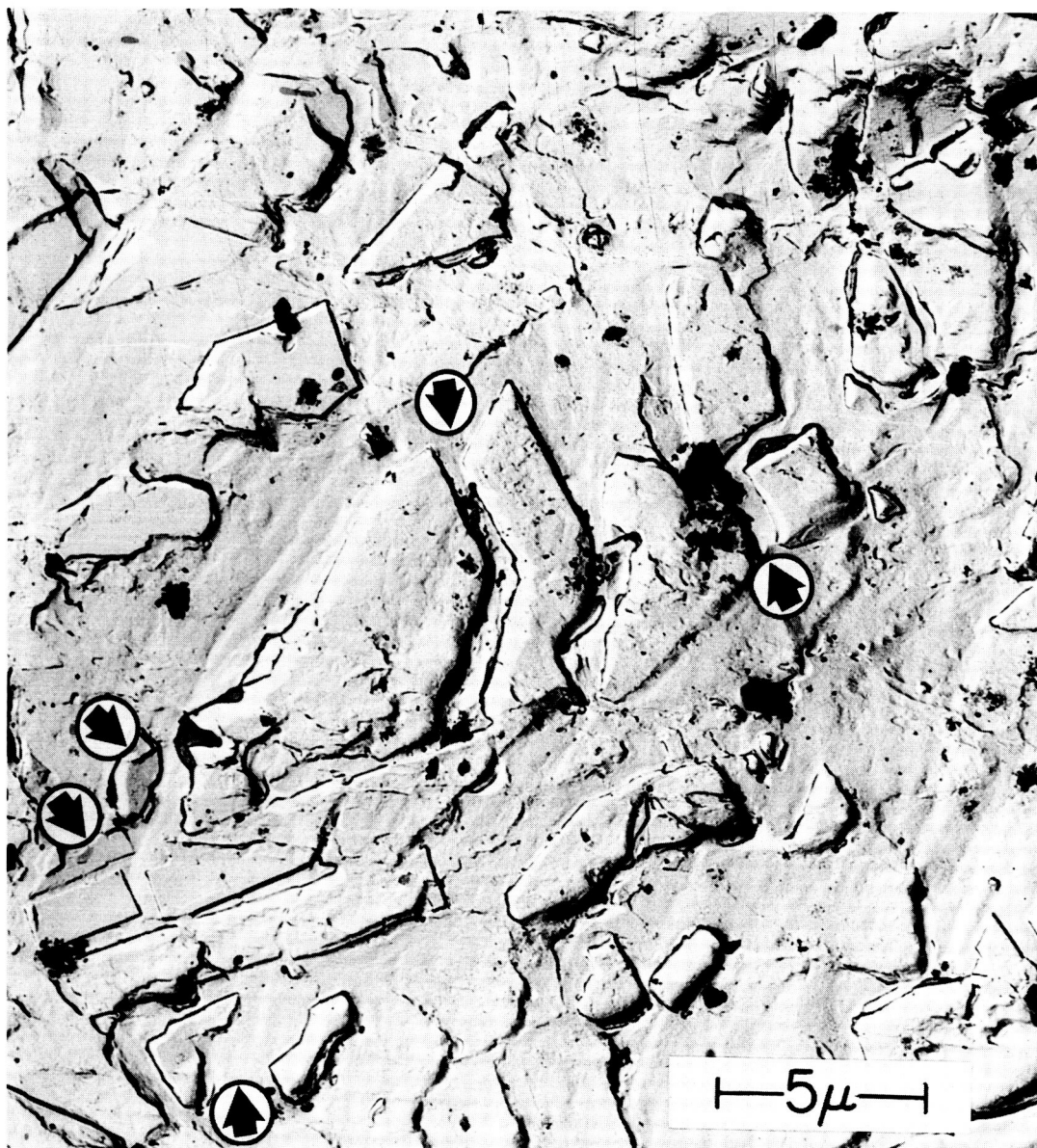
FIGURE 26. FRACTURE SURFACE OF 2219-T87 WELDED JOINT TENSILE SPECIMEN. Specimen tested with weld crowns intact. Fractograph taken from location within first weld pass (Area 2, Figure 19). Note the extent of elongation of the shear dimples.

initiation of voids could be responsible for lower ultimate strength of the weld metal observed in the mechanical tests conducted in this program.

Figures 27 and 28 show regions near the toe of the weld in the specimen tested with weld crowns intact. Those regions were notably flat and exhibited remnants of fractured second-phase platelets over relatively extensive areas. Such features can be attributed to the separation of the matrix and precipitate at the interface followed by plastic deformation of the matrix. Such regions were noted only near the toes of the weld. This observation is consistent with the indications of fracture initiation in the toes of the weld noted in the metallographic studies.

The following conclusions may be drawn from the fractographic study:

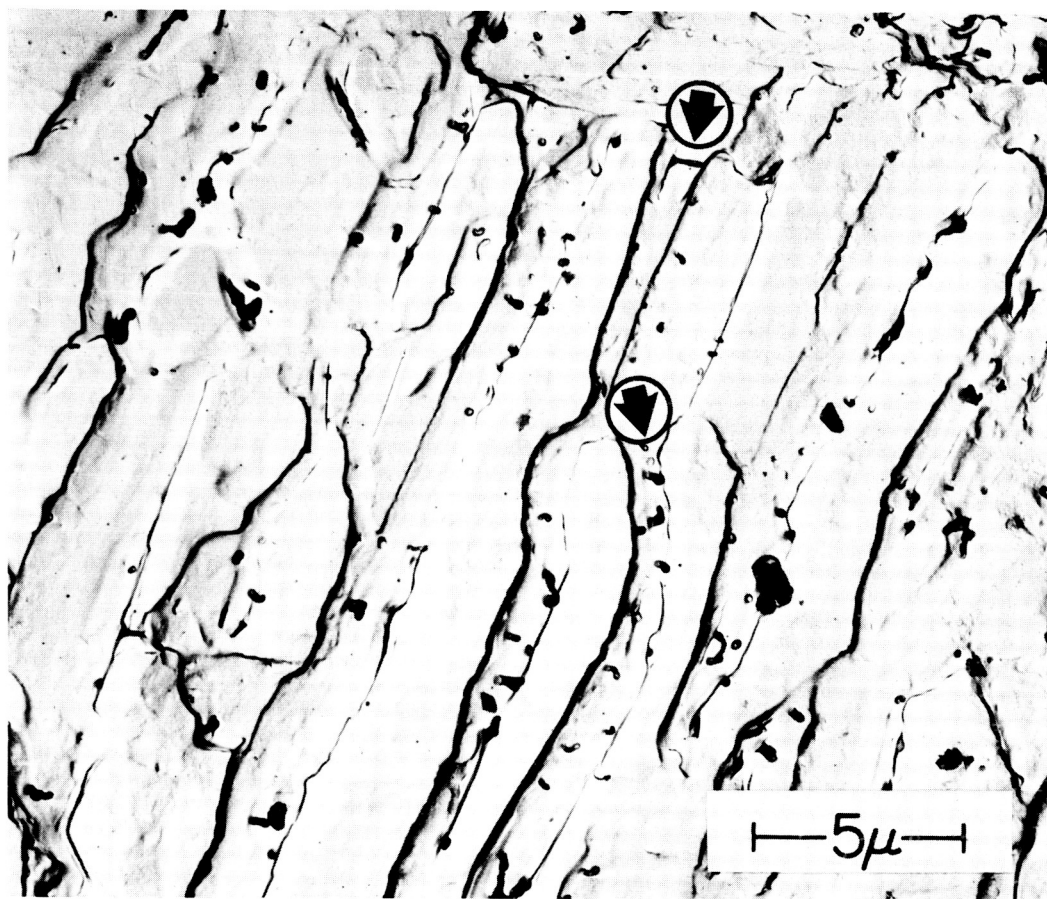
1. Tensile fracture of 2219-T87 base metal and weldments occurs generally by the nucleation and growth of voids during plastic deformation.
2. The size, shape and distribution of second-phase particles exerts a marked influence on the initiation and growth of voids. The larger precipitate platelets give rise to early nucleation and extensive growth of individual voids.
3. The surface topography of fractures in weld deposits exhibited distinctly different void shape and distribution than that of fractures in the base metal. The microstructure of the weld deposits is such as to



Two-Stage Plastic Carbon Replica

6000X

FIGURE 27. FRACTURE SURFACE OF 2219-T87 WELDED JOINT TENSILE SPECIMEN. Specimen tested with weld crowns intact. Fractograph taken from location near toe of second weld pass (Area 3, Figure 19). The region shows remnants of fractured second-phase platelet over extended area. Arrows indicate mating pieces of platelet.



Two-Stage Plastic Carbon Replica

6000X

FIGURE 28. FRACTURE SURFACE OF 2219-T87 WELDED JOINT TENSILE SPECIMEN. Specimen tested with weld crowns intact. Fractograph taken from location near toe of second weld pass (Area 3, Figure 19). The region shows remnants of fractured second-phase platelet over extended area. Arrows indicate mating pieces of platelet.

favor early nucleation of voids and the precipitates exert an influence on the direction and extent of void growth as well as serve on nucleation sites.

4. This examination indicated that massive second-phase particles at the toe of welds played a significant role in the initiation of the uniaxial tensile failures.

B. Biaxial Testing of 3/4 Inch 2219-T87 Weldments

Prior to selecting a method of subjecting the weldments to biaxial loading, a literature survey was conducted. Biaxial testing techniques that could be applied to the 3/4 inch thick weldment were considered. Four testing techniques appeared to be applicable. They were assessed on the basis of specimen preparation, necessary testing equipment and the value of results. These tests were:

1. Biaxial tensile tests of cruciform specimens.
2. Hydrostatic tests of welded tubular specimens.
3. Hydrostatic tests of welded miniature pressure vessels.
4. Hydraulic bulge tests of plate weldments.

Biaxial tests of cruciform specimens offer maximum stress ratio flexibility. A biaxial stress ratio of 1:1 is possible as well as 2:1 or other stress ratios depending only on the dimensions of the specimen and the method of loading. The limiting factor is specimen size. With equipment presently available only very small specimens can be treated. Sections in the order of 0.010" thick are the maximum. Since this limitation would

not permit the type of test contemplated, this method was not considered further in connection with this program.

Tests of welded tubular sections appear to be impractical both from a mechanical and a cost standpoint. Difficulties would be encountered in fabricating 3/4" thick 2219-T87 aluminum alloy into cylinders of reasonable diameter without structural changes which would seriously affect the test results. The same problem would be encountered were the tests made on model pressure vessels. The cost of pressure vessel testing on this particular program would be prohibitive.

The hydraulic bulge test offers advantages over all other techniques investigated. With a circular die a biaxial stress ratio of approximately 1:1 is developed. Other ratios are obtainable with the use of elliptical dies. Tests could be made on 3/4 inch thick 2219-T87 aluminum alloy plates as received from the supplier. Since no cold working would be required there would be no change in properties or in structure. Weldments of this material can be handled with equal ease.

Hydraulic bulge tests have been used successfully by various investigators to assess the performance of high strength steel and aluminum weldments in relatively thin material. This testing technique has also been used to study the effect of welding procedure variations on the performance of welds.

The test is carried out by clamping the test panel over a circular female die and applying a fluid pressure to the opposite side. As the

pressure increases, the panel bulges into the circular opening. The variables which are measured during the test are the pressure, bulge height and strain. Strain data may be obtained either by measuring the elongation of grids scribed or photoetched on the panel surface or by the use of resistance type strain gages.

When the relationship between test panel thickness and die diameter permit the formation of a sector of a true sphere during the test, the stress pressure relationship may be expressed as:

$$\sigma = \frac{P \times R}{2t} \quad (\text{equation 1})$$

where: σ = Stress in psi
P = Pressure in psi
R = Radius of bulge in inches
t = Panel thickness in inches

Previous investigations⁵ have shown that true spherical bulging exceeding 1-1/2 inch high could be developed in 0.125 inch thick high strength aluminum alloy panels through the use of a die with an 8-inch diameter circular opening. Smaller die openings were found in this particular case to increase the bending stresses around the clamped edges. The result is a greater deviation from the true spherical shape and from conformity with a mathematical relationship. Panel thickness is also a factor to be considered. When the panel thickness is increased there is an increase in the deviation from the mathematical formula. As a consequence, it was found that while the 8-inch die was adequate to determine biaxial

strength of 0.125 inch thick high strength aluminum alloy, it was inadequate when a thickness of 0.75-inch was involved. For this investigation, this fact was of secondary consideration. With a nominal size die made with a generous relief radius on the inner periphery, it is possible to thoroughly explore welded panels of 0.75-inch thick 2219-T87 aluminum alloy. While it is not possible to determine the absolute strength of various areas in the specimen, it is possible to readily and accurately detect the weaker areas of a welded panel and while the absolute tensile strength is not determined, a relative figure of equal value in the present investigation may be developed.

1. Design and Fabrication of Hydraulic Bulge Test Fixture

The hydraulic test fixture which was designed to test 3/4-inch thick aluminum weldments is shown in cross-section in Figure 29. The fixture consists of a top and bottom die which are clamped together with twenty, 3/4-inch diameter high strength steel bolts. Hydraulic pressure is introduced between the test panel and the bottom die forcing the test panel to bulge upward into the circular opening of the top die.

Figure 30 shows the bottom die of the fixture. This die was fabricated from 2-inch thick SA-212 Grade B carbon-silicon steel plate.

An "O" ring seal was provided to prevent leakage of the hydraulic fluid from the die-test panel interface. The groove detail for the "O" ring is also shown in Figure 30. A fitting at the center of the die is used to introduce the hydraulic fluid.

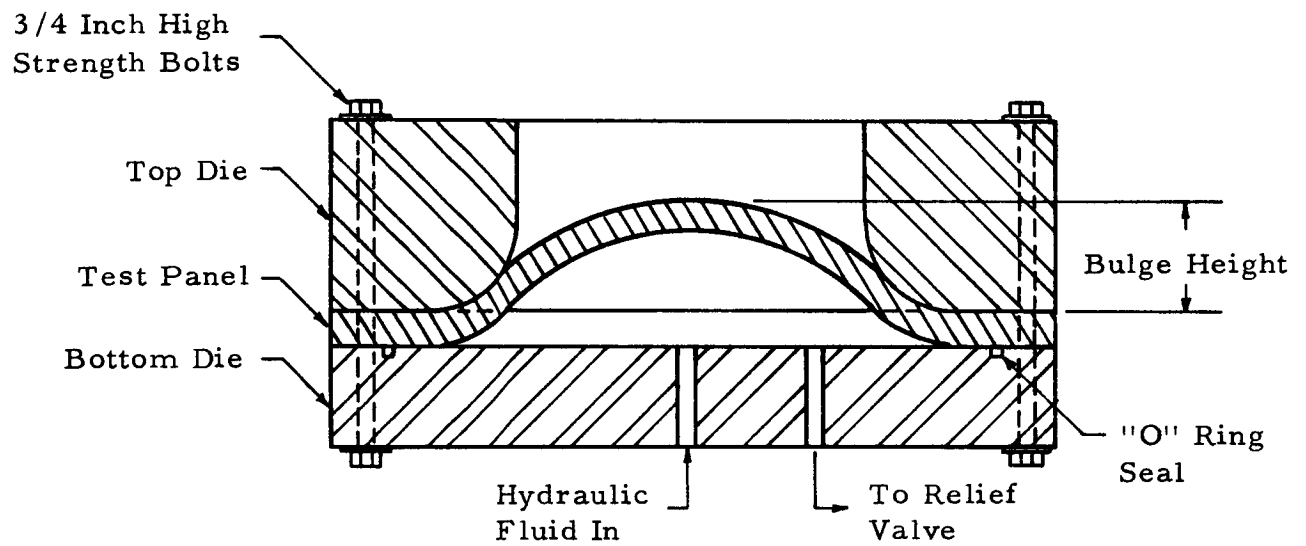


FIGURE 29. CROSS SECTION OF THE HYDRAULIC BULGE TEST FIXTURE

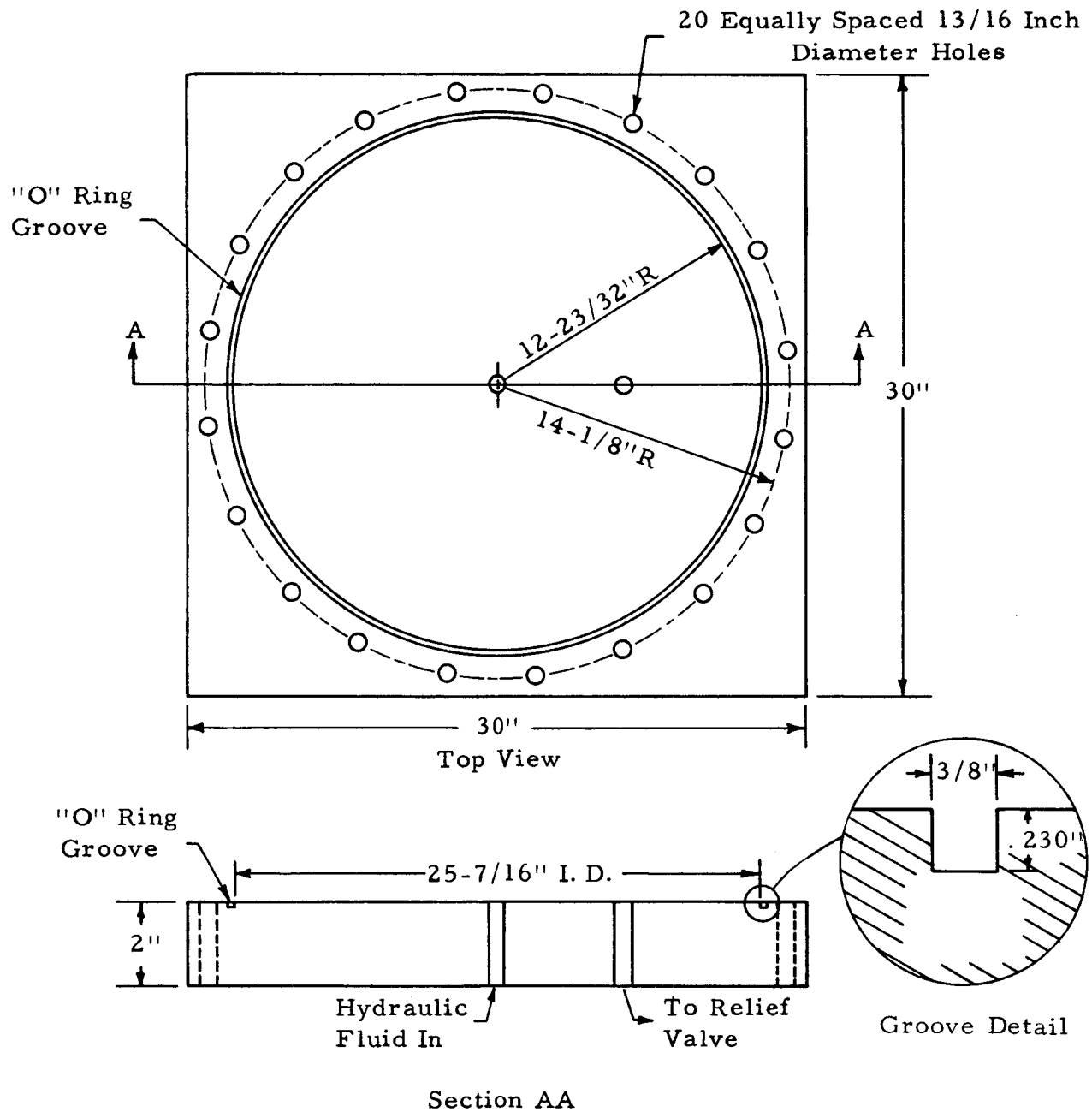


FIGURE 30. BOTTOM DIE OF HYDRAULIC BULGE FIXTURE

The top die of the fixture is shown in Figure 31. The material is AISI 4340 steel. The circular opening diameter is 18 inches at the top surface and increases to 24 inches at the bottom surface of the die. The 3-inch relief radius at the bottom surface of this die was used to minimize the bending stresses encountered in the bulging operation.

a. Initial Tests

Tests of the hydraulic bulge fixture were conducted using a 1/8-inch thick 32 x 32 inch 2014-T6 panel (not welded). This operation provided proof of the integrity of the "O" ring seal and the hydraulic system. Bulging became noticeable shortly after pressurization was started. An increase of pressure from 600 to 650 psi did not increase the height of the bulge, thus, pressurization was discontinued. Slippage of the test panel in the hold-down area was responsible for incomplete bulging. Measurements of the bulged panel after removal from the test fixture indicated that the radius (r) of the bulge was 11.5 inches and the bulge height (h) was 2.5 inches.

The radius of curvature (R) was determined to be 28 inches using the following relationship:

$$R = \frac{r^2 + h^2}{2h} \quad (\text{equation 2})$$

$$R = \frac{(11.5)^2 + (2.5)^2}{2(2.5)}$$

$$R = 27.8 \text{ inches}$$

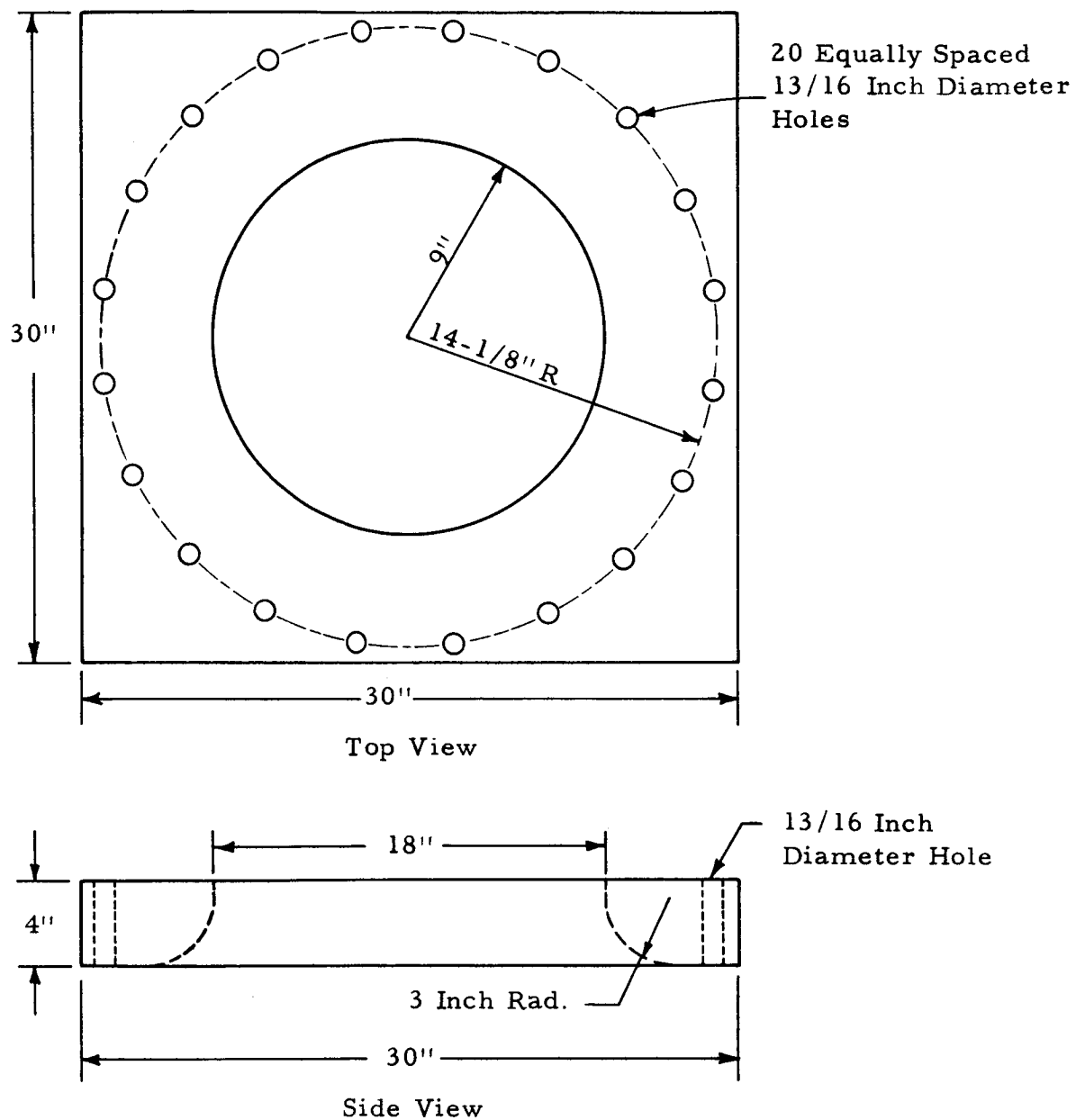


FIGURE 31. TOP DIE OF HYDRAULIC BULGE FIXTURE

Since the contour of the bulged area was spherical, the biaxial membrane stresses (1:1 tensile-tensile) were calculated using equation 1.

$$\sigma = \frac{F \times R}{2t} \quad (\text{equation 1})$$

$$\sigma = \frac{600 (27.8)}{2(.125)}$$

$$\sigma = 66,700 \text{ psi}$$

To test the "O" ring seal and the hydraulic system at higher pressures, a 1/4-inch thick 2014-T6 test panel (not welded) was prepared and bulged. A maximum pressure of 1400 psi was attained before slippage occurred. A 1-1/4-inch grid was scribed over portions of the surface of this panel in order to measure elongation due to bulging. This method of determining the maximum elongation of the bulged area was not satisfactory. Widening of the scribed lines of the grid masked the small increase in the grid dimensions. The radius for the bulged area of this panel was 11.5 inches and the bulge height was 2-7/8 inches. Radius of curvature was calculated to be 24.8 inches. Maximum stress attained in this panel was found to be 69,500 psi. The 2014-T6 test panel used for this preliminary test is shown in Figure 32. The results of both tests indicated that the hydraulic system and the "O" ring seal had performed as expected.

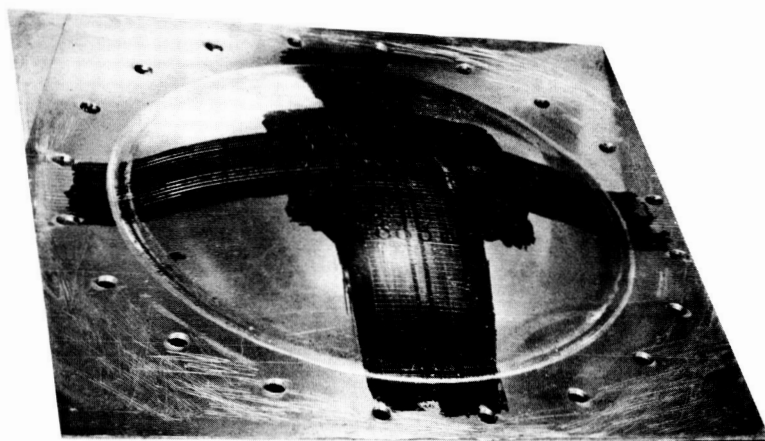


FIGURE 32. APPEARANCE OF TEST PANEL
(2014-T6) AFTER BULGING

b. Test on 3/4-Inch Thick 2219-T87 Aluminum Weldments

Four panels 32 x 32 inch were tested by the hydraulic bulge fixture. The welding procedure for these panels are described in Appendix II under "Hydraulic Bulge Test Panels". These panels were identified as follows:

Panel A. Single butt weld, crowns intact.

Panel B. Single butt weld, crowns ground flush with base metal.

Panel C. Single butt weld, crowns intact.

Panel D. "Tee" weld, crowns intact.

The weld configurations are illustrated in Figure 70. Each panel was radiographed prior to testing. The radiographic examination did not disclose the lack of penetration visible after testing.

c. Test Results

The hydraulic bulge test fixture was successfully used to test full 3/4-inch 2219-T87 weldments under biaxial loading condition. All panels were tested to rupture. The pressure sustained by each panel at rupture and the bulge height were measured and are listed below:

<u>Specimen</u>	<u>Pressure to Rupture (psig)</u>	<u>Bulge Height (inches)</u>
Panel A	805	Not recorded
Panel B	882	.656
Panel C	1,028	.788
Panel D	1,220	1.366

These data indicate that the 3/4-inch thick panels can be compared by the two parameters maximum pressure to rupture and bulge height. After bulge testing, three of the panels were sectioned and the fracture mechanism studied. Panel D was shipped to Marshall Space Flight Center, Huntsville, Alabama for examination. Upon sectioning Panels A and B incomplete penetration was detected. Panel C contained mismatch. Because of these defects, the panels cannot be critically evaluated with reference to load carrying capacity and weld configuration.

C. Failure Mechanism of Biaxial Test Plates

Information concerning the location, path and length of failure in the hydraulic bulge tests was obtained. After testing, the length of fracture in the weldment was measured and its location noted. Both single butt panels (Panels A and B) with incomplete penetration were studied metallogically. Cross-sections of the weld deposit were made at 1/2 inch intervals the full length of the weldment to study the path and extent of the fracture. Macroscopic and microscopic studies were made of several of the cross-sections in these two panels.

1. Panel A. Single butt weld, crowns intact

The surface measurements of the fracture which developed on this testing panel are shown in Figure 33. The outer surface of the bulged panel had a surface crack along 42 percent of its length. This was located in the bottom toe of the first weld pass. The crack on the inner surface was visible 14 percent of its length and was in the top toe of the

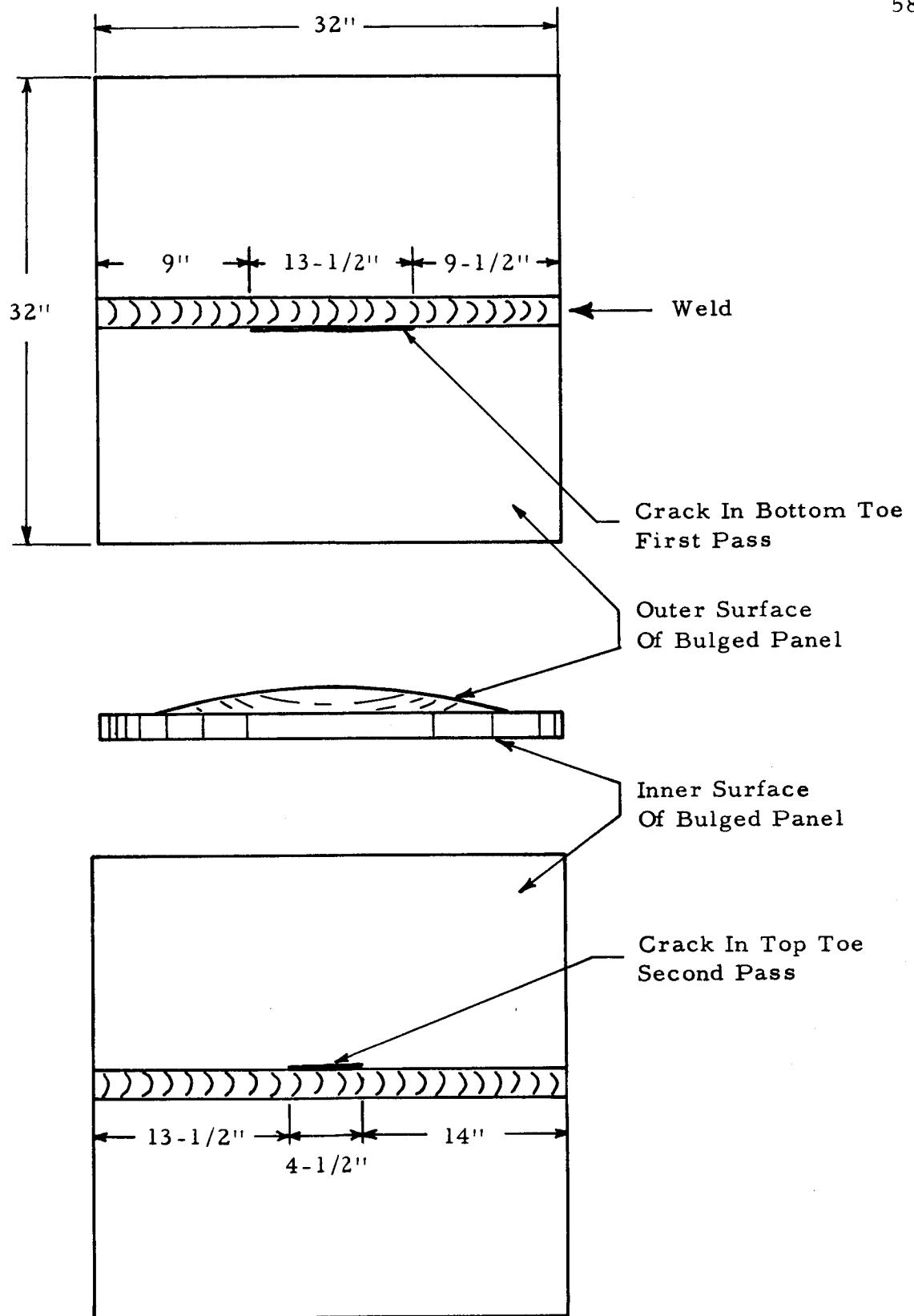


FIGURE 33. LOCATION AND MEASUREMENTS OF SURFACE CRACKS IN PANEL A

second weld pass. Both cracks were symmetrically located with respect to the ends of the panels. In Figure 34 the profile of the fracture and its length on both surfaces are shown. The fracture profile shows the failure to be extensive at all levels through the thickness except close to the inner surface.

The failure path on the macroscopic scale is shown in Figure 35. The figure shows three cross-sections of the weld at the ends of the surface crack and through the middle of the welded panel. The diagonal fracture pattern through the weld deposit is similar to the uniaxial fracture path. Fracture initiated in the bottom toe of the weld pass on the outer surface of the panel and progressed diagonally through the first weld pass to the small area of incomplete penetration. The crack progressed from this area in a direction at right angles to the thickness of the panel and finally veered diagonally through the weld deposit to the region close to the top toe of the second weld pass.

2. Panel B. Single butt weld, crown ground flush with base metal.

The surface measurements of the cracks in this panel are shown in Figure 36. The visible fracture on both sides of the panel was in the area of the weld metal that corresponded to the bottom toes.

The outer surface crack was along 36 percent of the weld length. On the inner surface it extended 18 percent.

The crack path at both ends of the outer surface crack and also the center cross-section of the weldment is shown in Figure 37. The

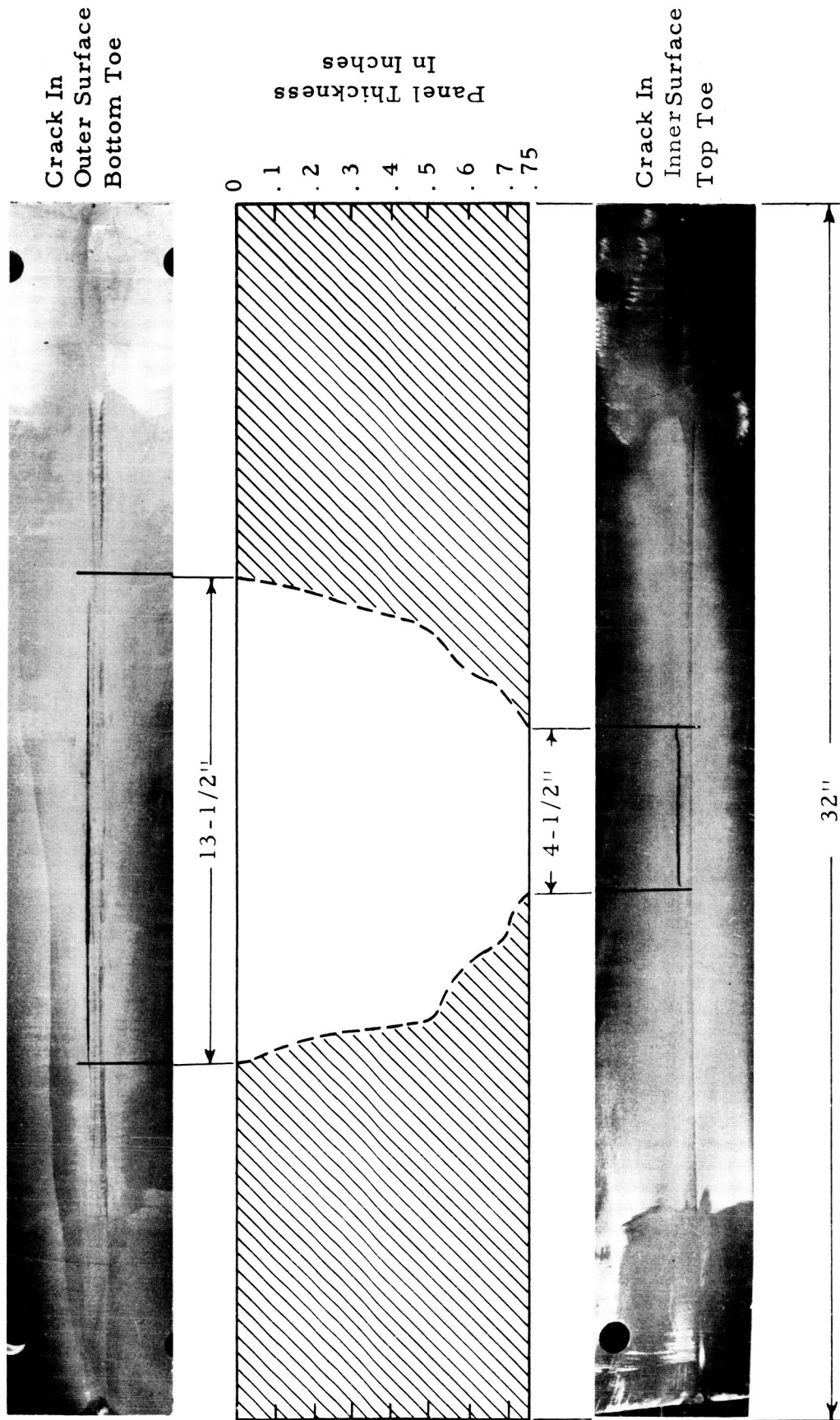
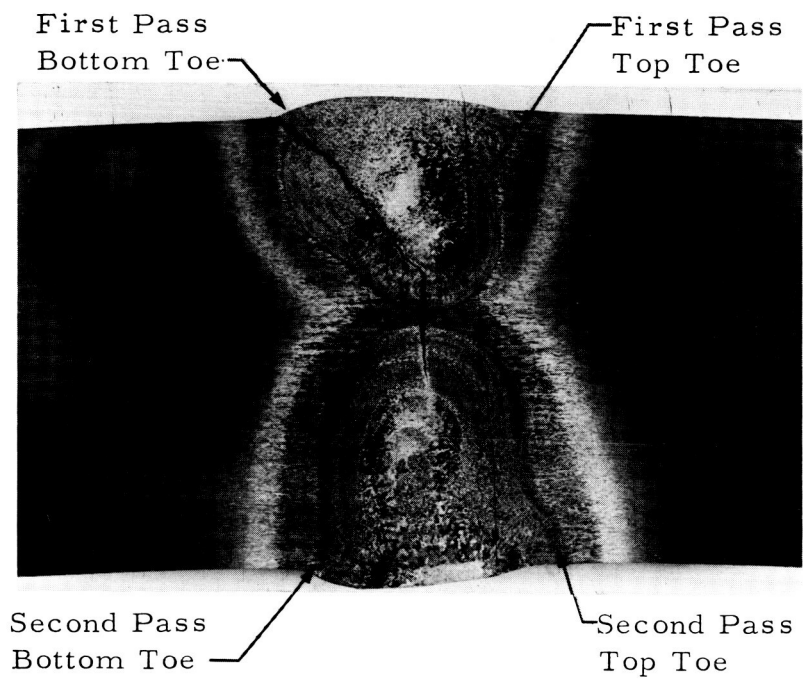
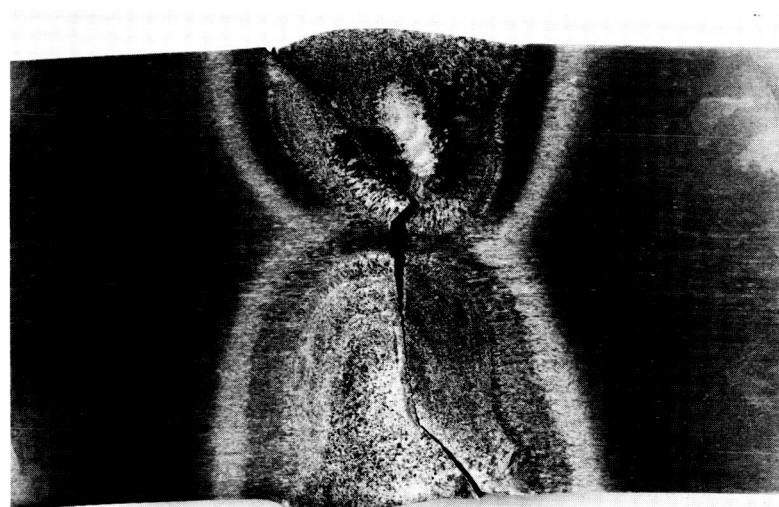
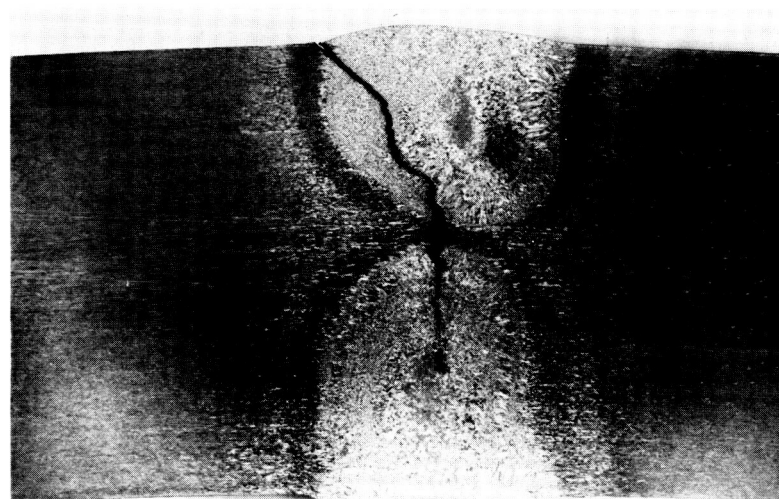


FIGURE 34. PROFILE AND LENGTH OF FRACTURE ON BOTH SURFACES IN PANEL A



Outer Surface

End Of Fracture
(Left)Inner
SurfaceCenter Cross
SectionEnd Of Fracture
(Right)

Etchant-Kellers

3X

FIGURE 35. CROSS SECTIONS THROUGH CENTER AND ENDS OF FRACTURE IN PANEL A. Single butt weld with lack of penetration.

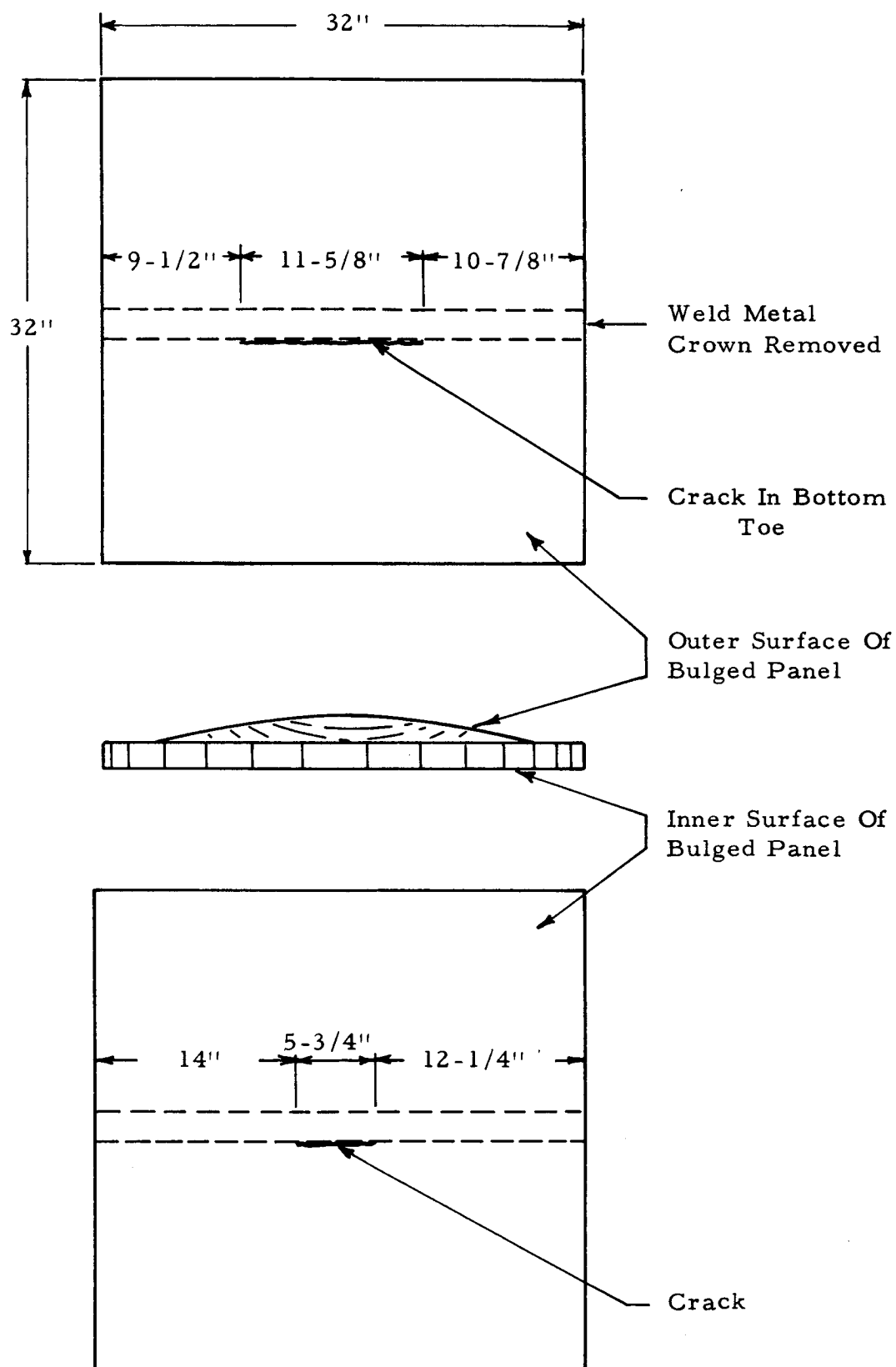


FIGURE 36. LOCATION AND MEASUREMENTS OF SURFACE CRACKS IN PANEL B. Weld crowns ground flush with base metal.

Second Pass

Bottom Toe

Filler Pass

63

Outer Surface

End Of Fracture
(Left)

Inner Surface

First Pass

Bottom Toe

Center Cross
Section

End Of Fracture
(Right)

Etchant-Keller's

3X

FIGURE 37. CROSS SECTIONS THROUGH CENTER AND ENDS OF FRACTURE IN PANEL B. Single butt weld, crowns off and with lack of penetration.

cross-sections of the ends show that the fracture progressed diagonally from Zone A where the bottom toe was located through the weld deposit to the area of incomplete penetration. The fracture propagated out of this area straight into the weld metal of the first weld pass. In the last 10 percent of the weld thickness the crack veered at an angle toward the bottom toe of the first pass (center cross-section).

3. Panel C. Single butt weld, crowns intact.

The surface cracks of the fracture on both sides of this bulge panel are shown in Figure 38. The outer surface crack extended 56 percent of the weld's length, while the inner surface crack extended 57 percent. Figure 39 is the photograph of the fracture in the outer surface of Panel C. The 18-1/2 inch length of the surface crack is indicated. The inner surface crack crossed the reinforcement three times starting at the top toe. The mismatch in this plate was considered to be one of the factors contributing to this irregular fracture pattern.

4. Panel D. "Tee" weld, crowns intact.

A panel with a "Tee" weld was fabricated and bulge tested. After locating and measuring the extent of the surface crack, this panel was shipped to George C. Marshall Space Flight Center, Huntsville, Alabama for evaluation. These measurements are shown in Figure 40.

Surface cracks occurred on the outer surface and in both welds comprising the "Tee". On the inner surface, cracks were limited to the long weld of the "Tee".

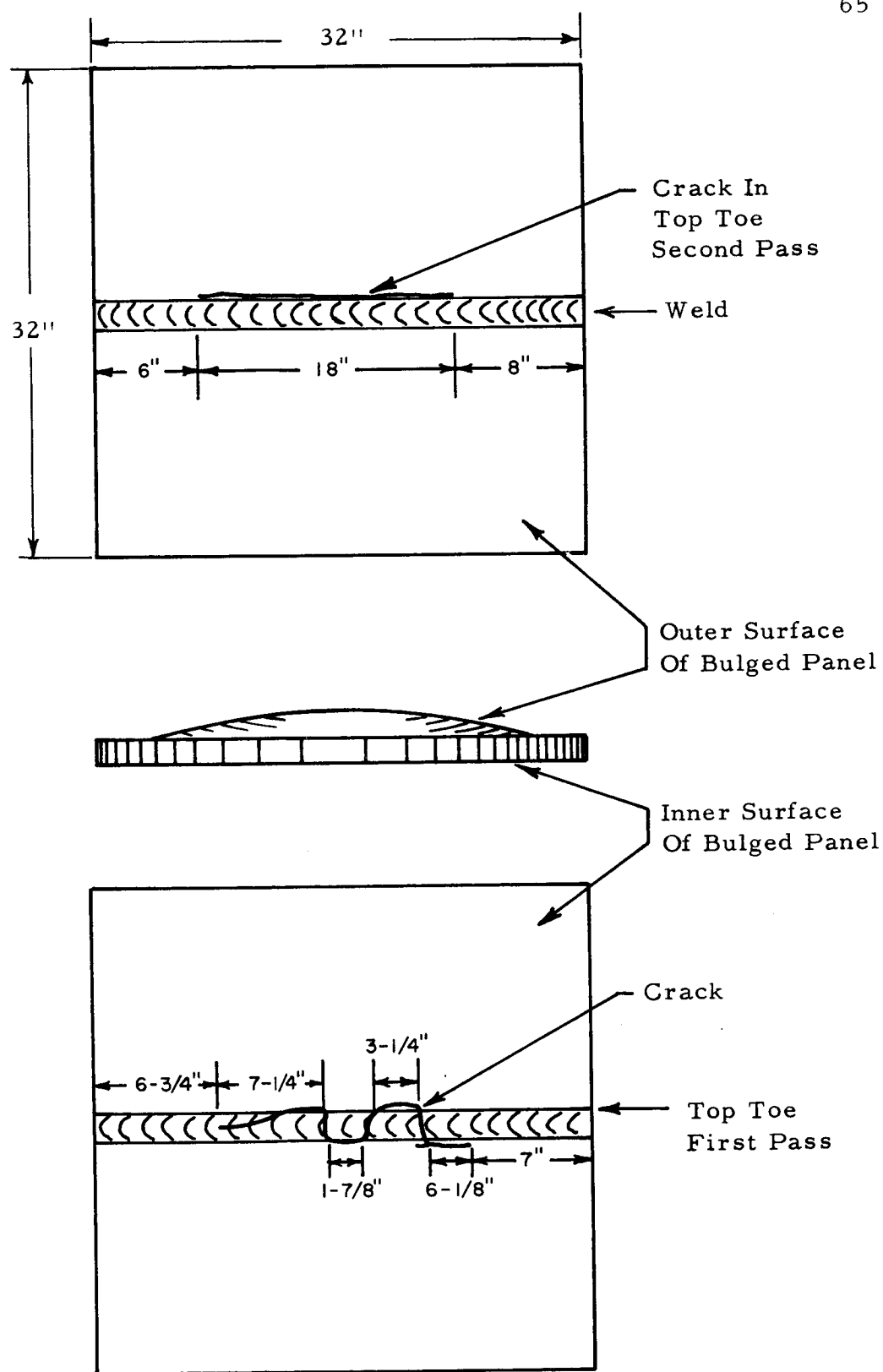


FIGURE 38. LOCATION AND MEASUREMENTS OF SURFACE CRACKS IN PANEL C

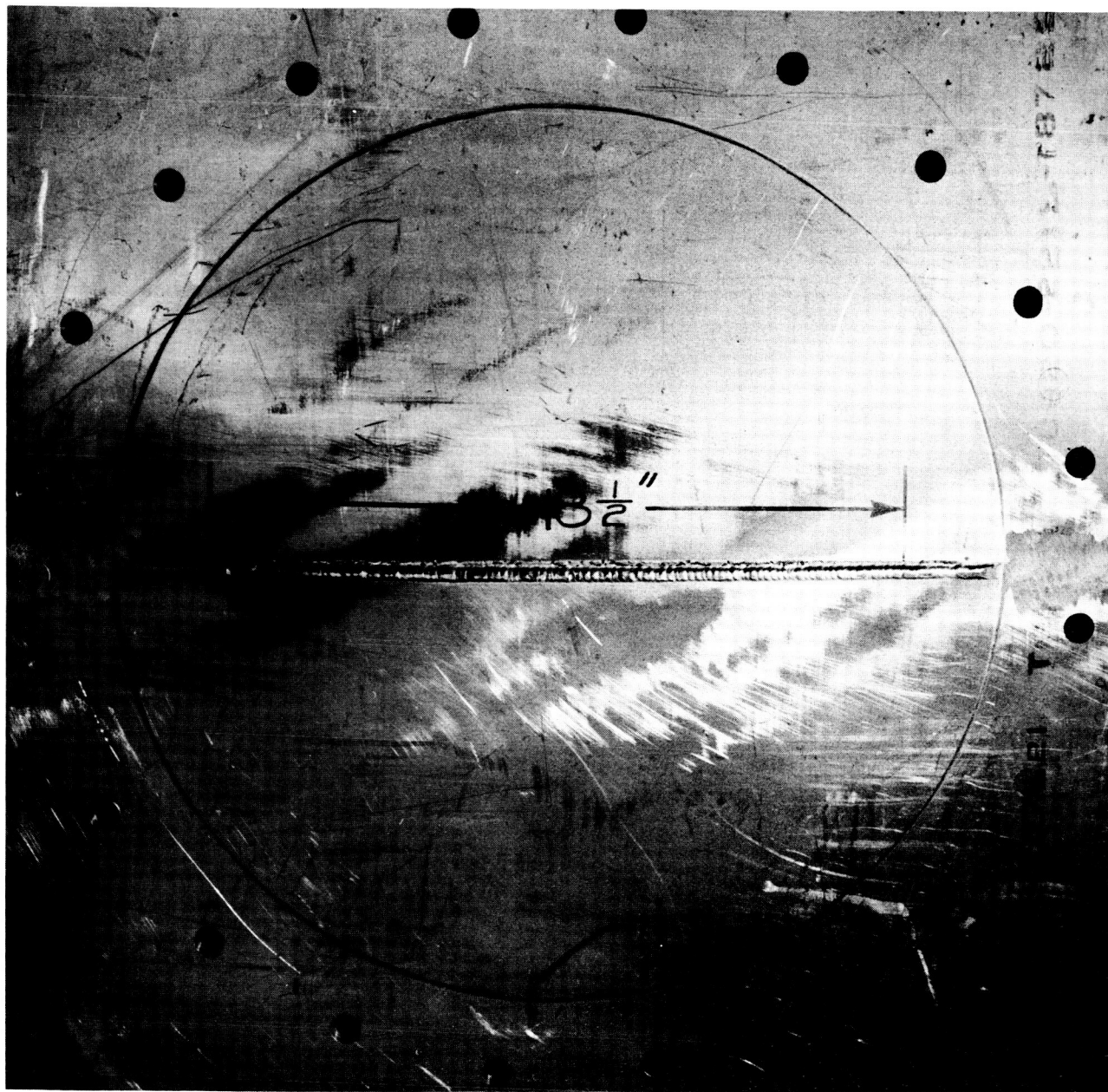


FIGURE 39. SURFACE CRACK IN PANEL C AFTER BULGE TEST

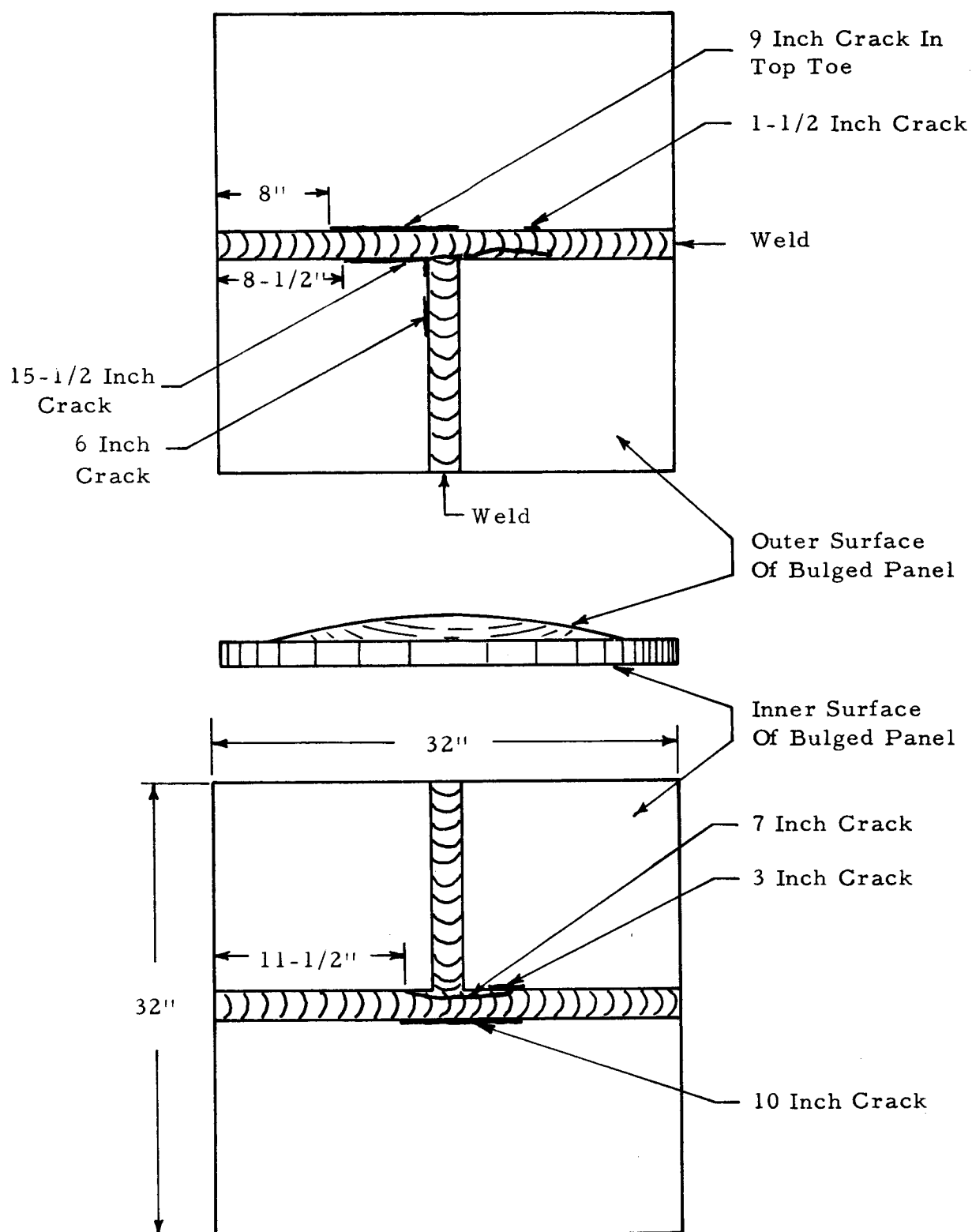


FIGURE 40. LOCATION AND MEASUREMENTS OF SURFACE CRACKS IN PANEL D

5. Microscopic Examination of Biaxial Failures

The mechanisms of failure of Panels A and B were microscopically examined. An examination of the surfaces of the biaxial panels showed that fracture initiated in the weld toes when the crowns were intact. Figure 41 is a cross-section through one end of the crack on the outer surface of Panel A. The three cracks present are identified by arrows. They are located in the bottom toe where the intermetallic precipitates are concentrated. The similarity between these cracks and those in a toe of a uniaxial specimen is illustrated by comparing Figures 41 and 12. The largest crack in Figure 41 indicates that the fracture path is through the intermetallic constituents. The lower portion of this crack can be seen to be intergranular.

A cross-section closer to the rupture at the center of the panel is shown in Figure 42. Two cracks originating in the toe of the weld are indicated by the arrows. The smaller crack had not propagated beyond the grain boundary from which it formed. Small intergranular branch cracks were evident. The fracture path in the weld metal is shown in Figure 43. This photomicrograph shows the end of a crack that originated at the outer surface of the panel and progressed into the weld metal as a result of biaxial stresses. The crack appears to be intergranular. Intermetallics are fractured or separated by this crack.

One specimen from bulge test Panel A was included in the

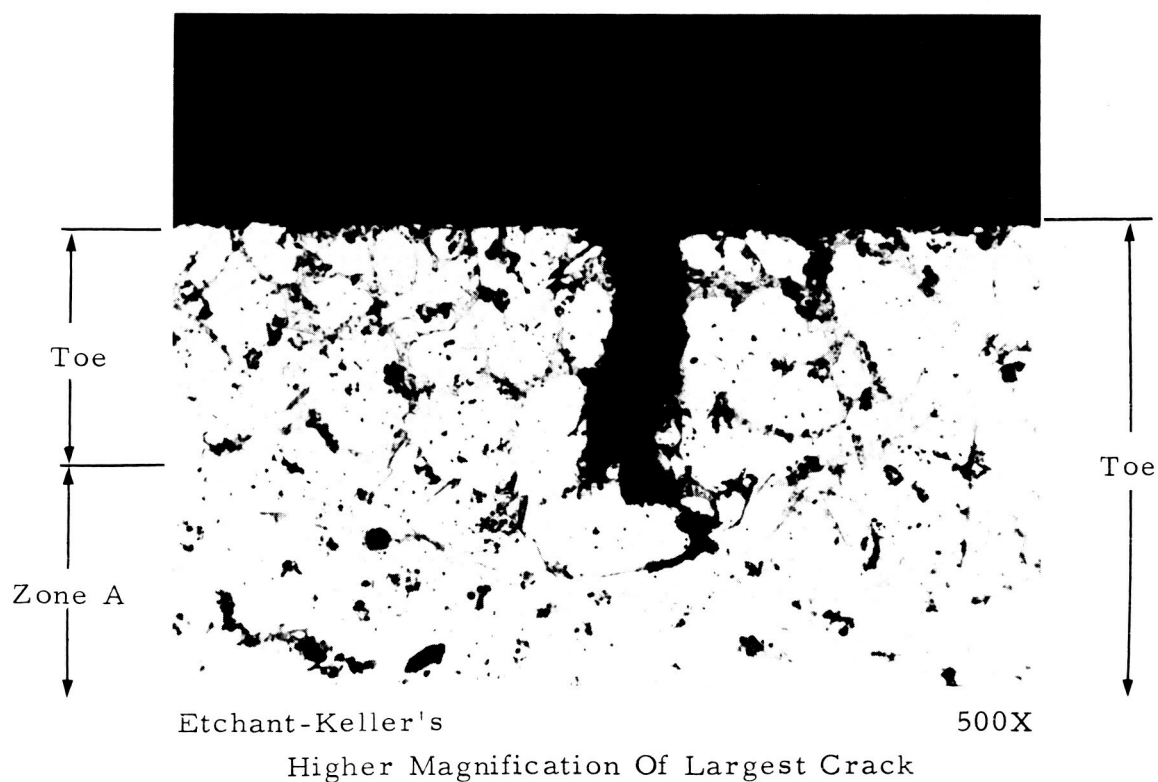


FIGURE 41. FORMATION OF CRACKS IN THE INTERMETALLIC CONSTITUENTS IN THE BOTTOM TOE OF A WELD PANEL AFTER BIAxIAL TEST



FIGURE 42. CROSS SECTION OF FRACTURE AT OUTER SURFACE OF WELD PANEL. Cracks initiating in weld toe indicated by arrows.

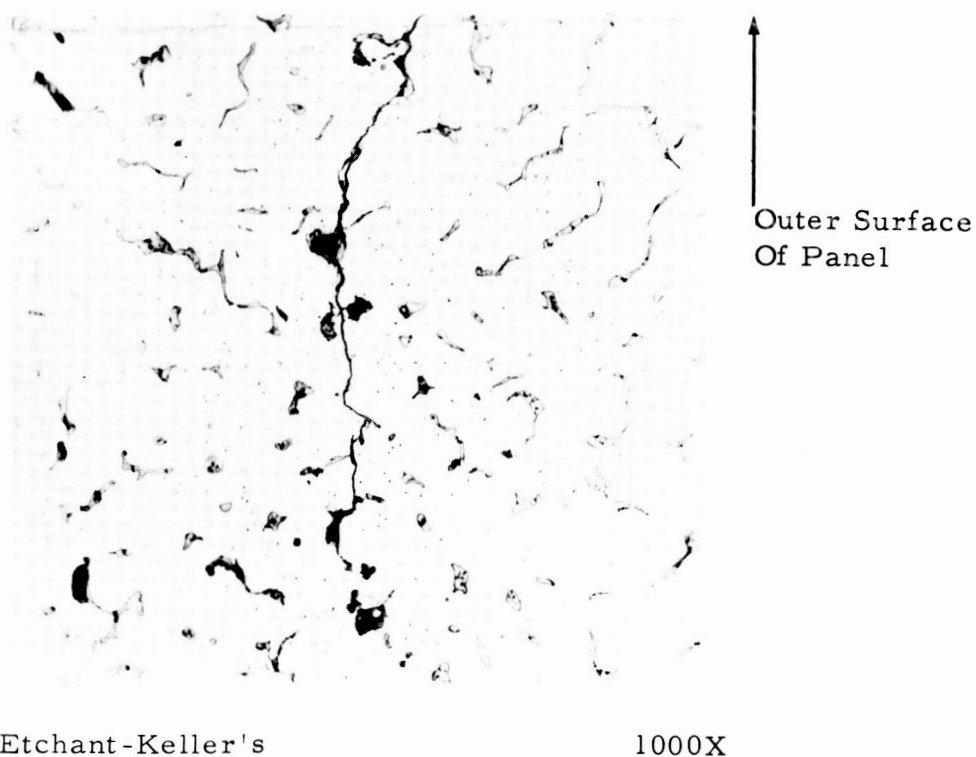


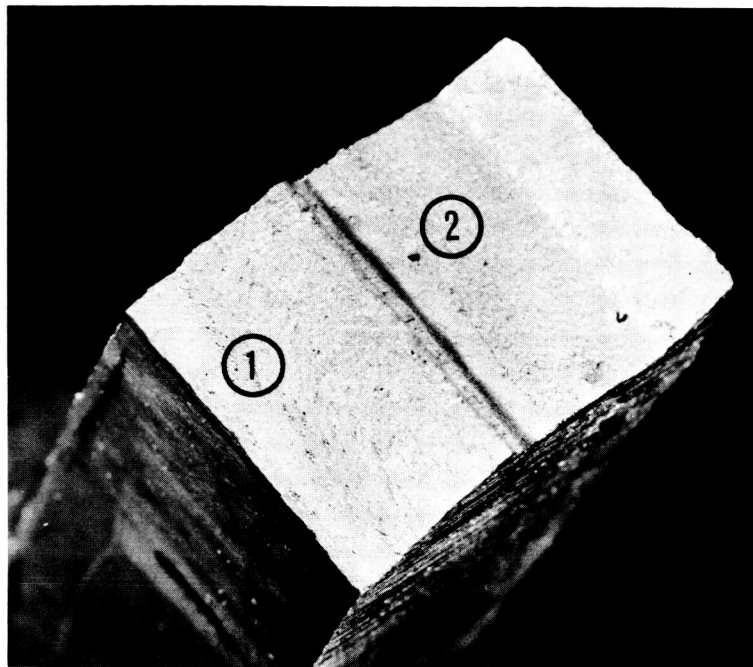
FIGURE 43. PATH OF FRACTURE IN WELD METAL
RESULTING FROM BIAXIAL STRESSING

fractographic study carried out in this program. The fracture surface of the specimen cut from the panel is shown in Figure 44.

The overall topographical features of this fracture resemble those of the uniaxial test fractures. The fracture surface exhibited the dimpled structure characteristic of transgranular plastic fracture.

A distinct difference in the surface topography of the two separate weld passes was noted, however. The fracture surface in the first weld pass, Figure 45, exhibited irregularly shaped dimples and numerous second-phase particles closely resembling the weld deposit fractures in the uniaxial tests. The region of the fracture surface extending through the second weld pass, on the other hand, was characterized by larger, smoother surfaced dimples, Figure 46. These dimples more closely resembled the larger dimples observed in the base metal uniaxial test specimen. The dimples in the second weld pass, however, were not as uniform in shape as those of the base metal.

The distinct difference in topography of the fracture surface in each of the weld passes indicates that in some cases the microstructure of the two weld passes may differ in such a way so as to produce entirely different conditions for the initiation and growth of voids involved in the fracture process.



4X

FIGURE 44. FRACTURE SURFACE OF 2219-T87 WELDMENT BULGE TEST PANEL. SPECIMEN TAKEN FROM PANEL A TESTED WITH WELD CROWNS INTACT.

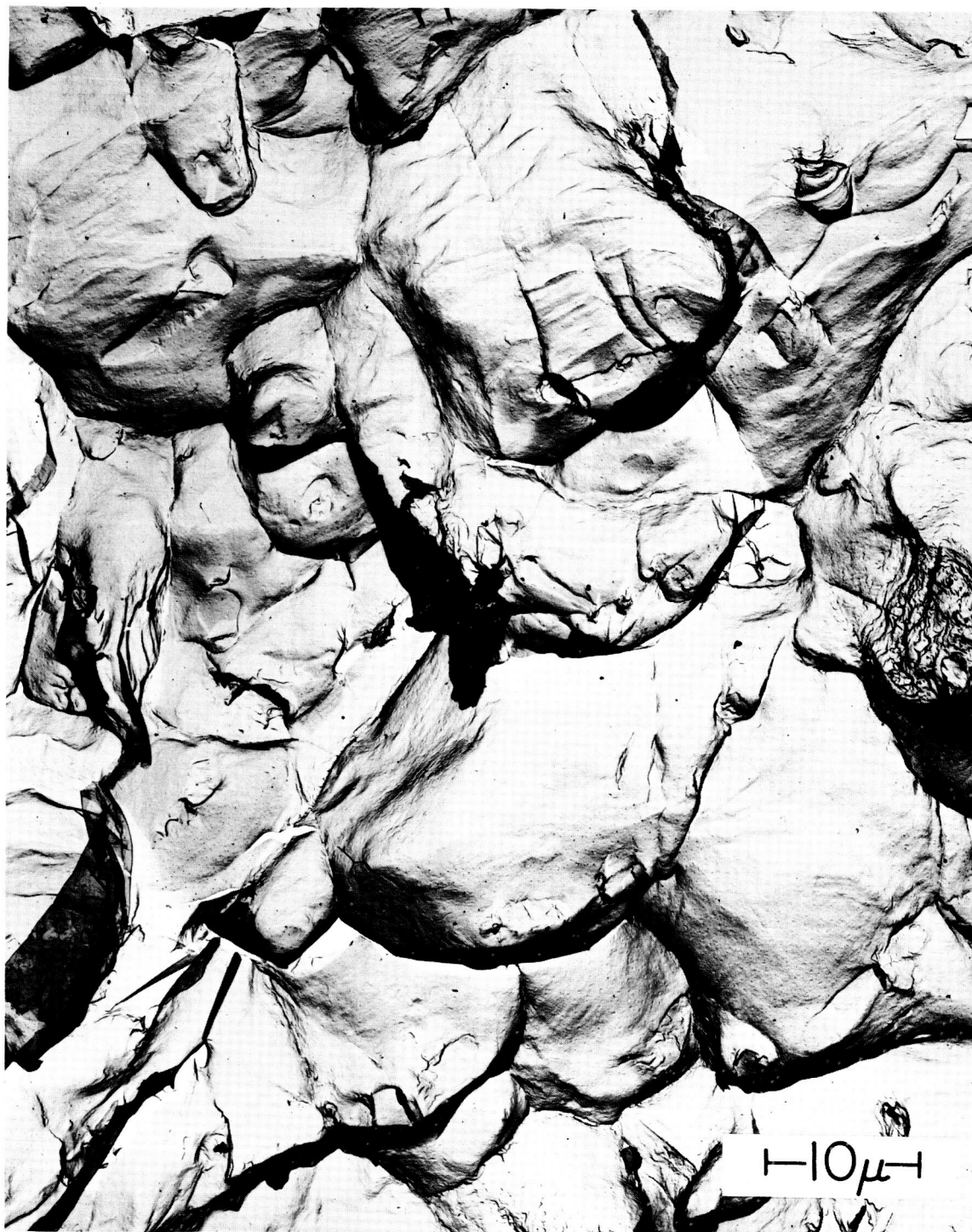
Numbered circles indicate location of fractographs shown in Figures 45 and 46.



Two-Stage Plastic Carbon Replica

2500X

FIGURE 45. FRACTURE SURFACE OF 2219-T87 WELDMENT BULGE TEST PANEL. Specimen tested with weld crowns intact. Fractograph taken from location within first weld pass in Panel A (Area 1, Figure 44). Note the irregular shape of dimples. Arrows indicate dispersed second-phase particles in fracture surface.



Two-Stage Plastic Carbon Replica

2500X

FIGURE 46. FRACTURE SURFACE OF 2219-T87 WELDMENT BULGE TEST PANEL. Specimen tested with weld crowns intact. Fractograph taken from location within second weld pass in Panel A (Area 2, Figure 44). Note the smooth surfaced nearly equiaxed dimples.

IV. METHODS FOR MEASURING YIELD STRENGTH AND DUCTILITY OF WELDS

A. Yield Strength

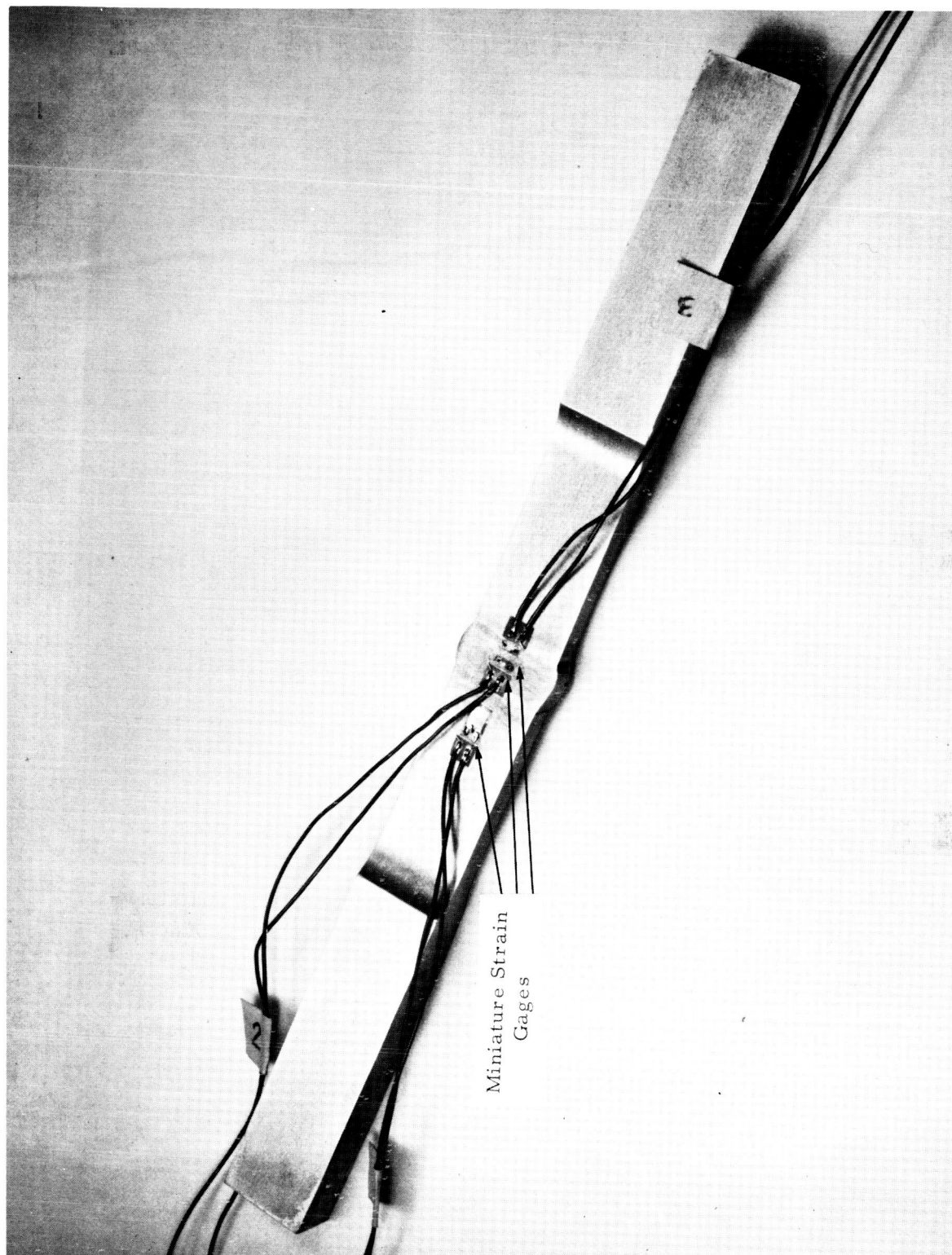
The American Society for Testing Materials defines yield strength as "the stress at which a material exhibits a specified limiting deviation from the proportionality of stress to strain. The deviation is expressed in terms of strain." For aluminum alloys the offset method with a limiting strain of 0.2 percent is specified.

This definition assumes a test piece of standard design and established relationships between critical dimensions. It also assumes that the test pieces are more or less uniform in strength, density and structure throughout their length. With these conditions fulfilled the results from a properly operated tensile test will be meaningful and should apply accurately to all parts of the test piece and/or the plate from which it has been properly sampled.

With a tensile test piece made with a butt weld as a part of the two inch gage length, the required uniformity does not exist, therefore the value for yield strength and elongation as determined by the standard testing methods will not reflect the properties of all sections of the specimen. It will be influenced by all materials of unequal strength included in the gage length.

Since the integrity of a structure is limited to that of its weakest part, it becomes imperative that a means be developed for the determination of the strength of all zones of the welded area. In an effort to develop a suitable method, a series of tests was made in which the behavior under tension of the various areas in the weld zone was studied. Three sets of tensile specimens were prepared. The first set was from a plate with a weld reinforcement intact. The second set was made from a plate from which the weld reinforcement had been completely removed. The standard procedure for butt welds with no gap was used for the first two sets of test pieces. For the third set a procedure directed to duplicating a repair weld was used. The width of the weld deposit was increased, the reinforcement was not removed.

Since, in addition to the weld deposit, three zones have been recognized in the weldment, (Figure 3) an attempt was made to evaluate the properties under tension of these three areas and of the weld deposit. After the tensile test specimens were prepared from the three types of samples, miniature resistance strain gages were mounted on the surface in the areas under consideration. 1/64-inch gages were used for the weld deposit and for Zone A. 1/8-inch gages were used for Zone C. Figure 47 illustrates the tensile specimen with strain gages attached. It does not include the two inch extensometer which was applied to each specimen prior to the tensile test.



IX

FIGURE 47. TENSILE COUPON WITH 1/64 AND 1/8 INCH MINIATURE STRAIN GAGES ATTACHED TO WELD DEPOSIT, ZONE A AND ZONE C

All specimens were tested in an Instron testing machine. Data from the strain gages were recorded by a Minneapolis Honeywell Model 906 A-1 Visicorder Oscillograph Honeywell Type M200-120 galvanometer. A continuous record was made of loading and strain gage deflection. The Instron testing machine and recording equipment are shown in Figure 48.

Figures 49, 50, and 51 were plotted from the data developed from these tests. For comparative purposes the stress-strain diagram previously obtained for the parent metal has been included. It is recognized that the measurements from the 1/64-inch and the 1/8-inch strain gages fixed to the standard size test piece do not record a true stress-strain diagram as defined by ASTM. However, since the values for the weld zone compare favorably with results from miniature tensile tests of weld metal, the data from this test is regarded to be of sufficient accuracy for comparative purposes.

Figure 52 was prepared from data plotted on Figure 49. The latter illustrates that when a standard ASTM two-inch gage length is employed to test weldments the yield strength of the weld deposit is likely to be exceeded long before the specified overall 0.2 percent offset is reached. It is also evident that the use of the "overall" yield strength for design purposes would be extremely hazardous. A more realistic testing method is desirable. The use of short gage lengths in a weld deposit and other limiting zones would be good in theory but rather impracticable in practice. It is felt

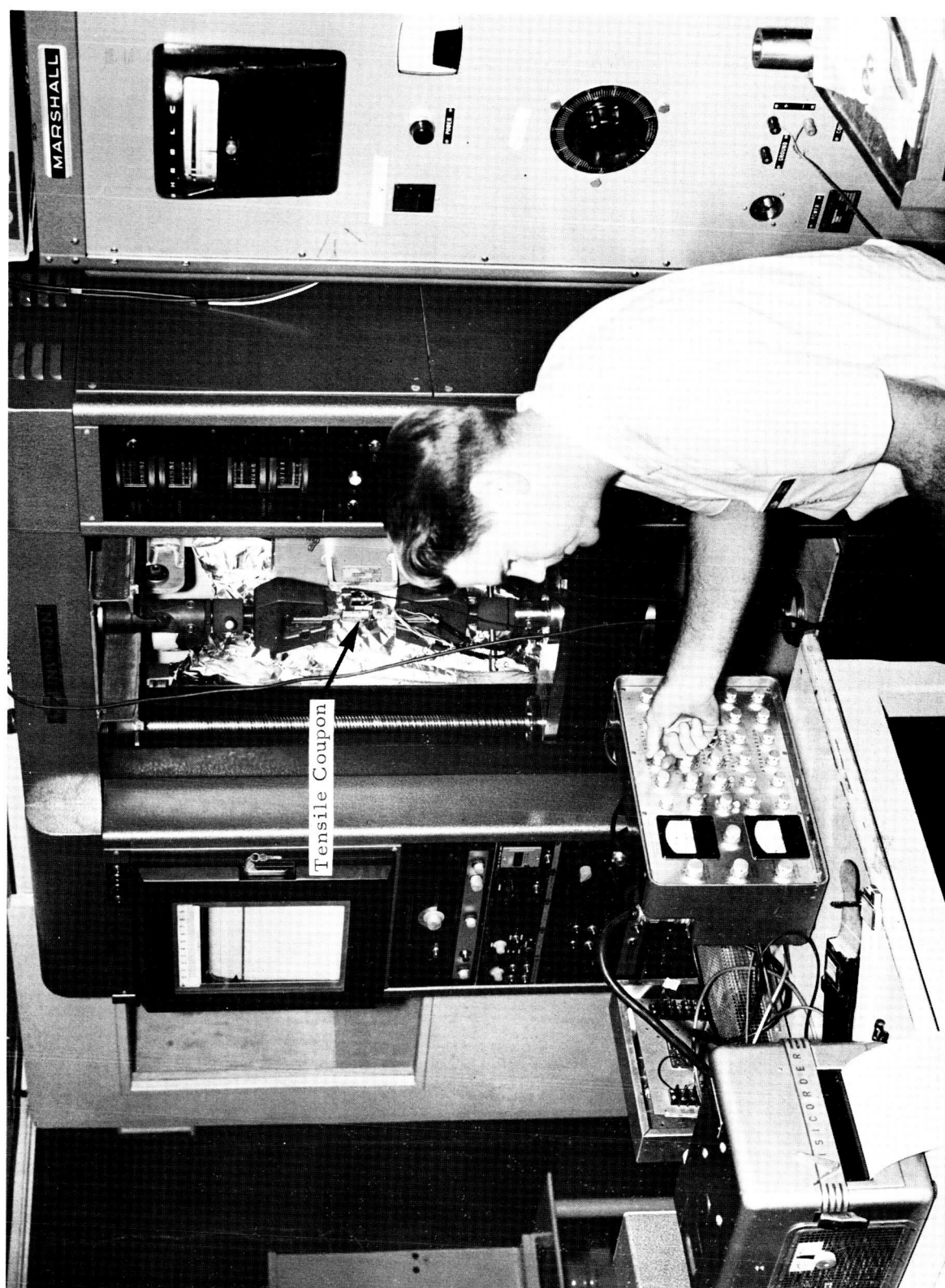


FIGURE 48. TESTING AND RECORDING EQUIPMENT. Arrow indicates tensile coupon.

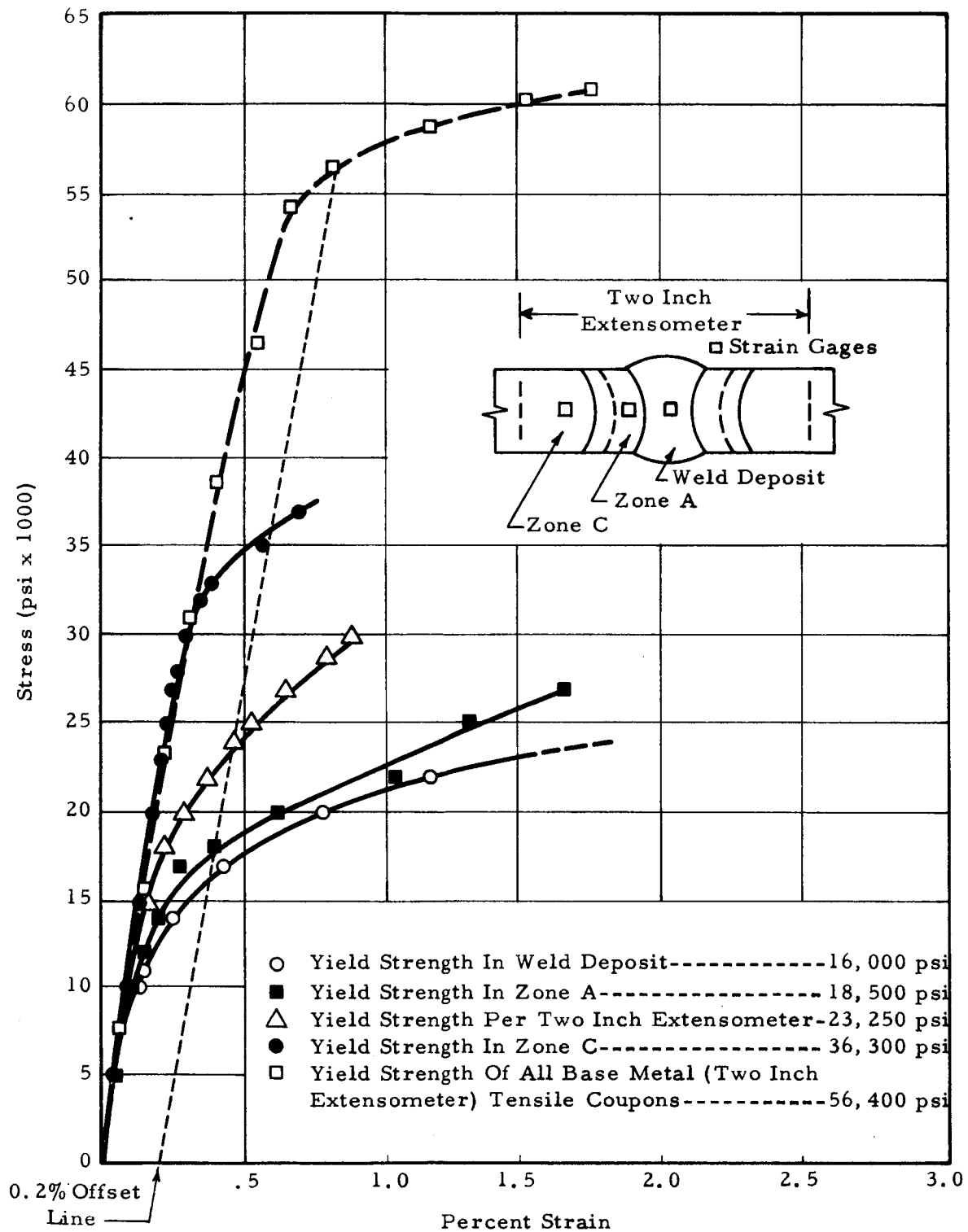


FIGURE 49. STRESS-STRAIN CURVES OF WELD DEPOSIT, ZONE A, ZONE C, AND PER TWO INCH EXTENSOMETER OF TENSILE COUPON. Note all base metal (two inch extensometer) curve from different tensile coupon.

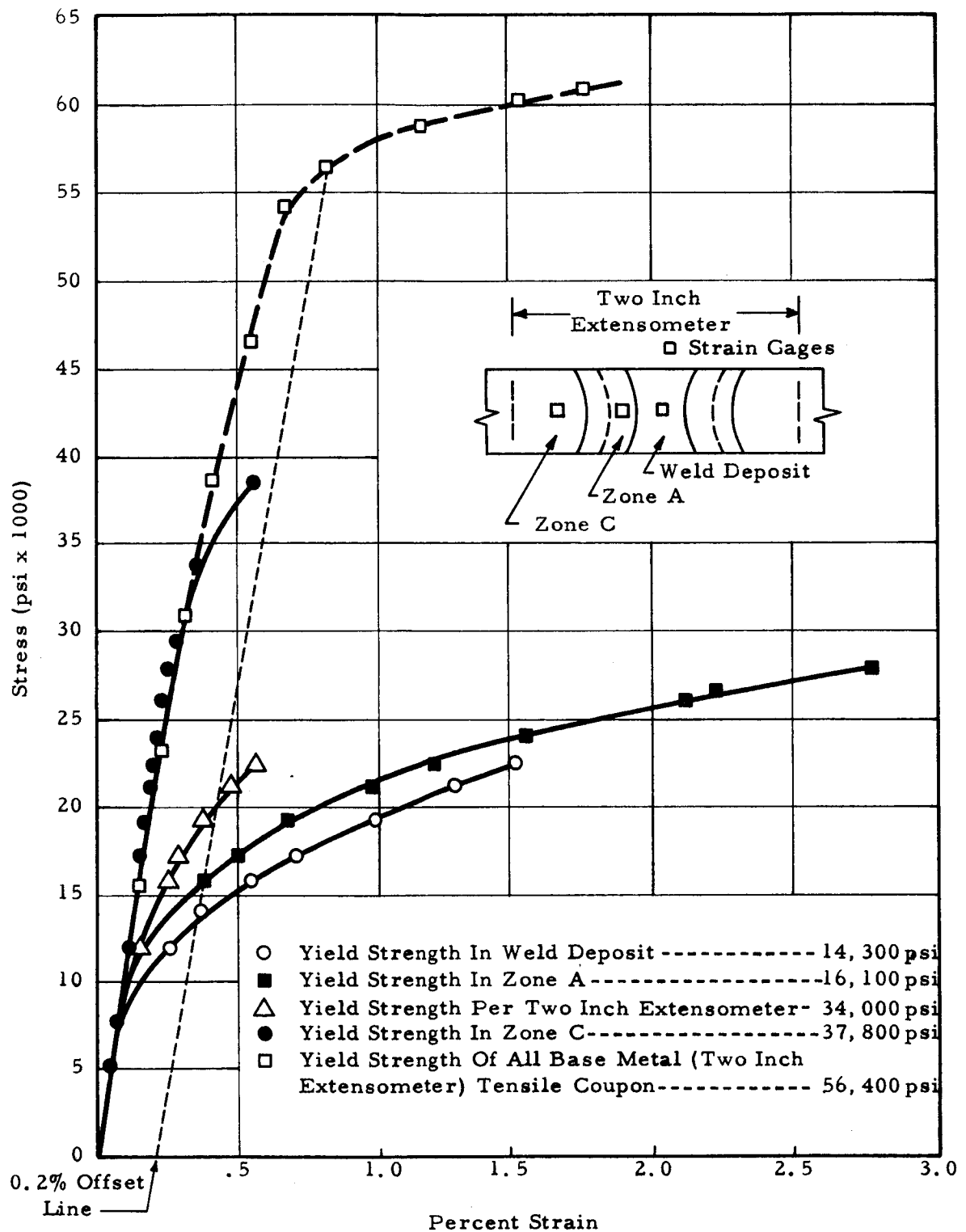


FIGURE 50. STRESS-STRAIN CURVES OF WELD DEPOSIT, ZONE A, ZONE C, AND PER TWO INCH EXTENSOMETER OF TENSILE COUPON WITH WELD CROWNS GROUND FLUSH WITH BASE METAL. Note all base metal (two inch extensometer) curve from different tensile coupon.

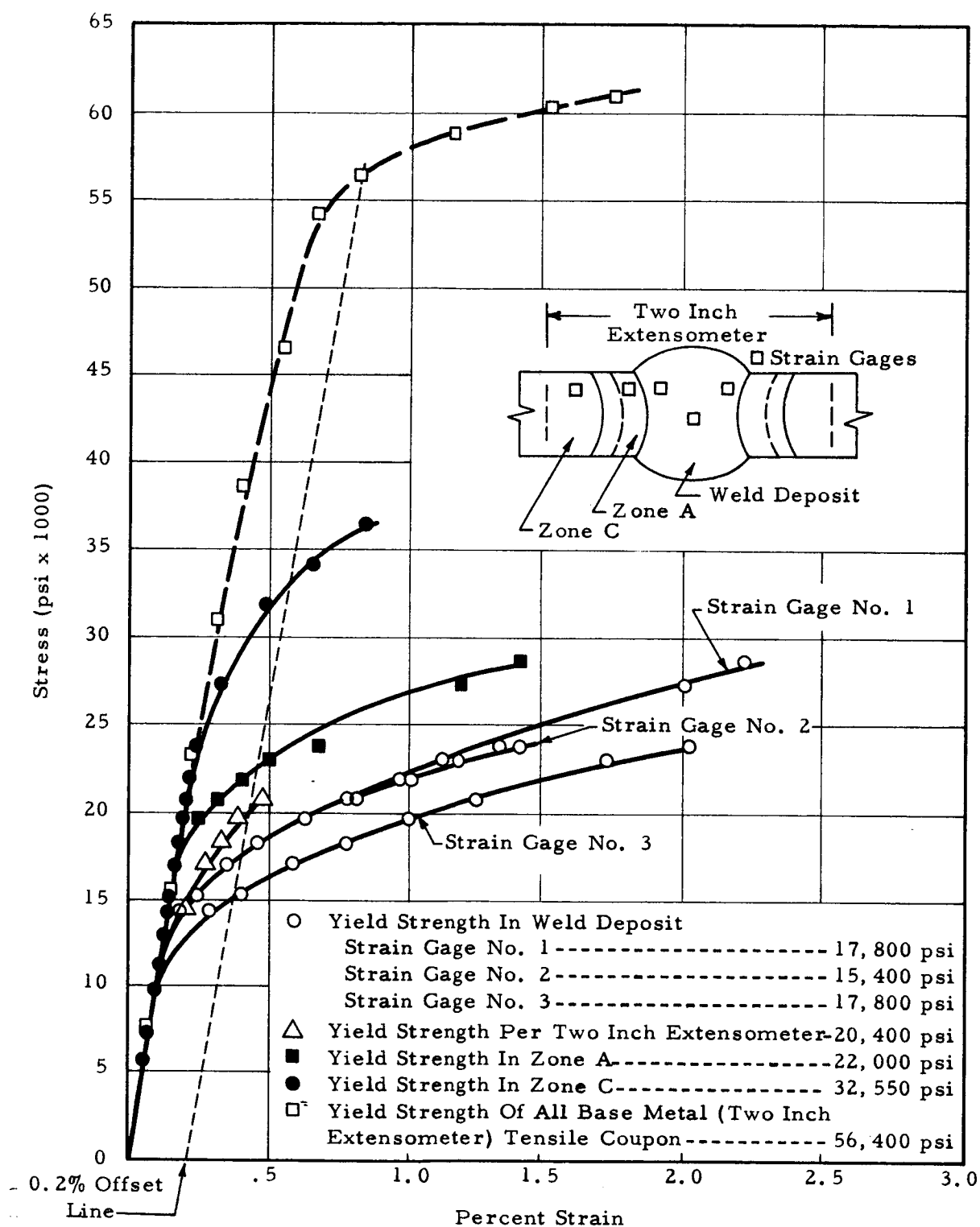


FIGURE 51. STRESS-STRAIN CURVES OF WELD DEPOSIT, ZONE A, ZONE C, AND PER TWO INCH EXTENSOMETER OF LARGE WIDTH-TO-DEPTH WELD RATIO TENSILE COUPON.

Note all base metal (two inch extensometer) curve from different tensile coupon.

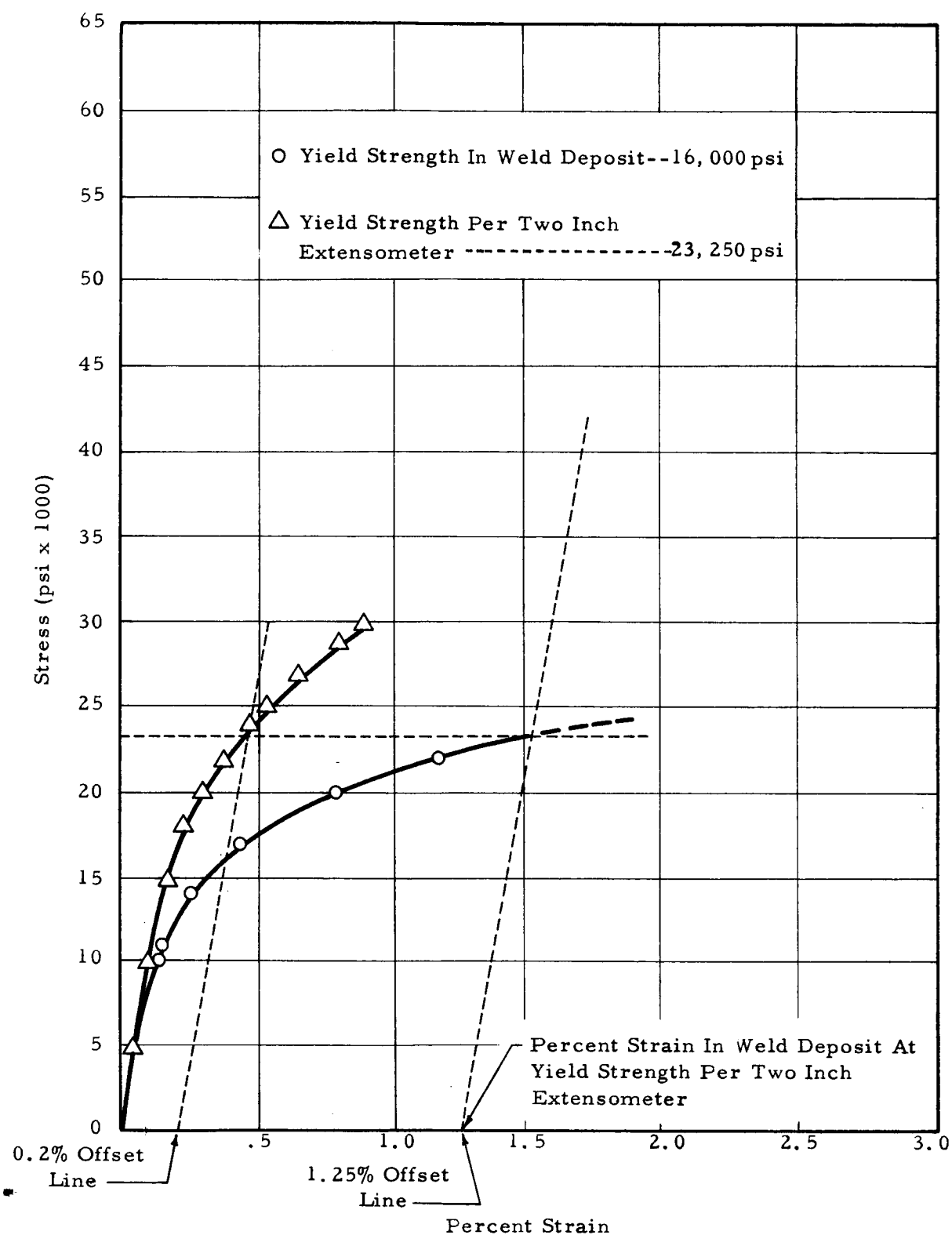


FIGURE 52. PERCENT STRAIN IN WELD DEPOSIT AT YIELD STRENGTH AS RECORDED BY THE TWO INCH EXTENSOMETER. These curves were extracted from Figure 49.

though that with data from a sufficient number of tests of weldments conforming rigidly to a given procedure, a relationship might be established which would permit the use of the two-inch gage length with a much lower offset value for a given material. Further systematic exploration in this area should produce useful data.

B. Ductility

In order to develop a better understanding of the ductility in the individual zones of the weldments and its relationship to the overall ductility, a series of special tensile tests were conducted. In this program, test specimens were prepared from welded panels which had been fabricated in accordance with the standard welding procedure described in Appendix II. Weld reinforcements were not removed. Figure 10 is a sketch of the finished test piece. After the test pieces were machined, the weld area was etched to define the various zones and the usual two inch gage length was scribed on the surface. The fusion lines and juncture between Zones A and B were further identified by Tukon microhardness indentations. Careful measurements were made of weld deposit, Zone A, Zones B and C and the two-inch gage length. Three surveys were made: 1) across the first weld pass, 2) across the center line where pass number one and two overlap, and 3) across the second pass. These surveys are shown in Figure 53.

After the specimens had been broken in the tensile machine, the fractured faces were mated together and all zones were measured again to determine the resultant plastic strain or elongation. The mechanical

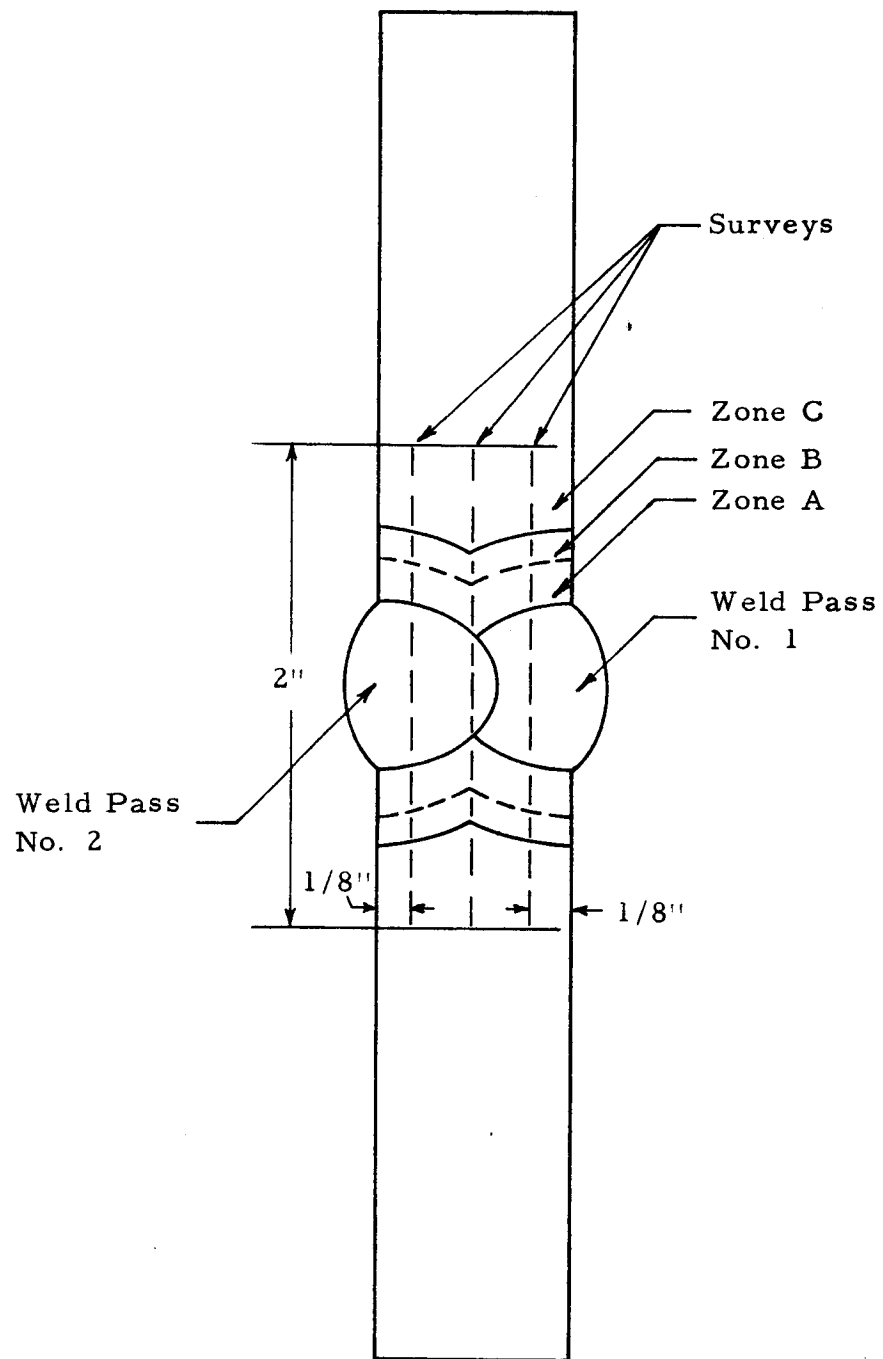


FIGURE 53. LOCATION OF THREE SURVEYS ACROSS TENSILE COUPON TO MEASURE PLASTIC DEFORMATION

properties of the specimens are tabulated in Table IV. Table V is a summary of the average plastic strain developed in the various zones in the five specimens tested. An examination of this table shows that strain is highly concentrated in the weld deposit. The percent strain in the weld deposit was 19.6 percent. This compares with 8.7 percent for Zone A and 0.97 percent for Zones B and C. The percent elongation over the two-inch gage length was 5.9 percent. The 19.6 percent strain value in the weld deposit checks very closely with 19.3 percent elongation developed by all weld metal tensile tests described in Section V.

The percent strain distribution across the weld joint is illustrated in bar graph form in Figure 54. This figure illustrates the incremental strain contributed by each zone to the total strain over the two-inch gage length. Of the total strain 57.1 percent occurred in the weld deposit, 8.4 percent in Zones A and 13.0 percent in Zones B and C. These values do not total 100 percent because of the gap and the inaccuracies inherent in the measurement process.

When mating the broken halves of the tensile specimens together to measure the strain in the various zones, it was noted that a gap existed across the first weld pass. This gap is shown in Figure 11. It was reasoned that possibly the first weld pass had less ductility and fractured first. The second pass being more ductile held together and strained a few more thousandths of an inch. However, a detailed analysis of the data did not show any significant difference in strain measurements between the first and second weld passes.

TABLE IV
MECHANICAL PROPERTIES OF SPECIMENS FROM 3/4 INCH THICK 2219-T87
ALUMINUM WELDMENTS USED IN DUCTILITY MEASUREMENTS¹

<u>Specimen</u>	<u>Yield Strength (0.2 Percent Offset) psi</u>	<u>Ultimate Strength psi</u>	<u>Percent Elongation (in 2 Inches)</u>
27-2	22,900	43,100	5.25
27-3	22,900	43,400	6.15
33-4	23,100	43,000	6.20
33-5	22,800	44,000	6.20
33-6	23,700	43,800	5.60
Average	23,080	43,460	5.88

¹ Horizontal square butt weld one pass from either side.

TABLE V

SUMMARY OF AVERAGE STRAIN IN WELD METAL, ZONE A AND ZONES B AND C OF
WELDED 3/4 INCH THICK 2219-T87 ALUMINUM TENSILE SPECIMENS

Average Percent Strain in Weld Zones				
<u>Specimen</u>	<u>Weld Deposit Average Strain (Percent)</u>	<u>Zone A Average Strain (Percent)</u>	<u>Zone B And C Average Strain (Percent)</u>	<u>Percent Elongation (in 2 inches)</u>
27-2	21.2	6.8	1.09	5.25
27-3	19.9	9.6	0.95	6.15
33-4	18.9	10.1	0.38	6.20
33-5	20.5	8.7	1.09	6.20
33-6	17.3	8.7	1.33	5.60
Average	19.6	8.7	0.97	5.90

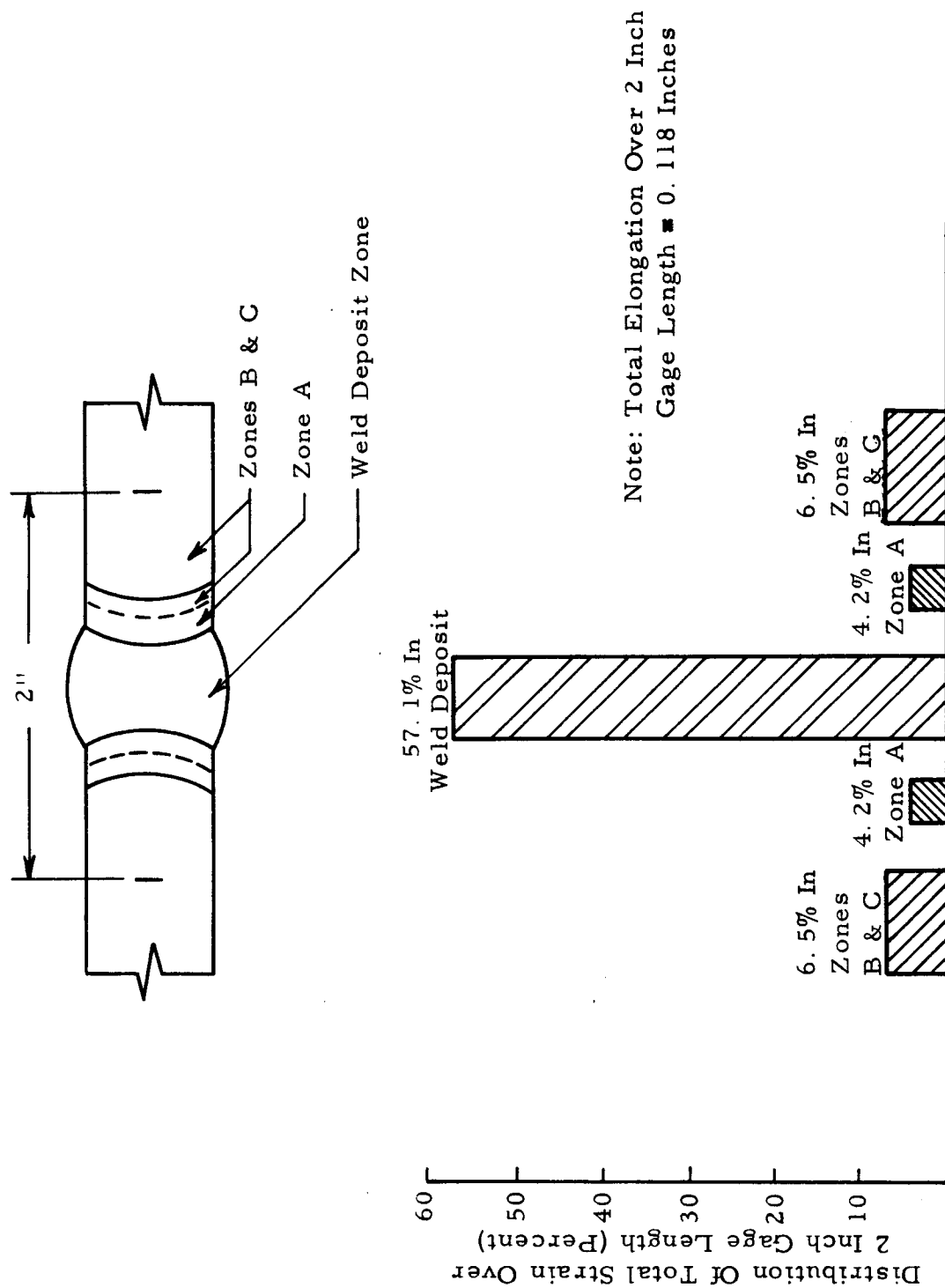


FIGURE 54. PERCENT STRAIN DISTRIBUTION ACROSS WELD JOINT

V. EXPLOSION IMPACT TREATING OF WELDMENTS

The feasibility of using explosive impact loading to improve the mechanical properties of 3/4 inch 2219-T87 weldments was investigated. The results obtained from the preliminary test indicate that a considerable increase in yield strength of the weld-metal can be obtained without incurring a drastic reduction in ductility. Tensile specimens taken transverse to the weld also exhibited a large increase in yield strength as a result of impact loading. The ultimate strength of all-weld-metal and of the transverse weld tensile specimens increased only slightly as a result of impact loading. Both the ultimate strength and the yield strength of the base metal decreased a small amount after explosive loading.

The test panels used in this study were fabricated in accordance with the "Standard Welding Procedure" in Appendix II. Two panels 3/4 x 16 x 24 inches were fabricated. Each panel was cut into two equal 16 x 12 inch sections. Only one section from each test panel was subjected to the explosive loading using the arrangements shown in Figures 55 and 56. The test panel was placed on a three-inch steel base plate and a solid explosive charge was positioned 18 inches above the panel. A four-pound charge of pentolite was used for Plate No. 30. The explosive was detonated from a safe distance using an electric blasting cap. Both panels were tested with the weld crown intact. All testing was carried out at ambient temperature.

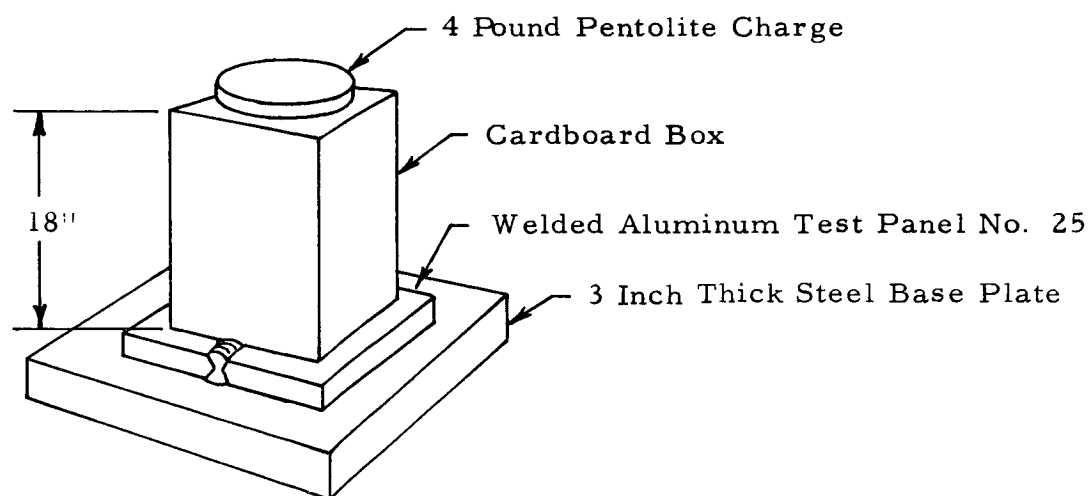


FIGURE 55. EXPLOSIVE IMPACT LOADING OF BUTT-WELDED
3/4 INCH THICK 2219-T87 TEST PANELS

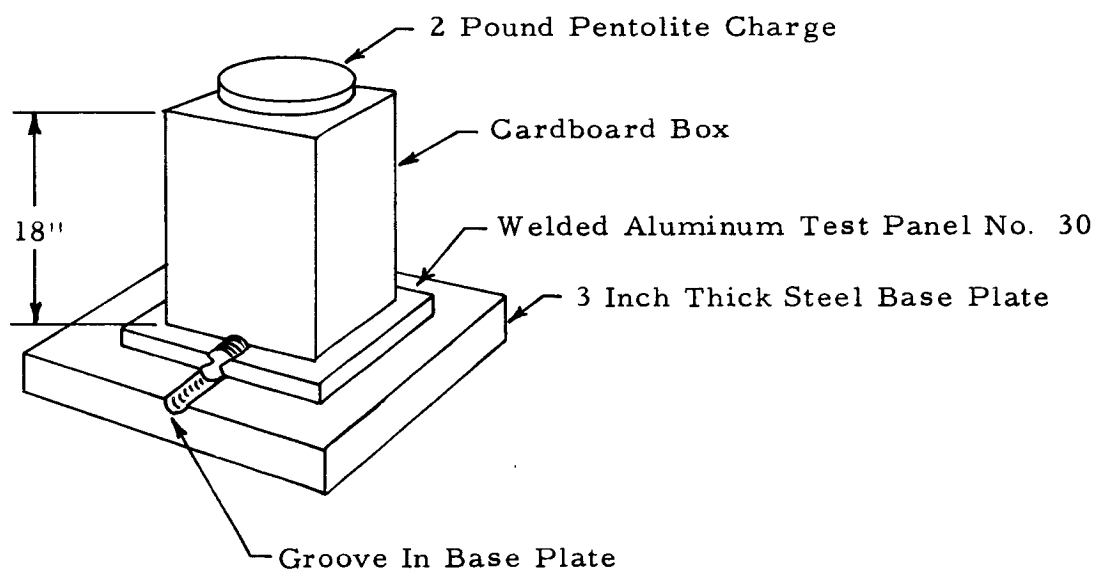


FIGURE 56. EXPLOSIVE IMPACT LOADING OF BUTT-WELDED
3/4 INCH THICK 2219 T87 TEST PANELS

The effect of the explosion on the top surfaces of the test weldments is shown in Figures 57 and 58. The texture of these surfaces was not unlike that of a sandblasted metal surface. The locations of all-weld-metal tensile specimens and of small rectangular metallographic specimens are outlined in both figures.

After the explosive loading, tensile specimens were prepared from the panels and tested. Specimens were also tested from the sections of the panels which had not been subjected to the explosive loading. Locations of tensile specimens are shown in Figure 59. The results of the individual tensile tests are shown in Table VI.

The results of the tensile tests indicated that the two-pound charge had produced a 138 percent increase in the yield strength of the weld metal and a 114 percent increase was produced by the four-pound charge. The yield strength of the base metal was slightly decreased as a result of loading with both the two and the four-pound charges. Results from tensile specimens taken transverse to the weld indicate a 42.5 percent increase in yield strength as a result of the two-pound charge and a 46 percent increase due to the four-pound charge. These results are summarized in Table VII.

The effect of explosive loading on the ductility of the transverse weld specimens was, for all practical purposes, negligible. This was also the case for the base metal. The only marked reduction in elongation was exhibited by the weld metal from panel No. 25. The elongation was decreased from 20 percent to 10 percent as a result of explosive loading. The

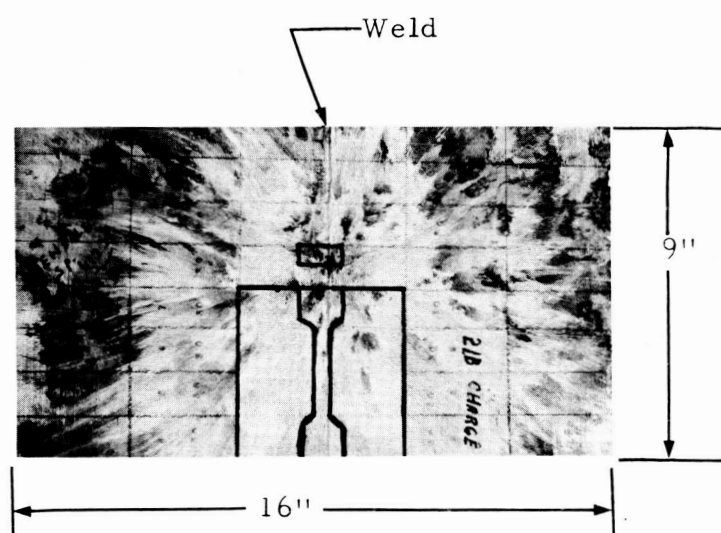


FIGURE 57. APPEARANCE OF 3/4" THICK 2219-T87 WELDMENT AFTER EXPLOSION IMPACT LOADING WITH A 2-POUND CHARGE OF PENTOLITE (PLATE NO. 30).

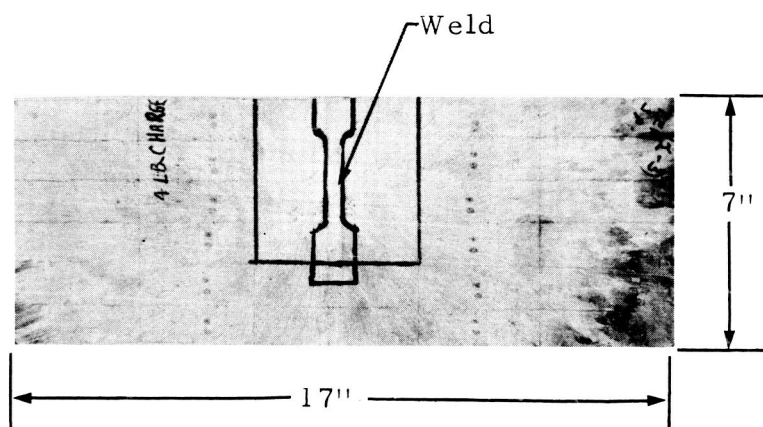


FIGURE 58. APPEARANCE OF 3/4" THICK 2219-T87
WELDMENT AFTER EXPLOSION IMPACT LOADING
WITH A 4-POUND CHARGE OF PENTOLITE (PLATE NO. 25).

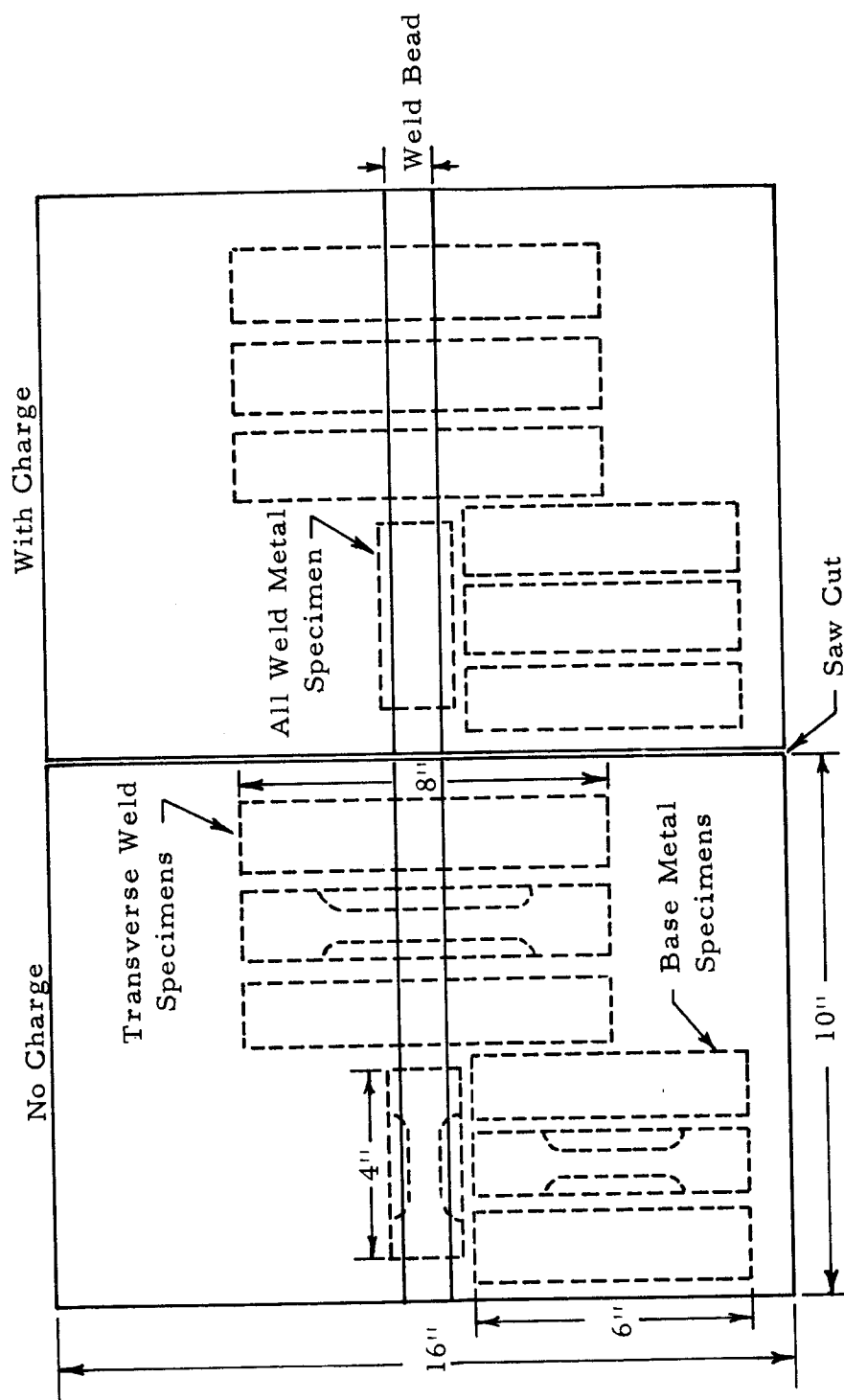


FIGURE 59. SEQUENCE USED IN REMOVING ALL WELD METAL, TRANSVERSE WELD AND BASE METAL TENSILE SPECIMENS FROM 3/4 INCH THICK 2219-T87 BUTT WELDED PANELS

TABLE VI
MECHANICAL PROPERTIES OF 2219-T87 WELDMENTS AND BASE
METAL BEFORE AND AFTER EXPLOSIVE IMPACT LOADING

Specimen Description	Plate No.	Plate Charge	Specimen No.	Ultimate Strength (psi)		Yield Strength (.2% Offset) psi		Percent Elongation (In 2 Inches))	
				No	Charge	No	Charge	No	Charge
Weld Metal	30	2	1	39,200	41,600	12,920	30,800	18.4	19.3
				39,300	41,400	15,430	33,100	20.2	10.1
Transverse to weld	30	2	1	39,600	40,800	21,150	31,750	4.7	4.9
			2 ^a	40,300	33,900	22,100	29,550	4.9	2.2
			3	40,100	39,850	21,700	31,250	4.9	4.0
			Av.	40,000	40,325	21,650	30,850	4.8	4.5
			1	41,400	41,900	22,900	32,700	5.4	5.7
Base Metal	30	2	2	40,500	--	21,900	--	5.4	--
			Av.	40,950	41,900	22,400	32,700	5.4	5.7
			1	64,800	64,300	57,700	52,900	14.0	15.8
			2	69,800	64,400	56,400	53,600	13.5	13.5
	25	4	3	68,700	64,400	56,700	53,300	14.6	14.1
			Av.	67,766	64,183	56,933	53,266	14.1	14.5
			1	64,600	63,200	52,800	52,600	12.8	11.3
			2	64,200	63,200	53,300	52,500	13.2	11.4
			3	66,400	62,800	53,000	51,300	13.7	14.5
			Av.	65,066	63,066	53,033	52,133	13.3	12.4

^a - contained lack of penetration

TABLE VII

EFFECT OF EXPLOSIVE LOADING ON THE MECHANICAL PROPERTIES OF 3/4 INCH
2219-T87 WELDMENTS AND BASE METAL, SUMMARIZED FROM TABLE VI

	Average Ultimate Strength (psi)				Average Yield Strength (.2% Offset) psi				Average Percent Elongation (2 Inch Gage Length)			
	With Charge		Percent Change		With Charge		Percent Change		No Charge		With Charge	
	No Charge				No Charge				No Charge			
<u>Weld Metal</u>												
Plate 30 ^a	39,200	41,600	+6.1%		12,920	30,800	+138%		18.4	19.3	*	
Plate 25 ^b	39,300	41,400	+5.3%		15,430	33,100	+114%		20.2	10.1	-50%	
<u>Transverse Weld Specimens</u>												
Plate 30	40,000	40,325	+0.8%		21,650	30,850	+42.5%		4.8	4.5	*	
Plate 25	40,950	41,900	+2.3%		22,400	32,700	+46.0%		5.4	5.7	*	
<u>Base Metal</u>												
Plate 30	67,766	64,183	-5.3%		56,933	53,266	-6.4%		14.1	14.5	*	
Plate 25	65,066	63,066	-3.1%		53,033	52,133	-1.7%		13.3	12.4	*	

a - 2 pound charge of pentolite

b - 4 pound charge of pentolite

* - Negligible

corresponding change in elongation for the weld metal specimen from plate No. 30 was negligible. The reason for the difference in the weld metal ductility of the two test panels is believed to be due to the explosive loading procedure rather than to the charges used (2 pounds vs. 4 pounds). This difference in procedure is shown in Figure 60. The weld crown on Panel No. 30 did not show any visible signs of deformation on either the top or bottom surface of the panel after explosive loading. On the other hand, the weld crown was completely flattened on the bottom surface of plate No. 25 since no base plate groove was provided for the weld crown. The gross plastic deformation of the weld metal is believed to be responsible for the lower ductility of the weld metal from Panel No. 25. Figure 61 shows a cross-section of the weld from Panel No. 25. A pronounced difference in the structure of the weld metal at the top and bottom of the joint is evident. The structure of the top reinforcement is the usual coarse dendritic structure. The bottom reinforcement was deformed by the force of the explosion and it appears that a certain amount of grain refinement was accomplished. Figure 62 shows the cross-section of the weld from Panel No. 30. The weld crown at the bottom surface of the panel was forced into the base plate groove and actually assumed the contour of the sides and bottom of the groove.

Knoop microhardness surveys were made across the weld zone to determine the effect of explosive loading. These surveys were run parallel to the top and bottom surfaces of the test panels. A small increase in

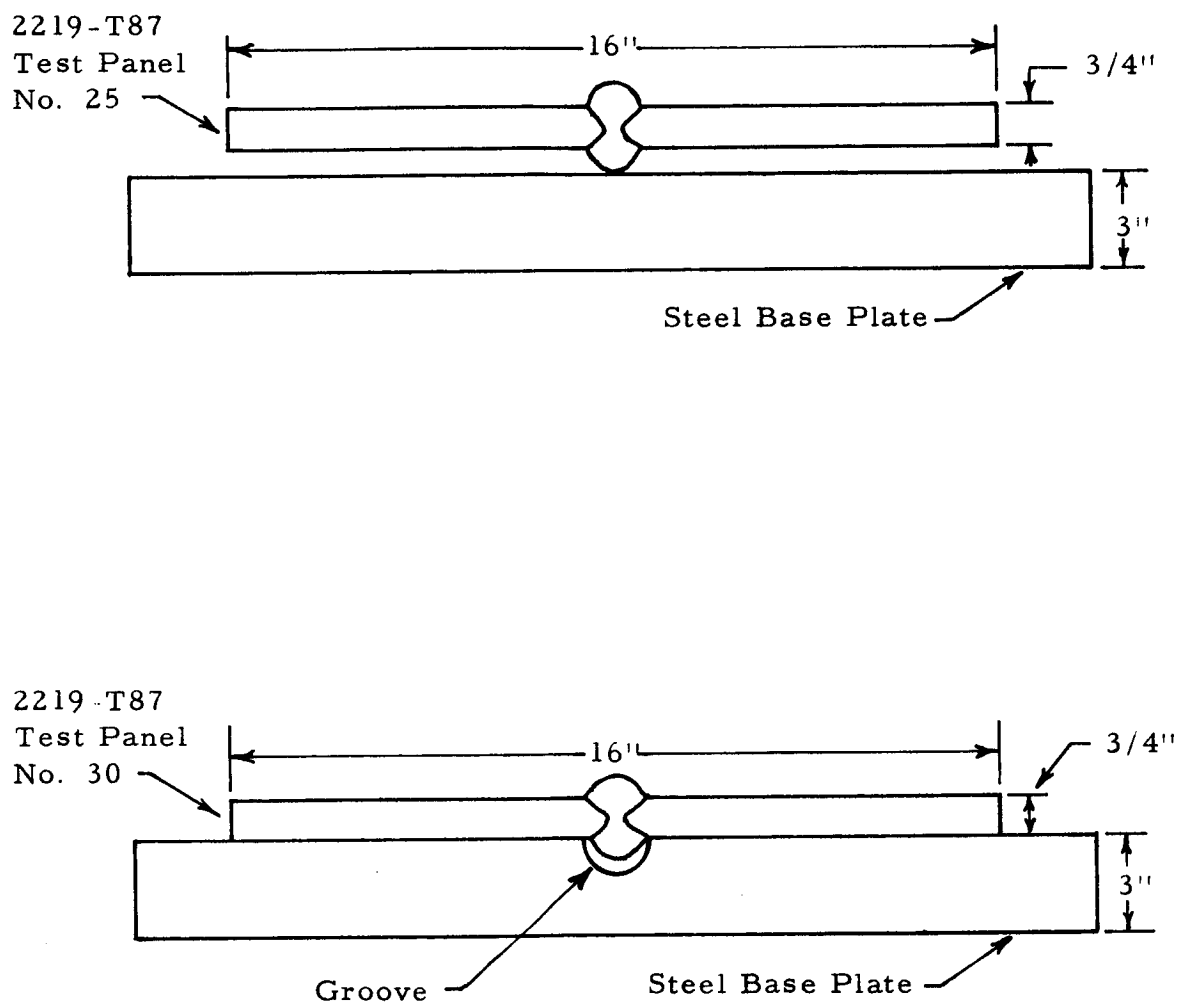


FIGURE 60. RELATIVE POSITIONS OF 3/4 INCH THICK 2219-T87 TEST PANELS NUMBERS 25 AND 30 ON THE STEEL BASE PLATE

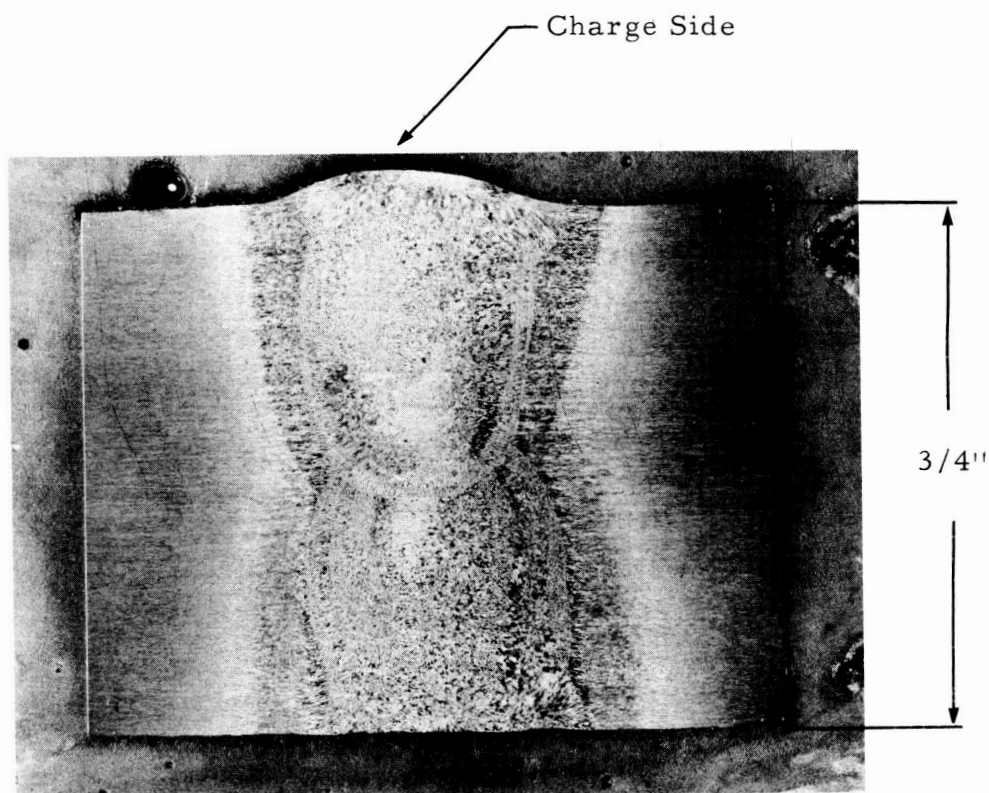


FIGURE 61. CROSS-SECTION OF THE WELD FROM TEST PANEL NO. 25. Panel was fabricated from $3/4$ inch thick 2219-T87 aluminum plate. A four pound charge of pentolite was fired above the panel. Note that the weld crown at the bottom surface was flattened out when the panel was forced against the steel base plate. This gross plastic deformation resulted in the refinement of the coarse columnar grain structure found in the crown area of the joint.

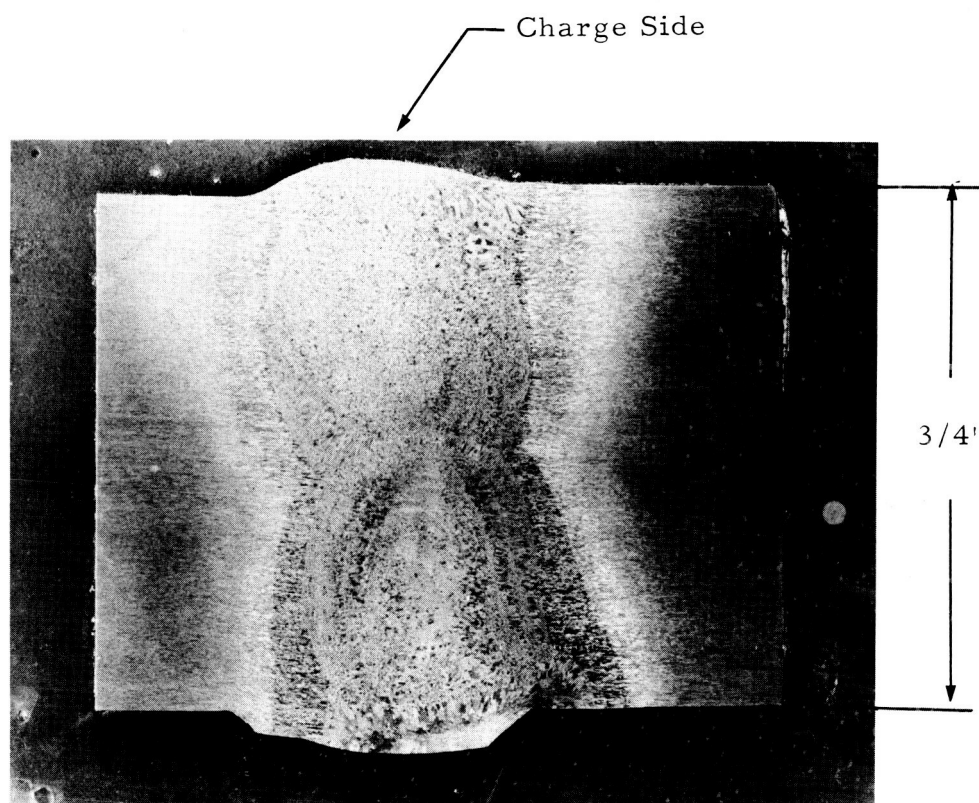


FIGURE 62. CROSS-SECTION OF THE WELD FROM TEST PANEL NO. 30. Panel was fabricated from 3/4 inch thick 2219-T87 aluminum plate. A two pound charge of pentolite was fired above the panel. The weld crown at the bottom surface of the panel was forced into the base plate groove and has assumed the contour of the sides and bottom of the groove.

hardness occurred in the different areas of the weld zone near the top (explosive charge) side of both panels. A larger increase in hardness occurred in the weld zone at the bottom side of the test panels. This was especially true for Panel No. 25 and is attributed to the gross plastic deformation which occurred when the weld crown was flattened. Figures 63, 64, 65, and 66 illustrate the hardness levels existing before and after impact loading near the top and bottom sides of both panels.

Figure 67 illustrates the difference in the hardness levels across the weld zones near the top and bottom sides of Panel No. 25 (four-pound charge). This difference was much greater than that found in Panel No. 30 (two-pound charge) and is attributed to the increase in hardness resulting from the flattening out of the bottom weld crown in Panel No. 25. The greater overall hardness of Panel No. 25 correlates well with the decrease in ductility observed after explosive impact loading.

The results of these tests indicate that strain hardening resulting from explosive loading appears to be an effective method of increasing the yield strength of 2219-T87 weldments. Although the ultimate strength is affected very little, the increase in yield strength is obtained without a drastic reduction in ductility which normally occurs when conventional cold working methods are used. This is probably due to the different manner in which metals deform when subjected to impulse loads of high magnitude and short duration as compared to steady, low magnitude loads.

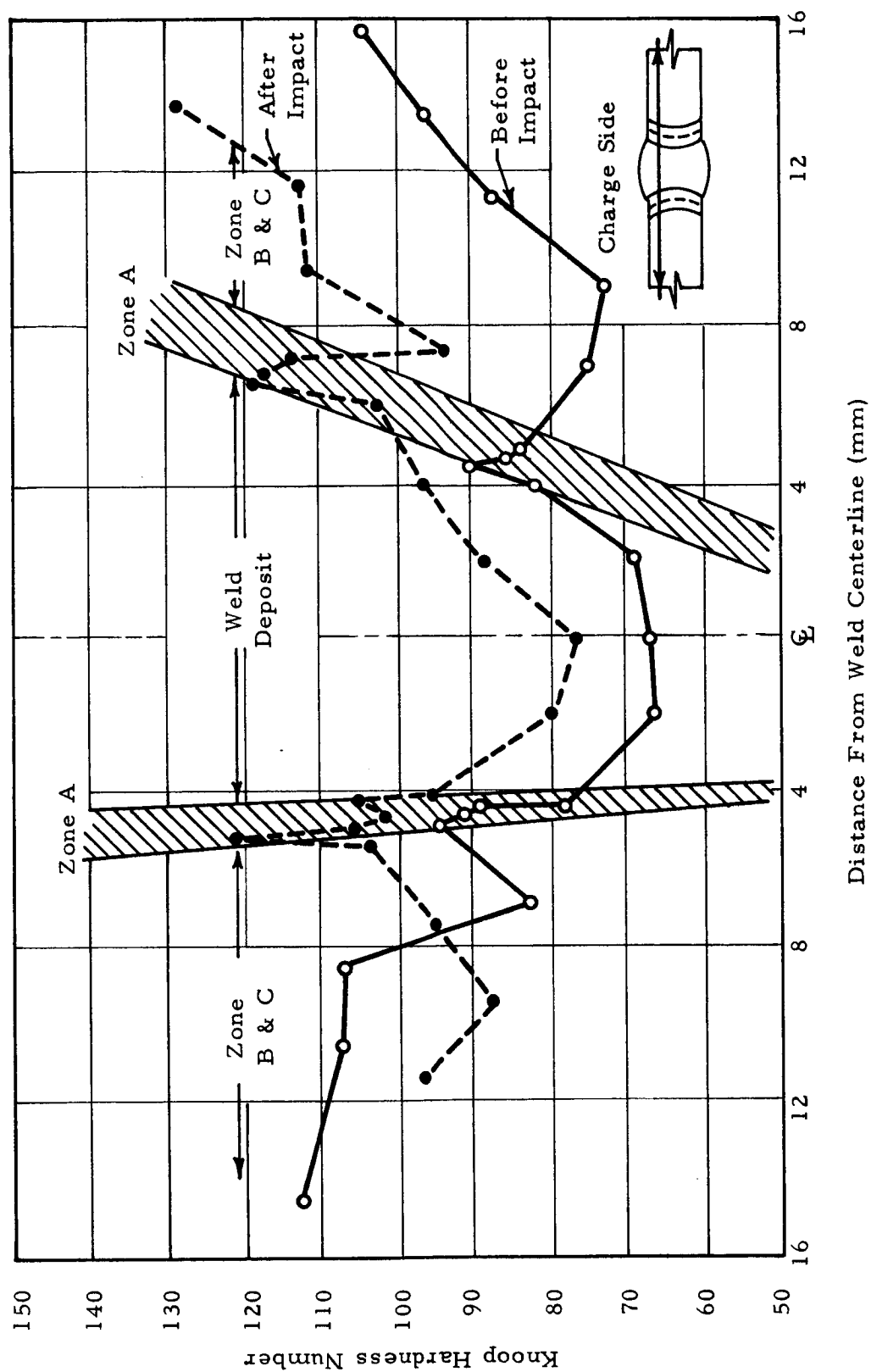


FIGURE 63. EFFECT OF EXPLOSIVE IMPACT LOADING ON WELD ZONE HARDNESS OF PANEL NO. 30. Panel was subjected to a two pound charge of pentolite.

Insert shows location of hardness traverses.

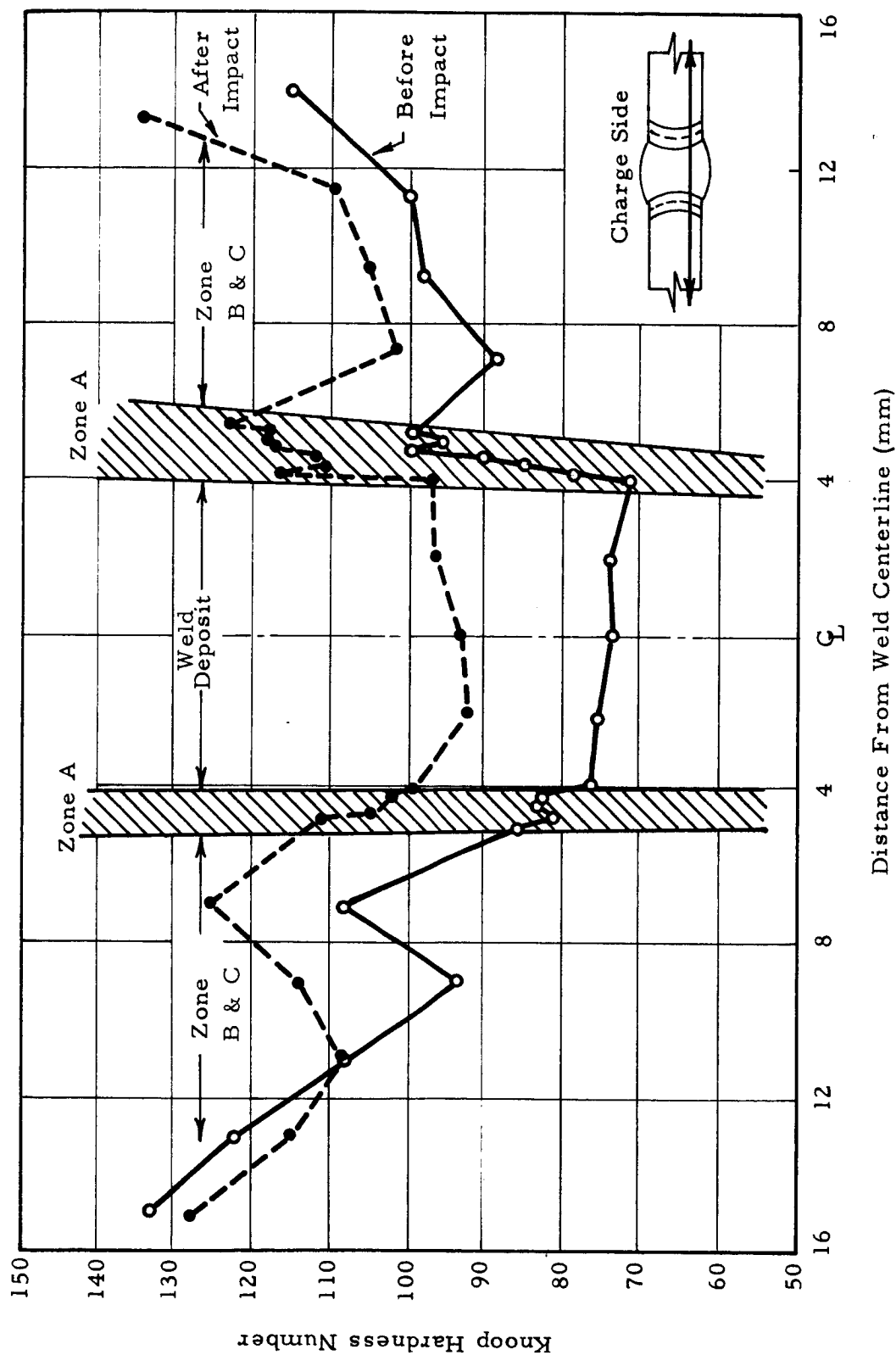


FIGURE 64. EFFECT OF EXPLOSIVE IMPACT LOADING ON WELD ZONE HARDNESS OF PANEL NO. 30. Panel was subjected to a two pound charge of pentolite. Insert shows location of traverses.

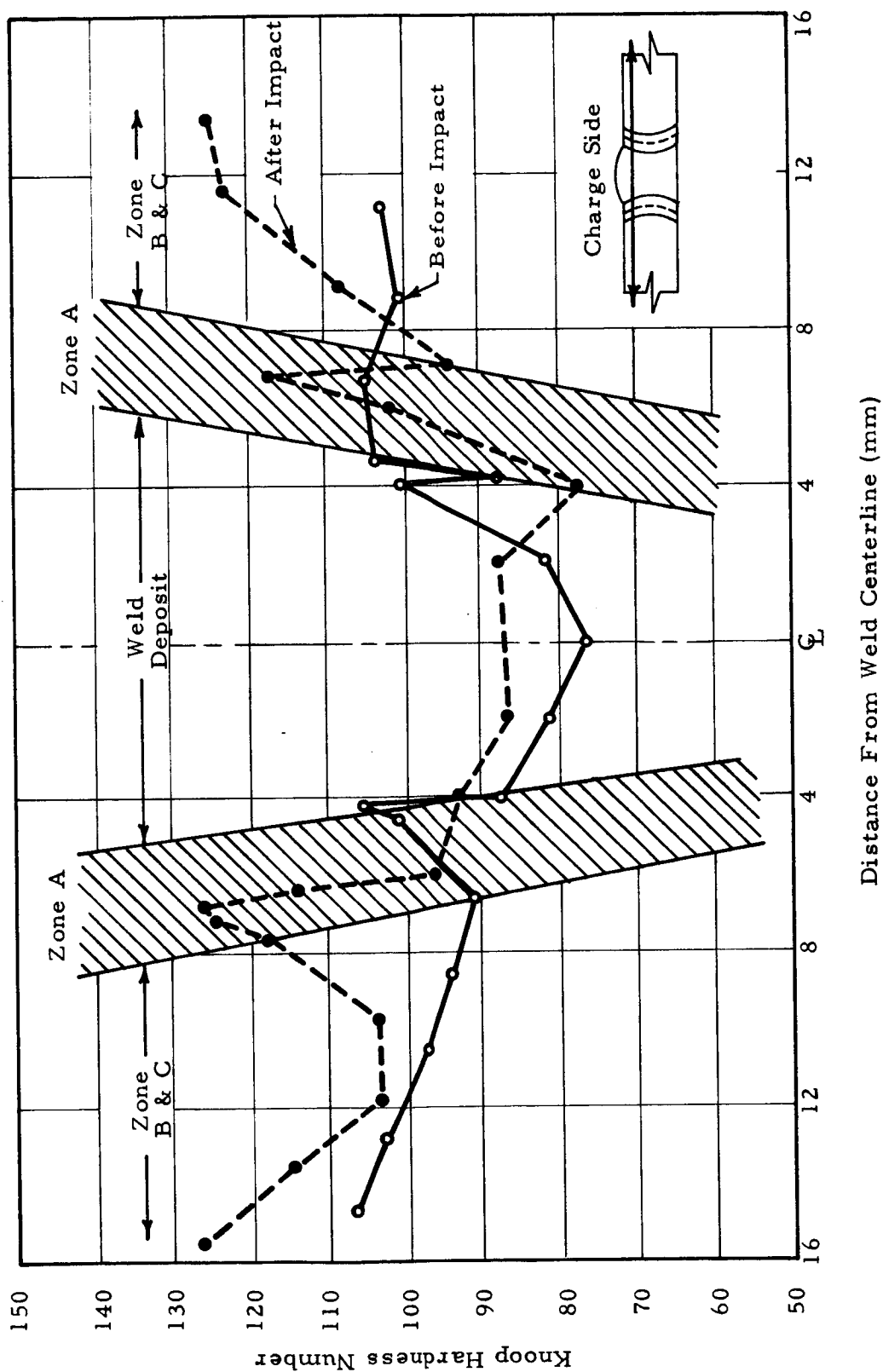


FIGURE 65. EFFECT OF EXPLOSIVE IMPACT LOADING ON WELD ZONE HARDNESS OF PANEL NO. 25. Panel was subjected to a four pound charge of pentolite. Insert shows location of traverses.

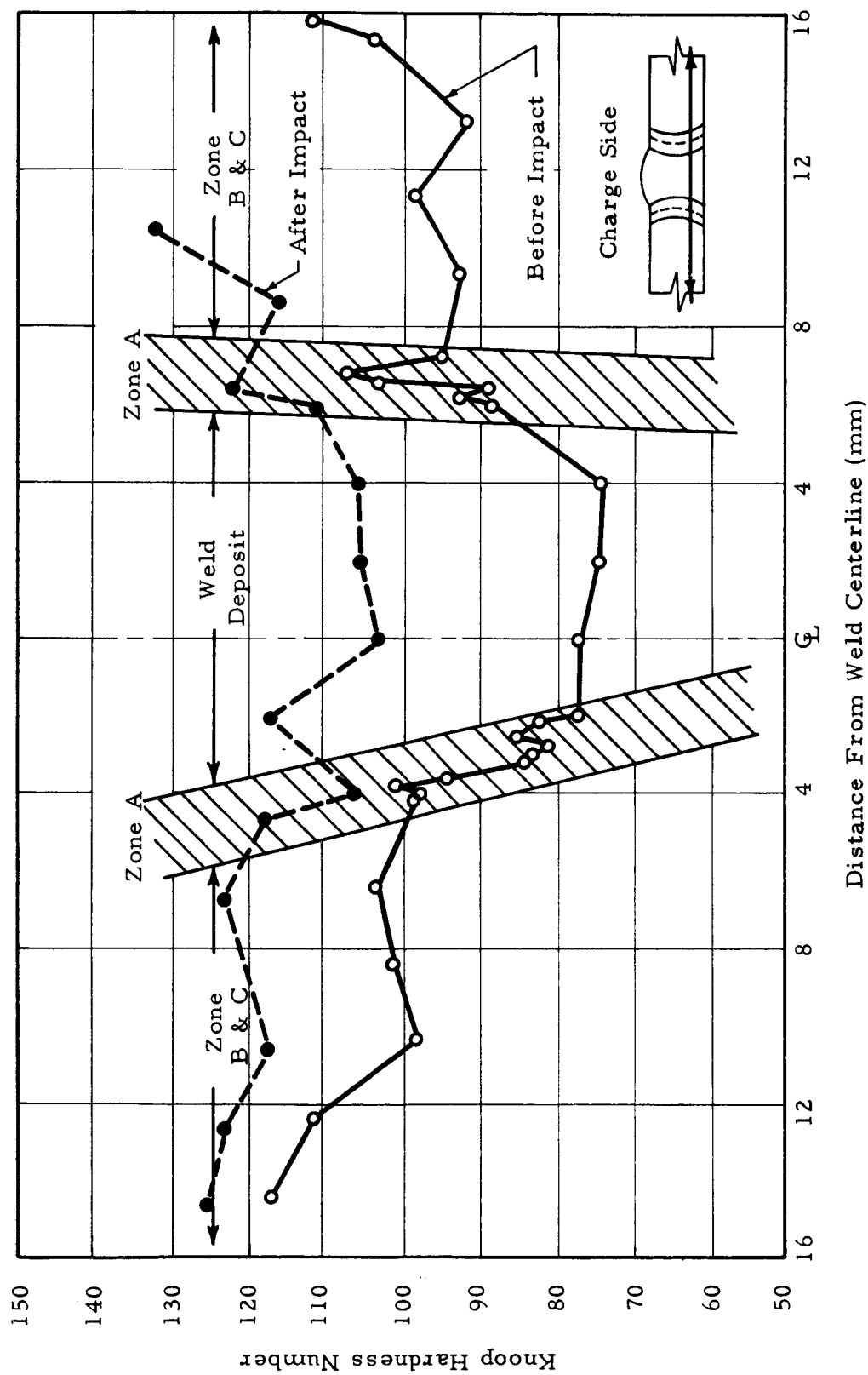


FIGURE 66. EFFECT OF EXPLOSIVE IMPACT LOADING ON WELD ZONE HARDNESS OF PANEL NO. 25. Panel was subjected to a four pound charge of pentolite.

Insert shows location of traverses. Weld crown was flattened out as a result of test procedure used.

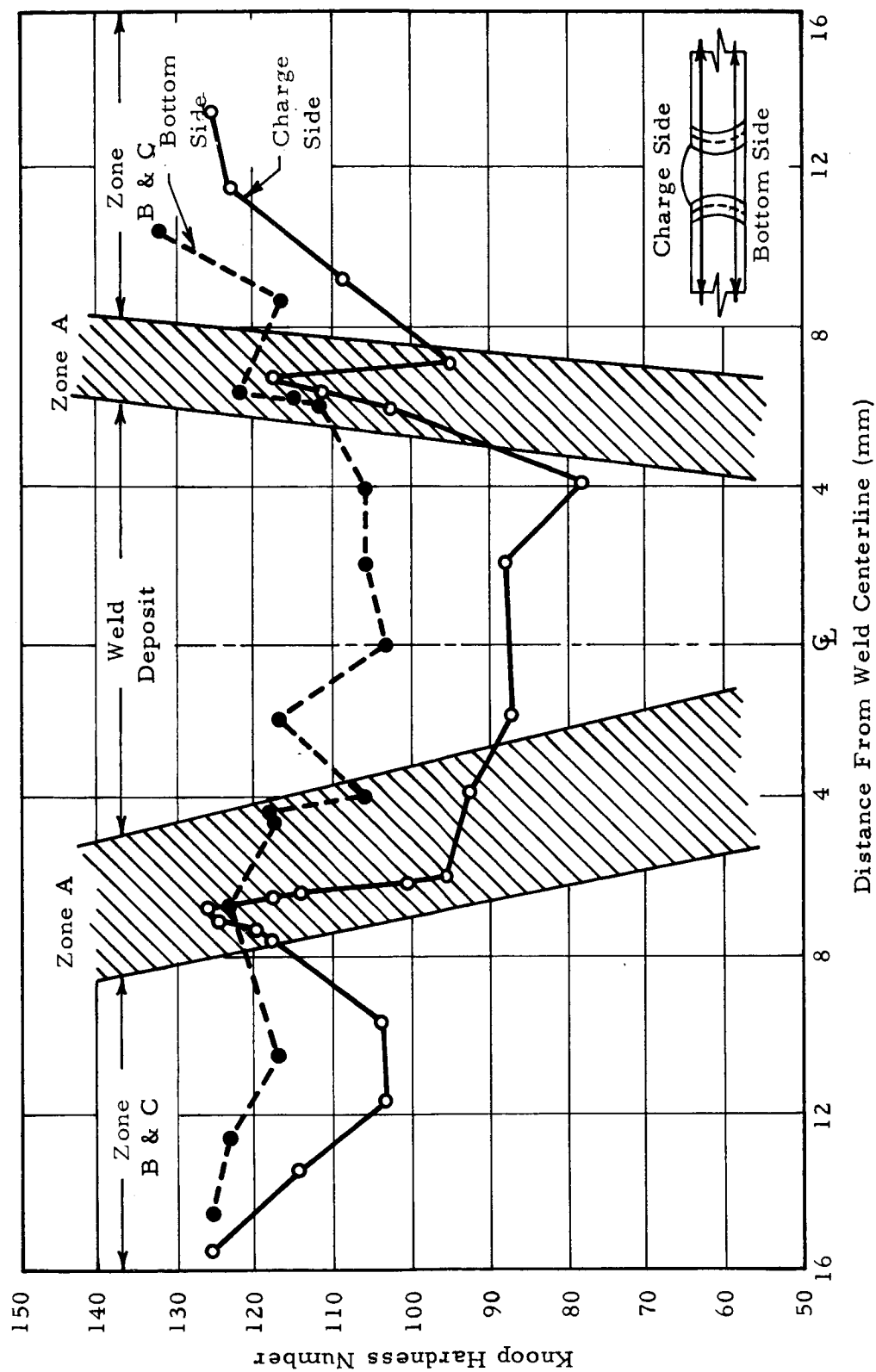


FIGURE 67. INCREASE IN WELD ZONE HARDNESS DUE TO FLATTENING OUT OF WELD CROWN ON BOTTOM SIDE OF PANEL NO. 25.

Insert shows locations of traverses.

These tests also indicate that the improvement in the yield strength of these weldments is derived mainly from improved yield strength in the weld metal since base metal properties were not changed appreciably by explosive loading. An alternate loading procedure could thus be used in which strips of plastic explosive would be attached to the weld so that only the weld metal would be subjected to the impact loading. Distortion would be minimized by placing the explosive on both sides of the weldment and detonating simultaneously.

VI. SUMMARY AND CONCLUSIONS

The behavior of welded 2219 aluminum plate under uniaxial loading was thoroughly investigated. The statistical limit of 38,000 psi as an ultimate strength level was obtained.

The major effort was directed toward a better understanding of the strain behavior of welded joints where the weld deposit strength greatly undermatches that of the base metal. It was determined that substantially all of the plastic strain which occurs in a transverse weld test takes place in the weld deposit or in the zone immediately adjacent to the weld fusion line which has been softened by the heat of welding. Determining the 0.2 percent offset yield strength based on a two-inch gage length extensometer consequently is erroneous, since at that level of stress substantial strain (about 1.25 percent) will have occurred in the weld deposit. The work suggests that a shorter gage length extensometer be used for engineering determinations or that strain gages be employed for more accurate determinations.

The fracture characteristics showed a consistent relationship between the point of initiation and the weld orientation. The cracks always initiated at the bottom toe of the weld and propagated diagonally through the weld. At this location there was a dense precipitate of an intergranular CuAl_2 eutectic, which is brittle. The fractures were primarily

intergranular. Removal of the weld crown by machining resulted in a slight decrease in strength and increase in ductility. Re-fusing of the toe area by welding resulted in a slight increase in strength and increase in ductility.

The biaxial test provides a good method for studying the fracture characteristics under combined loading conditions.

VII. LITERATURE SURVEY

BIBLIOGRAPHY

1. Keller, F. and Wilcox, G. W.: "Identification of Constituents of Aluminum Alloys." Alcoa Technical Paper #7, Revised 1958.
2. Mayer, L. W.: "Alcoa Aluminum Alloy 2219. "Aluminum Company of America, Sales Development Division.
3. Lankford, W. T.: "Hydraulic Bulge Testing of Sheet Metals." ASTM STP No. 87, June 1948, pp. 66-82.
4. Robinson, I. B., Collins, F. R., and Dowd, J. D.: "Welding High Strength Aluminum Alloys." Welding Journal, Research Suppl., 1962, 41 (5), 221-S to 228-S.
5. Robinson, I. B., Collins, F. R., and Dowd, J. D.: "Hydraulic Bulge Test For Welded Aluminum Sheet." Welding Journal, Research Suppl., 1961, 40 (12), 540-S to 545-S.
6. Corrigan, D. A., Travis, R. E., Ardito, V. P., and Adams, C. M., Jr.: "Biaxial Strength of Welds in Heat Treated Sheet Steel." Welding Journal, Research Suppl., 41 (3), 123-S to 128-S, 1962.
7. Baird, B. L.: "Studies of Design Criteria for Welded Structures Subjected to a Biaxial Stress Field." Rpt. Nr. ASD-TDR-62-1109, January 1963.
8. Terry, E. L. and McClaren, S. W.: "Biaxial Stress and Strain Data on High Strength Alloys for Design of Pressurized Components." Rpt. Nr. ASD-TDR-62-401, July 1962.
9. Kelley, K. K.: "Contributions to the Data on Theoretical Metallurgy." Vol. XIII, Bulletin 584, Bureau of Mines, 1960.
10. Liquid-Metals Handbook, NAVEXOSP-733, Atomic Energy Commission, Department of the Navy, Washington, D. C., 1950.
11. Smithells, C. J.: Metals Reference Book, Interscience Publishers, Inc. New York, 1949.

VII. LITERATURE SURVEY (Cont'd)

BIBLIOGRAPHY

12. Lessels, J. M. and MacGregor, C. W.: "Combined Stress Experiments on a Nickel-Chrome-Molybdenum Steel." Journal of The Franklin Institute, Vol. 230, No. 1, July 1940, pp 163-182.
13. "New High Strength Aluminum Alloy is Tough, Weldable". Materials in Design Engineering, February 1964, Vol. 59, No. 2, pp 88-89.
14. Petty, E. R.: "The Deformation Behavior of Some Aluminum Alloys Containing Intermetallic Compounds". Journal of The Institute of Metals, 1962-63, Vol. 91, Part 8, pp 274-279.
15. Adams, D. F. and Dinsdale, W. D.: "Effects of Chilling During Welding on the Static and Fatigue Properties of H30 Aluminum Alloy". British Welding Journal, October 24, 1962, Vol. 9, No. 10, pp 559-566.
16. "Tensile Testing With a Blunt Notch". Welding Handbook, 1962, Fifth Edition, Section 1, pp 6.10 - 6.12.
17. Brown, E. P. and Adams, C. M., Jr.: "Fusion-Zone Structures and Properties in Aluminum Alloys". Welding Journal, December 1960, Vol. 39, No. 12, pp 523s - 524s.
18. Phillips, A. and Bennet, G. V.: "The Electron Microscope - A New Tool For Examining Fractures". Metal Progress, May 1961, Vol. 79, No. 5, pp 97-102.
19. Elliot, E.: "Aluminum and Its Alloys in 1960". Metallurgia, Vol. 63, No. 376, February 1961, pp 65-70, No. 377, March 1961, pp 105-114.
20. Forsyth, P. J. E. and Ryder, D. A.: "Some Results of the Examination of Aluminum Alloy Specimen Fracture Surfaces". Metallurgia, Vol. 63, No. 377, March 1961, pp 117-124.
21. Jaeger, J. C.: Elasticity, Fracture and Flow, John Wiley and Sons, Inc., New York, 1962, pp 92-97.
22. "Determination of Failure Stress For Parent Metal and Weldments (Space Vehicle Systems All Phases)". NASA Inhouse Publication.

VII. LITERATURE SURVEY (Cont'd)

BIBLIOGRAPHY

23. Beachem, C. D.: "An Electron Fractographic Study of the Influence of Plastic Strain Conditions Upon Ductile Rupture Processes in Metals". Transactions ASM, Vol. 56, No. 3, September 1963, pp 318-326.
24. Pelloux, R. M. N.: "The Analysis of Fracture Surfaces by Electron Microscopy". Boeing Scientific Research Laboratory Report No. D1-82-0169-R1, December 1963.
25. Beachem, C. D. and Pelloux, R. M. N.: "An Electron Fractography - A Tool for the Study of Micro-Mechanisms of Fracturing Processes", Preprint of paper presented at the ASTM Annual Meeting, June 1964.

"IDENTIFICATION OF CONSTITUENTS OF ALUMINUM ALLOYS"*

Keller-Wilcox

A means of identifying twenty aluminum constituents was presented. The procedure outlined consisted of polishing and etching an unknown sample and comparing the resultant structure with standard photomicrographs. The structure and appearance of twenty individual constituents for six different aluminum etchants were recorded. The as-polished appearance of the standards was also recorded

* Abstract of Article No. 1 as noted in Bibliography.

"ALCOA ALUMINUM ALLOY 2219"*

Mayer

This article deals with chemical composition, high and low temperatures, mechanical properties, heat treatment and other aspects of 2219. Aluminum copper alloy, 2219, was originally developed for use at elevated temperatures. The alloy is quite amenable to heat treatment and results in high strength at ambient temperature.

* Abstract of Article No. 2 as noted in Bibliography.

"HYDRAULIC BULGE TESTING OF SHEET METALS"*

Lankford

This article describes the results of a fundamental study of the strain hardening characteristics and the ductility of sheet metals under biaxial stresses produced by bulging the sheet. The author traces the development of the hydraulic bulge test and describes the test procedure used for thin gage sheet. The extent of bulging was determined by measuring the radius of curvature at the top of the bulge using a three point spherometer carrying a dial gage reading to 0.0001 inch. Strains were determined with the aid of a twenty line to the inch photogrid applied at the center of the specimen. The distortion undergone by the grid during bulging was taken as a measure of elongation. In addition to the circular bulge test, the author also describes an elliptical bulge test which produces an unbalanced biaxial stress system in the bulged material.

* Abstract of Article No. 3 as noted in Bibliography.

"WELDING HIGH STRENGTH ALUMINUM ALLOYS"*

Robinson-Collins-Dowd

The authors evaluate the weldability of the 2000 series and the 7000 series high strength aluminum alloys. It was pointed out that the results obtained with the common uniaxial tensile test do not correlate well with the performance of pressure vessels made with these high strength alloys. A better correlation is obtained using either the hydrostatic test of cylinders or small size pressure vessels or the hydraulic bulge test. This latter test is used to evaluate the effect of variations in welding procedures on the performance of the resulting welds. The results obtained indicate that 2219 alloy is the easiest to weld and the least sensitive to variations in welding procedure. Of the higher strength alloys, 7178 is the most weldable, being appreciably better than 7075 in ease of welding, resistance to weld cracking, and consistency of weld properties.

* Abstract of Article No. 4 as noted in Bibliography.

"THE HYDRAULIC BULGE TEST FOR WELDED ALUMINUM SHEET"*

Robinson-Collins-Dowd

Described in this article was a laboratory bulge testing machine capable of bulging 0.125 inch thick high strength aluminum alloy sheet. The results of such tests are known to correlate well with the performance of welded structures of high strength aluminum alloys. This is not the case for results of cross-weld tensile tests. The tester described has an 8 inch circular die opening and features instrumentation designed to measure pressure and bulge height during testing. Biaxial tensile stress is calculated from values of pressure and bulge height measured during the test.

* Abstract of Article No. 5 as noted in Bibliography.

"BIAXIAL STRENGTH OF WELDS IN HEAT TREATED SHEET STEEL"*

Corrigan-Travis-Ardito-Adams

A technique was developed to study the mechanical behavior of high strength steel sheets and weldments under conditions of biaxial tensile loading. This technique utilizes a slotted sheet tensile specimen in which a large plastic bulk is used to restrain plastic flow in a direction perpendicular to that of the applied tensile load. Specimen geometry used to produce a 2:1 ratio of principal stresses called for a slot width of $3t$ with a specimen width (slot length) of $30t$, where t is the thickness of the sheet material being tested. The amount of plane strain attained was determined with the aid of a 20 line per inch grid applied to the specimen. The results of these tests indicated that uniaxial tensile strength increases of greater than 10 per cent are possible for both base metal and weldments under 2:1 biaxial loading conditions.

* Abstract of Article No. 6 as noted in Bibliography.

"STUDIES OF DESIGN CRITERIA FOR WELDED STRUCTURES
SUBJECTED TO A BIAXIAL STRESS FIELD"*

Baird

Parent and weld metal biaxial stress-strain data were obtained in a 2:1 tension-tension stress field from four steels and one titanium alloy at three test temperatures. Honed and ground tubular specimens containing two longitudinal seam welds were tested using strain gage rosettes attached in both weld and parent metal zones to develop biaxial stress-strain relationships. Values of fabrication stress concentration factors were obtained from burst testing welded vessels made from the test materials. The text also illustrates the use of biaxial stress-strain data along with the fabrication stress concentration factor values into design high strength vessels.

* Abstract of Article No. 7 as noted in Bibliography.

"BIAXIAL STRESS AND STRAIN DATA ON HIGH STRENGTH ALLOYS
FOR DESIGN OF PRESSURIZED COMPONENTS"*

Terry-McClaren

A cross-shaped specimen was developed for generating complete biaxial stress-strain curves under 1:1 and 2:1 biaxial tension stress ratio loading. Tests on several materials have shown that the specimen has good reliability.

The influence of strength level on the behavior of a 5 Cr-Mo-V steel under biaxial loading was investigated. These tests showed that by lowering the uniaxial strength level from 280 to 260 ksi, the shattering type failure observed at the 280 ksi level ceased to exist. Good correlation was obtained between the failure stresses from these biaxial specimens and from small scale pressure vessels hydrostatically tested to failure.

* Abstract of Article No. 8 as noted in Bibliography.

"CONTRIBUTIONS TO THE DATA ON THEORETICAL METALLURGY"*

Kelley

High-temperature heat content, heat capacity and entropy data for the elements and inorganic compounds were tabulated. Values were intercompared and the best values selected.

* Abstract of Article No. 9 as noted in Bibliography.

"LIQUID-METALS HANDBOOK"*

R. N. Lyon, Editor

In this book the information available concerning the use of liquid metals as a heat transfer medium was summarized. Among the topics discussed were industrial use, chemical and physical properties, and liquid-metal heat transfer.

* Abstract of Article No. 10 as noted in Bibliography.

"METALS REFERENCE BOOK"*

Smithells

Data relating to metallurgy and metal physics was compiled. The presentation was in the form of tables and diagrams. Certain short monographs were also included.

* Abstract of Article No. 11 as noted in Bibliography.

"COMBINED STRESS EXPERIMENTS ON A NICKEL-CHROME-
MOLYBDENUM STEEL"*

Lessels - MacGregor

The authors describe a tubular specimen for obtaining uniaxial and biaxial stresses. To obtain biaxial stress internal pressure was applied to the specimen. A wide range of biaxial stresses can be obtained with this type of specimen by the application of both tensile load and internal pressure.

This type specimen was considered as a means of checking the stresses developed in the hydraulic bulge welded panels.

* Abstract of Article No. 12 as noted in Bibliography.

"NEW HIGH STRENGTH ALUMINUM ALLOY IS
TOUGH, WELDABLE"*

- - - - -

This article describes a relatively new high strength aluminum alloy designated as 7039. A comparison was made between this alloy, 2219, 5083 and 2014. The 7039 alloy was reported to have good cryogenic properties and will be quite useful for ordnance and missile structures. At 75° and -350°F the strength of 7039-T6 was found to be superior to 2219-T81 and 5083-H113 in both strength and notched-unnotched strength ratio. At 75°F, 7039-T6 was slightly lower in strength than 2014-T6, but had a slightly higher notched-unnotched tensile strength ratio. At -320°F the tensile strength and notched-unnotched tensile strength ratio was about the same.

Fatigue strength of 7039-T6 was superior to the other alloys studied. After 10^8 cycles, the fatigue strength of 7039-T6 was approximately 5,000 psi higher than the 5083-H113, and almost 12,000 psi higher than the 2219-T81.

The weldability was reported to be quite good from the standpoint of resistance to cracking. A comparison was made between 7039, 7079 and 2219. These tests showed that 7039 was superior.

* Abstract of Article No. 13 as noted in Bibliography.

"THE DEFORMATION BEHAVIOR OF SOME ALUMINUM
ALLOYS CONTAINING INTERMETALLIC COMPOUNDS"*

Petty

Tensile and rolling tests were made on aluminum alloys containing various dispersions of CuAl_2 and FeAl_3 . This study showed the importance of size, shape and amount of the phases on strength, plasticity and deformation over a range of temperatures. Tensile test of alloys containing 1.9 and 10 percent Fe resulted in equal strengths at all temperatures up to about 500°C . In fact, at temperatures above 400°C these alloys were stronger than alloys containing up to 40.4 percent Cu.

The iron alloys were rolled at temperatures up to 500° to investigate the plasticity of the particles. Samples were then examined metallographically. Little difference was noted in the behavior of the FeAl_3 particles. Of particular interest were micrographs of FeAl_3 . These particles were relatively large and rectangular in shape.

* Abstract of Article No. 14 as noted in Bibliography.

"EFFECTS OF CHILLING DURING WELDING ON THE
STATIC AND FATIGUE PROPERTIES OF H30 ALUMINUM ALLOY"*

Adams - Dinsdale

The effect of modifying the heat-affected-zone of a 1/4 inch thick aluminum-manganese-silicon alloy by water chilled back up bars was studied. It was noted that static joint strength could be increased by 6,000 psi by this technique. Hardness surveys were made in the weld, HAZ and base metal of the material welded with the water chilled back up bar and compared with normally welded joints. This test also verified the fact that the HAZ could be greatly modified.

Fatigue tests were made and the results showed that fatigue strength was not affected. It was noted that post-weld aging of welds with the reinforcement left on, reduced the fatigue strength by 16 percent. The strength was improved slightly by removing the crown, although a complete analysis could not be made due to porosity inclusions.

* Abstract of Article No. 15 as noted in Bibliography.

"TENSILE TESTING WITH A BLUNT NOTCH"*

Under this topic in the first section of the Welding Handbook, The Massachusetts Institute of Technology biaxial tensile test specimen is described. It is reported that the increase in uniaxial ultimate strength of high strength aluminum is between 5 and 15 percent as a result of using this type specimen. In addition a drawing of the test specimen is shown. The effect of specimen geometry on tensile strength is illustrated by curves. A specimen width about 25 to 30 times the slot thickness is required for maximum tensile strength.

* Abstract of Article No. 16 as noted in Bibliography.

"FUSION-ZONE STRUCTURES AND PROPERTIES IN ALUMINUM ALLOYS"*

Brown - Adams, Jr.

A study of the fusion zone in 2014 arc deposits was made. The relationship between finer dendritic size and lower heat input was established. It was noted that arc deposits represent more severe quenching rates than any form of chill casting. Time of solution treatment was reduced and ductility improved when the lower levels of heat input were used.

* Abstract of Article No. 17 as noted in Bibliography.

"THE ELECTRON MICROSCOPE -- A NEW TOOL FOR
EXAMINING FRACTURES"*

Phillips - Bennet

The greater depth of focus, resolution and obtainable magnification of the electron microscope over the optical microscope can be used in fracture studies. The 200,000X for the electron microscope as compared to the 2,000X of the optical indicates that many details hitherto undetermined can be revealed. Replica of the fractured surface can be made and examined. Fatigue, shear, ductile and brittle failures can be identified by this technique.

* Abstract of Article No. 18 as noted in Bibliography.

"ALUMINUM AND ITS ALLOYS IN 1960"*

Elliot

This review of aluminum highlights, 254 references, deals with all aspects of the metal for its extraction and fabrication through its properties. Developments in MIG and TIG welding are noted, and literature dealing with weld failure is also included.

* Abstract of Article No. 19 as noted in Bibliography.

"SOME RESULTS OF THE EXAMINATION OF ALUMINUM
ALLOY SPECIMEN FRACTURE SURFACES"*

Forsyth - Ryder

This paper discusses the use of the electron microscope as applied in fractography of aluminum alloy failures. Brittle intercrystalline tensile fracture was one of the types of failure examined and theory for its occurrence is advanced.

* Abstract of Article No. 20 as noted in Bibliography.

"ELASTICITY, FRACTURE AND FLOW"*

Jaeger

The author discusses the von Mises yield criterion. The criterion is expressed as $\sigma_1^2 - \sigma_1\sigma_2 + \sigma_2^2 = \sigma_0^2$. σ_1 and σ_2 are the maximum and minimum stresses in a biaxial stress field.

* Abstract of Article No. 21 as noted in Bibliography.

"DETERMINATION OF FAILURE STRESS FOR PARENT METAL AND
WELDMENTS (SPACE VEHICLE SYSTEMS, ALL PHASES)"*

This is a NASA "inhouse" publication of design criteria. Failure stresses are to be determined on a statistical basis with a 95 percent confidence level. Weld strength data should be representative of fabrication practices.

* Abstract of Article No. 22 as noted in Bibliography.

"AN ELECTRON FRACTOGRAPHIC STUDY OF THE INFLUENCE
OF PLASTIC STRAIN CONDITIONS UPON DUCTILE RUPTURE
PROCESSES IN METALS"*

Beachem

Electron microscopic studies of a large number of metal fracture surfaces have shown that a considerable proportion of mechanical fractures occurs by some form of ductile rupture usually by void coalescence, regardless of the macroscopic appearance of the fracture surfaces. A long-term study of ductile rupture surfaces revealed three different but closely related modes of void coalescence: depending upon the stresses in the material surrounding it, a group of voids may coalesce by normal rupture, shear rupture, or tearing.

* Abstract of Article No. 23 as noted in Bibliography.

"THE ANALYSIS OF FRACTURE SURFACES BY
ELECTRON MICROSCOPY"*

Pelloux

This work reviews and illustrates the characteristic features of fracture in the categories listed below:

- 1) Transgranular Fracture
 - (a) Cleavage along crystallographic planes.
 - (b) Formation and coalescence of microvoids.
 - (c) Fatigue.
- 2) Intergranular Fracture
 - (a) Brittle fracture associated with perfect separation along grain boundaries.
 - (b) Ductile fracture associated with void formation at grain boundaries.

* Abstract of Article No. 24 as noted in Bibliography.

"AN ELECTRON FRACTOGRAPHY-A TOOL FOR THE STUDY OF
MICRO-MECHANISMS OF FRACTURING PROCESSES"*

Beachem - Pelloux

Uses of the electron microscope for the study of fracture surfaces and the subsequent formulation of models of fine-scale fracture mechanisms are demonstrated. Electron fractography is shown to be a valuable tool in obtaining a better understanding of fracture and in the analysis of service failures.

Various types of fracture surfaces produced by single cycle overload and by fatigue in various materials are discussed in order to indicate the usefulness of this relatively new tool.

The scope of application in the general field of fracture research is indicated.

* Abstract of Article No. 25 as noted in Bibliography.

APPENDIX I

One of the objectives of this program was to study the phases formed in the weld zones of 3/4 inch thick 2219-T87 aluminum weldments using 2319 as the filler metal. This portion of the program was presented in Section II "Weld Zone Investigation". A considerable number of tests were conducted to identify a "needle" like phase occurring in the toes of the weldments. However, in order to keep the presentation from becoming too lengthy, details of some of the tests were not given. For anyone desiring complete and detailed descriptions, the tests are discussed at length in this Appendix.

The dark "needle" like phase was tentatively identified as $\beta(\text{Al-Cu-Fe})$. However, it was not possible to establish this on a quantitative basis by either electron microprobe or X-ray diffraction techniques. In both instances, the laboratories conducting the respective tests indicated that sufficient quantity of the constituent was not present for positive identification.

The greatest concentration of "needles" has been located only in the bottom toes of the horizontal welds. Figure 8 shows a high concentration of "needles" in the toe of such a weld. The "needles" did not occur in all four toes of any one weld. Small amounts of "needles" were found near the fusion lines of some welds. The tests conducted to identify this phase follow:

1. A selective etching technique described in an Alcoa paper¹ was used in an effort to identify the "needle" phase. A similarity between the needles in the toes of welds and the $\beta(\text{Al-Cu-Fe})$ illustrated in the pamphlet for various etches was observed. However the results were not conclusive.

2. Electron microprobe analysis of the "needles" in a weld toe was conducted by Mr. J. R. Churchill, Chief, Analytical Chemistry Division, Aluminum Company of America. The following results were reported:

- a. Major amounts of Al, Cu and Fe were found together with minor amounts of Mn.
- b. The "needles" were too small for absolute quantitative analysis, but the relative concentrations of the major elements were indicative of the β (Al-Cu-Fe) phase.
- c. Metallographic examinations were made and the following was confirmed.

Mr. Churchill stated that β (Al-Cu-Fe) is commonly a constituent in welds of the 2219 alloy type and forms as a result of nonequilibrium conditions existing in welding. When equilibrium conditions exist, the β (Al-Cu-Fe) phase has a composition in the range of 27.0 - 32.0 percent copper and 14 - 17.5 percent iron. Other elements such as manganese can substitute for elements in this phase. It was also brought out that heat treatment is ineffective in removing the "needles."

3. A study was made to evaluate the possibility that segregation of alloying elements in the 2219 material or 2319 filler metal could be the cause of the "needle" formation.

This was achieved by examining the microstructures of a series of master alloys containing the elements in 2219. These master alloys were:

Al-Mn, Al-Fe, Al-Ti, Al-Zr, Al-V and two Al-Cu alloys. Al-Fe, Al-Mn, Al-Ti and Al-Zr had acicular structure somewhat resembling the "needles" in shape. However, etching these specimens and the toe region of a weld with the same etchants provided no correlation. From this investigation it was concluded that the presence of needles was unlikely to be the result of binary system; however, the possibility of element segregation was not ruled out.

4. The possibility that atmospheric contamination produced the "needles" was investigated. Hydrogen was considered because it could be produced from the decomposition of water vapor or migration from the base metal. However, porosity generally results from H_2 and it is unlikely that this gas is a factor in the presence of "needles". It seemed most likely that if atmospheric contamination produced the "needles", nitrogen would be the cause and aluminum nitride the product. A review of available literature did not produce any information concerning metallurgical studies of aluminum nitride in aluminum, but thermochemical data of a reaction between molten aluminum and N_2 to form aluminum nitride were obtained ^{2, 3, 4}.

Nitrogen was injected into the welding arc and also into molten metal. The following series of tests were made.

- a. N_2 injected into the arc at 4 psi and at 20 psi.
- b. N_2 injected into molten metal. A portion of the molten metal was air cooled and part water quenched.

Metallographic examination of these specimens were made and the results follows.

1. A massive plate-like precipitate was found in the welded sample with 20 psi N_2 injection. This was thought to be aluminum nitride; however, it did not resemble the "needles". No precipitates were observed in the 4 psi N_2 injection into the weld.

2. A "needle" like formation having some of the "needle" characteristics of the weld was found in the sample in which N_2 was injected into molten 2219 aluminum and air cooled.

3. No "needle" formation was found in the water quenched sample in which N_2 had been injected.

The last two tests indicated that possibly the rate of cooling influenced the formation of "needles" rather than some external contaminant such as N_2 . In addition to the "needle" formation in the air cooled sample, a concentration of $CuAl_2$ in the form of Chinese script was noted. Additional tests were made to study the influence of cooling rate on the formation of both the "needle" phase and the $CuAl_2$ network. The top surface of blocks of 2219 aluminum plate material approximately $2 \times 3/4 \times 1/2$ inch was melted with an oxy-acetylene flame. Heating was discontinued when the melted portion began to sag over the sides. The blocks were then quenched in several media that would result in different cooling rates. These media were water, oil, air blast and still air.

Metallographic examination revealed that the "needle" phase was almost absent in the water quenched sample. A considerable amount of "needles" plus the $CuAl_2$ network was noted in the sample cooled in still air. Both "needles" and $CuAl_2$ were found in varying degrees in the other samples quenched in oil and air blast; however, the water and still air samples contained the least and the greatest amounts of the two phases respectively.

The area where the "needles" and CuAl_2 phase in the melted 2219 plate material most closely resembled the condition in the weld toes was where the metal sagged over the side of the blocks. It appears, although it has not been confirmed, that cooling rate and/or concentration of elements in the sagging metal of both the blocks and weldments promotes the formation of the "needles" and CuAl_2 Chinese script network.

4. X-ray diffraction analysis was made of a toe region by Meta-Chem Laboratories, Inc., Houston, Texas, in an effort to identify the "needles". As with the electron microprobe analysis, positive identification was not possible. Their analysis showed that Fe and Mn were concentrated in the toe containing needles. Alcoa reported that other elements such as manganese could substitute for the elements in the $\beta(\text{Al-Cu-Fe})$ phase. Therefore it seems quite likely that the "needle" phase is $\beta(\text{Al-Cu-Fe})$.

APPENDIX II

WELDING PROCEDURES

All welding was done by the automatic inert gas tungsten arc welding process (TIG) using a Linde HWM-2 Mechanized Contour Welder. All test panels were prepared in the horizontal position to simulate conditions at Marshall Space Flight Center in Huntsville, Alabama. The weld position is shown schematically in Figure 68. Plates were prepared for welding by first machining and then draw filing just prior to welding.

Several welding procedures were used in this investigation to study different conditions and each is discussed according to the type of study that was made. The various welding procedures follow.

STANDARD WELDING PROCEDURE

This welding procedure was established to duplicate the welding at Marshall Space Flight Center, Huntsville, Alabama, and is listed in Figure 69. Plates 24 x 8 inches were placed in a horizontal positioner and tack welded approximately 1-1/4 inches on either end to maintain alignment during welding. The weld joint was perpendicular to the rolling direction of the material. After the first side was welded the panels were allowed to cool to ambient temperature before removing from the positioner and welding the back side. The finished panels were stamped with an identification number and X-rayed. The X-ray procedure is as follows:

- Source - Dental X-ray unit
- Strength - 85 KV, 4 ma
- Source to film distance - 24 inches
- Exposure time - 90 seconds
- Type of film - Kodak type M without lead screens

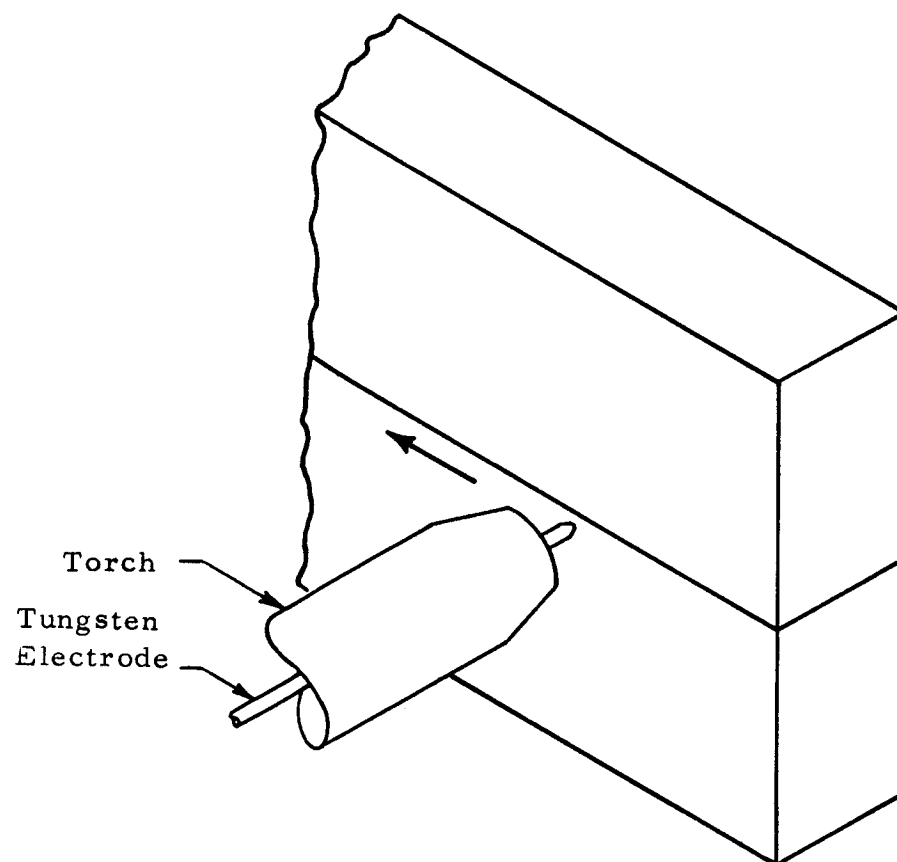
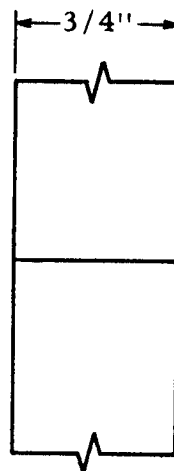


FIGURE 68. HORIZONTAL TIG WELDING



Square Butt Joint

Material	2219-T87
Filler Material	2319, 3/64 Inch Dia. , 12 ipm
Volts	11.5 V
Amperes	395 A
Welding Speed	7 in/min.
Polarity	DCSP
Shielding Gas	Helium (60 cfh)
Welding Process	Gas Tungsten-Arc (TIG)

One pass from each side

FIGURE 69. STANDARD WELDING PROCEDURE

Density - 2
Penetrameter - .75 inch ASME, 1/16 inch shim stock
Developing solution - Kodak D-19 developer
Developing time - 8 minutes at 68°F
Fixing solution - Kodak X-ray fixer
Fixing time - 10 minutes at 68°F

HYDRAULIC BULGE TEST PANELS

Test panels were fabricated for the bulge tests and identified as A, B, C and D. The panels are shown in Figure 70.

Panel A:

Two 3/4 x 16 x 32 inch plates were butt welded together along the 32-inch dimension according to the "Standard Welding Procedure".

Panel B:

Two 3/4 x 16 x 32 inch plates were butt welded together along the 32-inch dimension similar to Panel A except that two passes were deposited on each side. Welding variables are listed in Figure 71. After welding, the crowns were ground flush with the base material.

Panel C:

This panel was prepared identical to Panel A.

Panel D:

This panel was fabricated to simulate the intersection of a longitudinal and a circumferential weld in a cylindrical pressure vessel. This type weld is quite common on many space vehicles. Two 16 x 18 inch plates were butt welded to form a 32 x 16 inch section according to the "Standard Welding Procedure". This section was then butt welded to a 32 x 16 inch plate according to the same procedures to form a 32 x 32 inch panel.

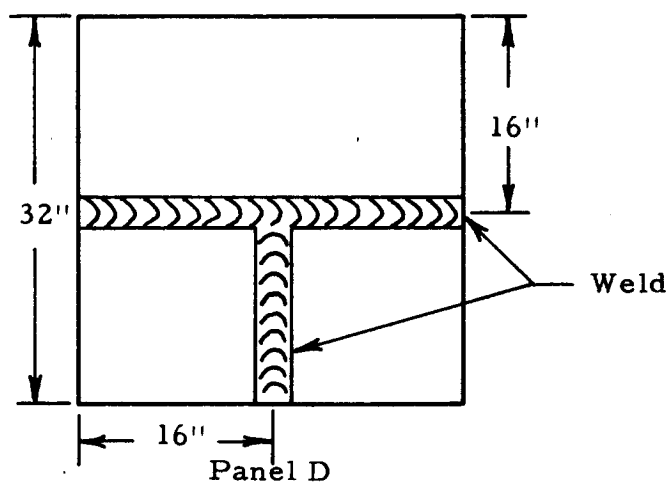
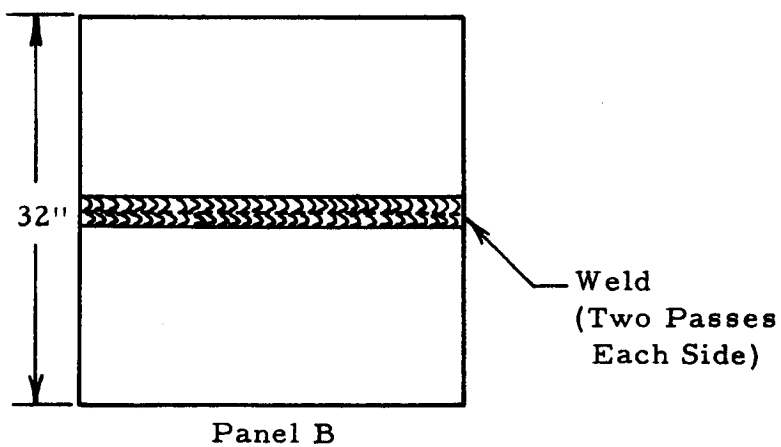
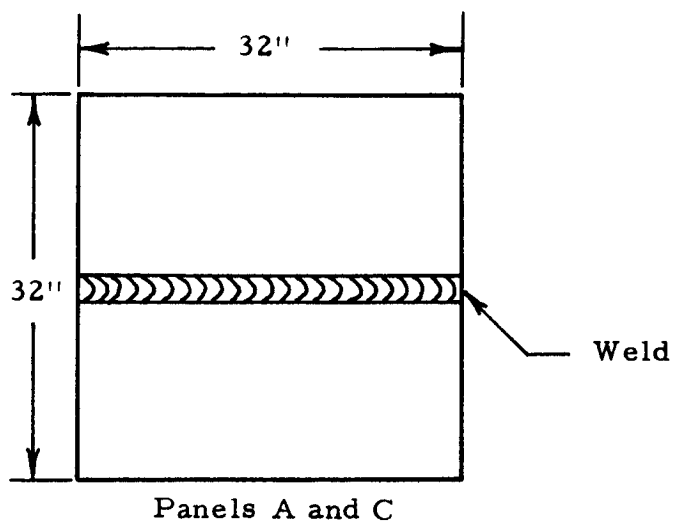
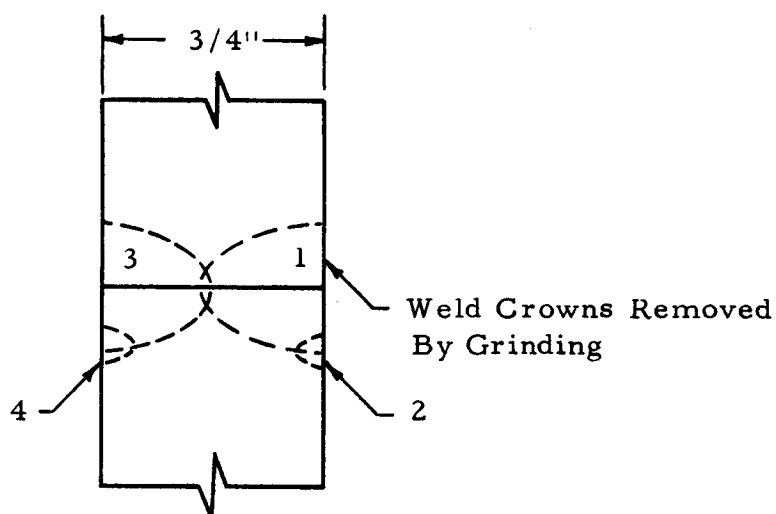


FIGURE 70. WELD CONFIGURATIONS OF HYDRAULIC BULGE PANELS A, B, C AND D



Joint Preparation and Welding Sequence

Welding Procedure*

<u>Pass No.</u>	<u>Amps</u>	<u>Volts</u>	<u>Filler Material Diameter (inches)</u>	<u>Filler Material Feed Rate (ipm)</u>	<u>Travel Speed (ipm)</u>
1	380	11.5	3/64	9	5
2	244	11.5	3/64	9	5
3	366	11.5	3/64	9	5
4	244	11.5	3/64	9	5

* All passes made in the horizontal position using a 5/32 inch diameter thoriated tungsten electrode and 60 cfh (Helium) gas flow rate.

FIGURE 71. WELDING PROCEDURE USED IN THE PREPARATION OF HYDRAULIC BULGE TEST PANEL B

LARGE WIDTH-TO-DEPTH RATIO

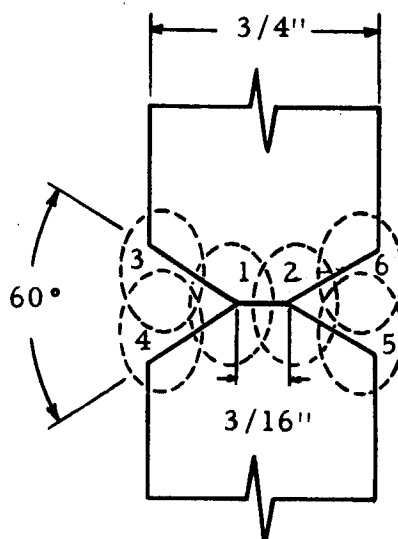
This welding procedure was used to simulate repair procedures on vehicles, and the various parameters are listed in Figure 72.

FUSION PASSES

Small fusion weld passes (without filler) were made in the toes of a panel prepared in accordance with the "Standard Welding Procedure".

A sketch of the cross-section of the prepared joint is shown in Figure 73.

The welding procedure is also listed.

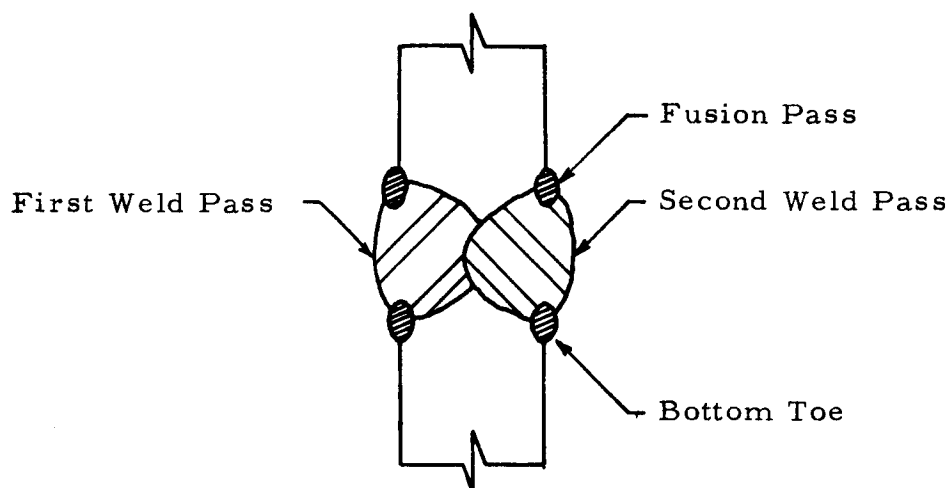


JOINT PREPARATION AND WELDING SEQUENCE

<u>Pass Number</u>	<u>Amps</u>	<u>Volts</u>	<u>Filler Material Diameter (Inches)</u>	<u>Filler Material Feed Rate (ipm)</u>	<u>Carriage Travel Speed (ipm)</u>
1	392	11.5	3/32	11.5	10
2	392	11.5	3/32	11.5	10
3	392	11.5	3/64	3	10
4	392	11.5	3/64	3	10
5	392	11.5	3/64	3	10
6	392	11.5	3/64	3	10

- Notes: (a) 3/16 inch diameter tungsten used for all passes.
 (b) 2319 filler material used for all passes.
 (c) 60 cfh helium flow rate used for all passes.
 (d) All welding done in the horizontal position.

FIGURE 72. WELDING PROCEDURE OF LARGE WIDTH-TO-DEPTH WELD RATIO



WELDING PROCEDURE FOR ALL FUSION PASSES

Amperes	160
Volts	11.5
Carriage Travel Speed	7 ipm
Filler Material Speed	9 ipm
Shielding Gas	Helium (60 cfh)
Filler Material	3/64 inch diameter 2319
Electrode	3/32 inch thoriated tungsten

FIGURE 73. WELDING PROCEDURE AND LOCATION OF FUSION PASSES IN TOES OF WELD